Mach probes

2012 Plasma Sources Sci. Technol. 21 063001

(http://iopscience.iop.org/0963-0252/21/6/063001)

Plasma Sources Sci. Technol. **21** (2012) 063001 (47pp) doi:10.1088/0963-0252/21/6/063001

INVITED REVIEW

Mach probes

Kyu-Sun Chung

Department of Electrical Engineering, Hanyang University, Seoul 133-791, Republic of Korea

E-mail: kschung@hanyang.ac.kr

Received 4 February 2008, in final form 6 August 2012
Published 16 November 2012
Online at stacks.iop.org/PSST/21/063001

Abstract

A Mach probe (MP) is an electric probe system to deduce the plasma flow velocity from the ratio of ion saturation currents. Generally, a typical MP is composed of two directional electric probes located at opposite sides of an insulator, which is mostly used as a parallel MP, but there are other MPs such as perpendicular MP (PMP), Gundestrup probe (GP) or rotating probe (RP), and visco-MP (VMP), depending on the shape of the probe holder, location of different probes or the method of collecting ions. For the parallel MP (to be called simply an MP), the relation between the ratio of the upstream ion saturation current density (J_{up}) to the downstream (J_{dn}) and the normalized drift velocity ($M_\infty = v_d/\sqrt{T_e/m_i}$) of the plasma has generally been fitted into an exponential form ($R = J_{up}/J_{dn} \approx \exp[K M_\infty]$). For the GP or RP, with oblique ion collection, the relation becomes $R = \exp[K(M_\parallel - M_\perp \cot\theta)]$, where $K \simeq 2.3$–2.5, $M_\parallel = M_\infty$, $M_\perp$ is the normalized perpendicular flow to the magnetic field, and θ is the angle between the magnetic field and the probe surface. The normalized drift velocity of flowing plasmas is deduced from the ratio (R_m) measured by an MP as $M_\infty = \ln[R_m]/K$, where K is a calibration factor depending on the magnetic flux density, collisionality of charged particles and neutrals, viscosity of plasmas, ion temperature, etc. Existing theories of MPs in unmagnetized and magnetized flowing plasmas are introduced in terms of kinetic, fluid and particle-in-cell models or self-consistent and self-similar methods along with key physics and comments. Experimental evidence of relevant models is shown along with validity of related theories. Calibration and error analysis are also given. For probes other than the typical parallel MP, the relation between the ratio of ion saturation currents and M_∞ can be expressed as a combination of the functional forms: exponential and/or polynomial form of M_∞ for PMP; two Rs of two separate MPs for VMP. Collisions of ions/electrons/neutrals, asymmetries of ion temperatures and the existence of hyperthermal electrons, existence of ion beam, supersonic flow and negative ions can affect the deduction of flow velocities by an MP.

(Some figures may appear in colour only in the online journal)

NOMENCLATURE

B:	magnetic field intensity
E:	electric field intensity
ϕ:	electric potential (with respect to the probe)
$\phi_{p,f}$:	plasma and floating potential
ψ, ψ_w:	normalized electric potential to electron temperature ($\equiv e\phi/T_e$) at an arbitrary position and at the wall (i.e. probe surface)
e:	electron charge
Z:	ion charge state
q:	ion charge ($\equiv Ze$)
T_-:	negative ion temperature
T_N:	neutral temperature
T_e:	electron temperature
T_i, $T_{i\infty}$:	ion temperature at an arbitrary position and in the out of perturbation region (i.e. infinitely far from the probe).
τ:	ratio of ion to electron temperature ($\equiv \sqrt{T_i/T_e}$)
m_i:	ion mass
m_e:	electron mass
f_M, f_N:	forms of velocity distribution function of molecular ion and neutral particles, respectively

f_i or $f(z, v)$:	form of ion velocity distribution function
g_i or $g(y, M)$ or $g(y, M)$:	form of normalized ion velocity distribution function ($\equiv V_s f_i(z, v)/n_\infty$
P_i:	ion pressure
$\mathcal{E}$:	total energy of ions
ϵ:	normalized total ion energy of ions ($\equiv \mathcal{E}/T_e$ or $\mathcal{E}/ZT_e$)
a:	radius of probe
b:	radius of sheath; $b - a =$ sheath thickness
A:	probe area
θ:	angle to the probe for particle collection ($= 90^\circ$: normal incidence, $= 0^\circ$: grazing incidence)
n_i, $n_{i\infty}$:	ion number density at an arbitrary position and infinitely far from the probe, respectively
n_e, $n_{e\infty}$:	electron number density at an arbitrary position and infinitely far from the probe, respectively
n, n_s:	normalized ion density ($\equiv n_i/n_\infty$) at an arbitrary position and sheath edge, respectively
n_∞:	normalized ion or electron number density out of the perturbation region since $n_\infty = n_{e\infty} = n_{i\infty}$ for quasi-neutrality
n_{st}:	stagnation density
J:	current density
J_∞:	unperturbed current density (out of the perturbation region)
J_s:	current density at the sheath edge
$J_{up,dn}$:	upstream and downstream current density of ions at the sheath edge
$N_{in,out}$:	number of ions entering/coming from the ion flux tube
J_{net}:	net current density to the ion flux tube
ρ_i:	ion gyro-radius
λ_D:	Debye length
λ:	normalized Debye length to the probe radius
$\vec{x}$:	an arbitrary position vector
z:	coordinate for parallel direction to the probe
r:	coordinate for perpendicular direction to the probe
y:	normalized distance to parallel perturbation length ($\equiv z/L_{\|\|}$), for a magnetized plasma, and to probe radius ($\equiv z/a$) for an unmagnetized plasma
s:	dimensionless distance for non-uniform meshing ($y = s^\delta$, $\delta > 1$)
$L_{\|\|}$, $L^*_{\|\|}$:	parallel components of perturbation length expressed by $a^2 V_s/\zeta^* D_\perp$ and $a^2 C_s/\zeta^* D_\perp$. ζ^*: scale factor for parallel perturbation length ($L_{\|\|}$ or $L^*_{\|\|}$)
ζ:	self-similar variable ($\equiv z/y$). Here y is the perpendicular coordinate to the flow direction (z).
R:	ratio of upstream to downstream current densities, $R_{\|\|}$ for a parallel Mach probe, $R_\perp$ for a perpendicular Mach probe, R_s for a small separator in a visco-Mach probe, R_l for a large separator in a visco-Mach probe
v:	ion kinetic velocity (or coordinate for the ion velocity)
V:	ion fluid velocity at an arbitrary position
v_d:	drift velocity outside the perturbation region
v_{th}:	ion thermal velocity ($\equiv \sqrt{T_i/m_i}$)
v_{ph}:	ion phase velocity
$v_{\|\|}$:	tangential ion velocity component
$v_\perp$:	radial ion velocity component
$v_{up,dn}$:	negative ion drift velocities of upstream and downstream sides
V_s:	ion sound velocity without ion temperature ($\equiv \sqrt{T_e/m_i}$ or $\sqrt{ZT_e/m_i}$)
C_s:	ion acoustic velocity with ion temperature ($\equiv \sqrt{(T_e + T_i)/m_i}$ or $\sqrt{(ZT_e + T_i)/m_i}$)
u:	normalized ion kinetic velocity to ion sound velocity ($\equiv v/V_s$)
M, M_∞:	normalized drift velocity to ion sound velocity ($\equiv V/V_s$ and $\equiv v_d/V_s$) at an arbitrary position and at infinity from the probe, respectively
M^*, M^*_∞:	normalized drift velocity to ion sound velocity ($\equiv V/C_s$ and $\equiv v_d/C_s$) at an arbitrary position and at infinity from the probe, respectively
K:	calibration factor for Mach probe when using M_∞
K^*:	calibration factor for Mach probe when using M^*_∞
M_c:	(inverse) calibration factor ($\equiv 1/K$)
$W(z, v)$:	transverse transport coefficient, which is expressed by $D_\perp$ ($\equiv D_\perp(z, v)/a^2$)
$D_\perp$, $D_\perp(z, v)$, $D_\perp(z)$:	forms of cross-field diffusion coefficient
η:	shear viscosity
α:	normalized shear viscosity ($\equiv \eta/n_i m_i D_\perp$)
S_t, S_i, S_r, S_a:	source terms for transport, ionization, recombination and atomic processes, respectively
$\langle\sigma v\rangle_{ion,rec,MAR,EIR}$:	reaction rate for ionization, recombination, molecular-activated recombination and electron–ion recombination, respectively.

1. Introduction

1.1. What is a Mach probe?

A Mach probe (MP) is an electric probe system to deduce the plasma flow velocity or Mach number from the measurement

of ion saturation currents. There are several types of MPs: (1) a parallel MP is composed of two directional electric probes located at opposite sides of a common insulator between them, and both probes collect the ions in the parallel direction with respect to the plasma flow or the magnetic field direction. This is mostly used for flow measurements, and is usually called the MP (figure 1). The relation between the Mach number and the ratio of the upstream (ram) and the downstream (wake) is expressed as an exponential form such as $R = J_{up}/J_{dn} \approx \exp[K M_\infty]$; (2) a rotating (Mach) probe (RP), which consists of one directional probe, or two planar collectors separated by an insulator, rotates and measures the polar distribution of ion saturation currents of all the angles with respect to the flow or magnetic field direction (figures 2 and 3); (3) a Gundestrup probe (GP) is composed of several collectors installed around a cylindrical or octagonal insulator, and measures the polar distribution of ion currents at different angles simultaneously (figure 4); (4) a perpendicular Mach probe (PMP) is composed of two cylindrical probes mutually perpendicular to each other. Although the axis of one probe is parallel to the flow, and that of the other is perpendicular, PMP measures the parallel plasma flow (figure 5); (5) a visco-Mach probe (VMP) consists of two parallel MPs, i.e. four separate directional probes, to deduce the parallel Mach number and the normalized shear viscosity simultaneously. One small MP (SMP) is located within the presheath generated by the other large MP (LMP) (figure 6).

1.2. How can we deduce the Mach numbers?

If there is no flow ($M_\infty = 0$), the collection of ions at the one-sided probe (J_{up}) is the same as that at the opposite sided-probe (J_{dn}), i.e. $R = J_{up}(1)/J_{dn}(1) = 1$, while if there is directional flow ($M_\infty > 0$), the ratio of the current density at the upstream side (J_{up}) to the downstream side (J_{dn}) is larger than one, $R = J_{up}(2)/J_{dn}(2) > 1$, as shown in figure 7. Experimental data for $R > 1$ can be clearly seen from the data taken by the retarding ion mass spectrometer (RIMS) on DE 1 (Dynamic Explore 1) spacecraft [2], as shown in figure 8. Generally, the magnitude of the drift flow is a function of the ratio of upstream current to downstream current, i.e. $R = R(M_\infty)$, where M_∞ is the normalized drift velocity.

The relationship between the Mach number (M_∞) and the ratio (R) of upstream (J_{up}) to downstream (J_{dn}) ion saturation current densities can be expressed as

$$R = \exp[K M_\infty],$$

where K is a calibration factor to be provided by the model. This exponential form of the ratio of current densities was used as an empirical formula in order to deduce the plasma flow velocity at the scrape-off layer in the DITE tokamak [1], and it was adopted in order to fit the ion current data from the Explorer 31 magneto-spheric satellite [2]. As for theories, one can derive exponential forms exactly from a self-similar fluid model for coherent inflow [4]. One can approximately deduce it from a magnetized fluid model [5–7] and a kinetic model [8] as well. Thus, if one measures the ratio ($R_m = J_{up}/J_{dn}$) of upstream to downstream ion saturation currents, and the calibration factor K is given by the relevant model, then the Mach number can be deduced as

$$M_\infty = \ln[R_m]/K,$$

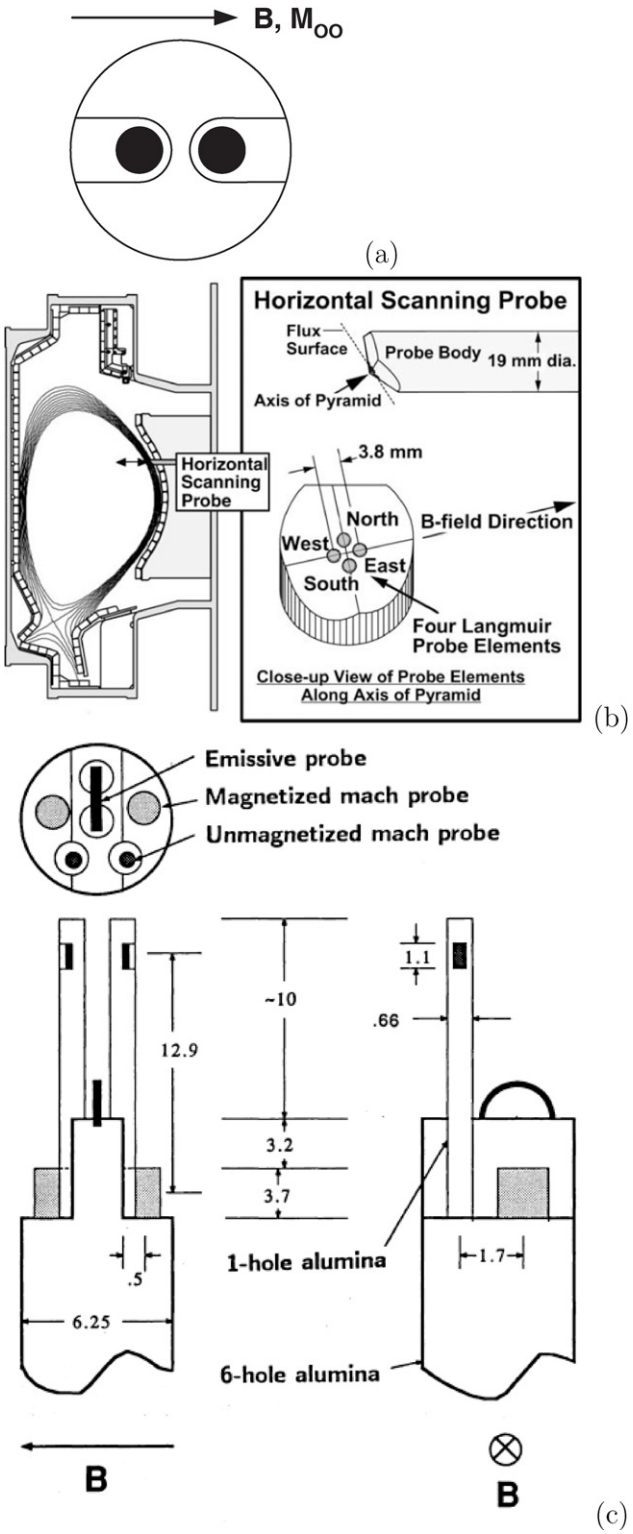

Figure 1. (Parallel) MP. (*a*) Schematic drawing of a (parallel) Mach probe (MP), (*b*) actual drawing of an MP (Alcator C-Mod) [140], (*c*) actual drawing of a MP set (PISCES-A: Chung) for unmagnetized plasma is the case of $\rho_i > a$, and MP for magnetized plasma is for $\rho_i < a$ [113].

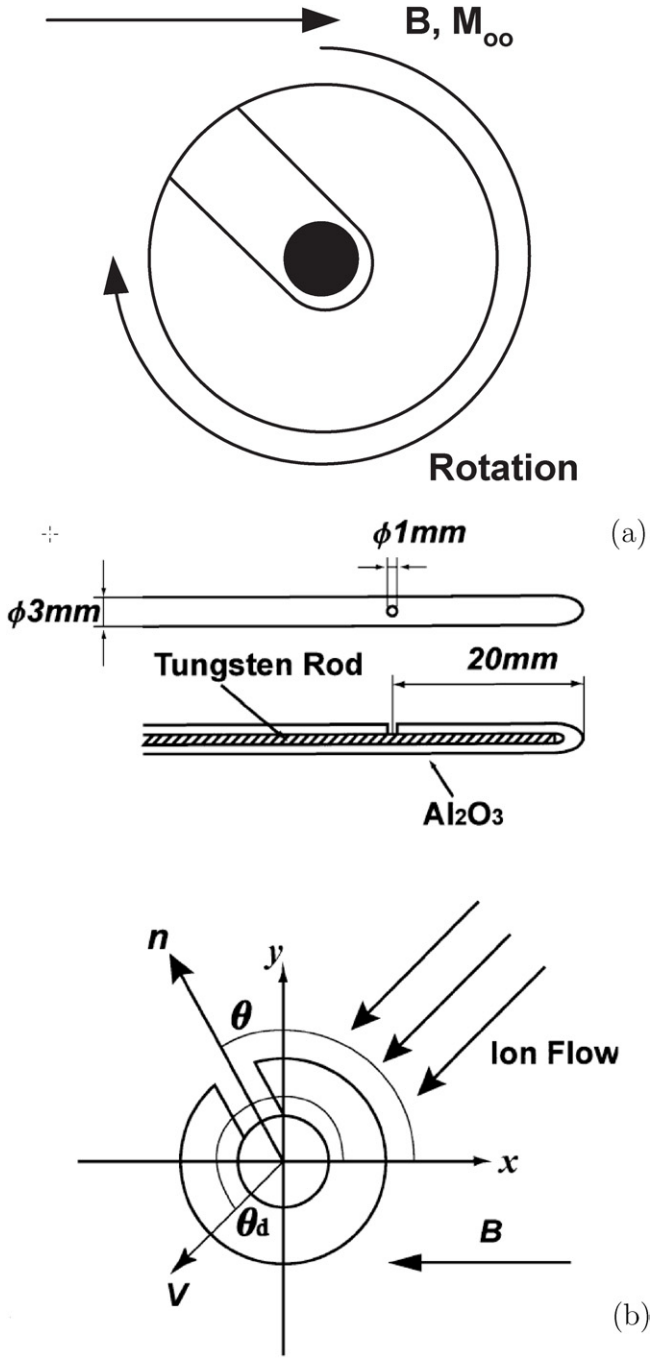

Figure 2. Rotating directional probe. (*a*) Schematic drawing of a rotating directional probe, (*b*) actual drawing of a rotating directional probe (Hyper-I device) [156].

where the calibration factor (K) is to be affected by the magnetic flux density, collisions of charged particles and neutrals, viscosity, ion temperature of plasmas, etc, which will be explained in detail in the following sections.

1.3. Why do we care about an MP?

The MP is the cheapest and easiest device to be used among various methods of flow measurement, but it is somewhat cumbersome to analyze the data due to the complexity of its theory. Since the same measured data can produce quite

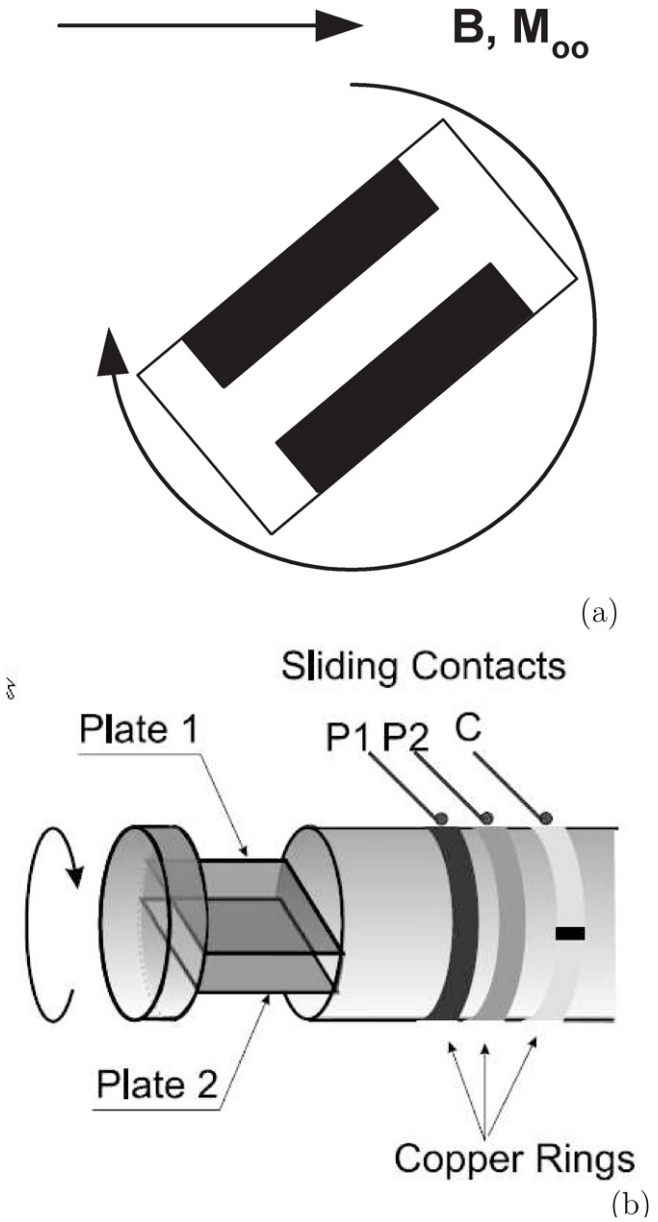

Figure 3. Rotating MP. (*a*) Schematic drawing of a rotating MP, (*b*) actual drawing of a rotating MP (CASTOR) [88].

different flow velocities depending on the applied theories, one should be cautious in choosing the proper model to interpret the measurement, i.e. one should characterize the plasma properly in a given machine, survey the available theories and build a probe for which a relevant theory exists, if possible. Otherwise, the MP would just become a flow meter giving the direction of flow, or producing a Mach number with a large uncertainty. Spectroscopic and laser methods [27–29] rely on line emission by excited electrons, therefore they cannot be used to measure ionized hydrogenic ions in fusion plasmas. An MP could deduce the plasma flows with spatial variation, if reliable theory would be provided, even for the hydrogen plasma, by taking the ion saturation currents of two separate electric probes.

The physics of the plasma flow to the probes used to measure the edge plasma flows is very similar to the physics

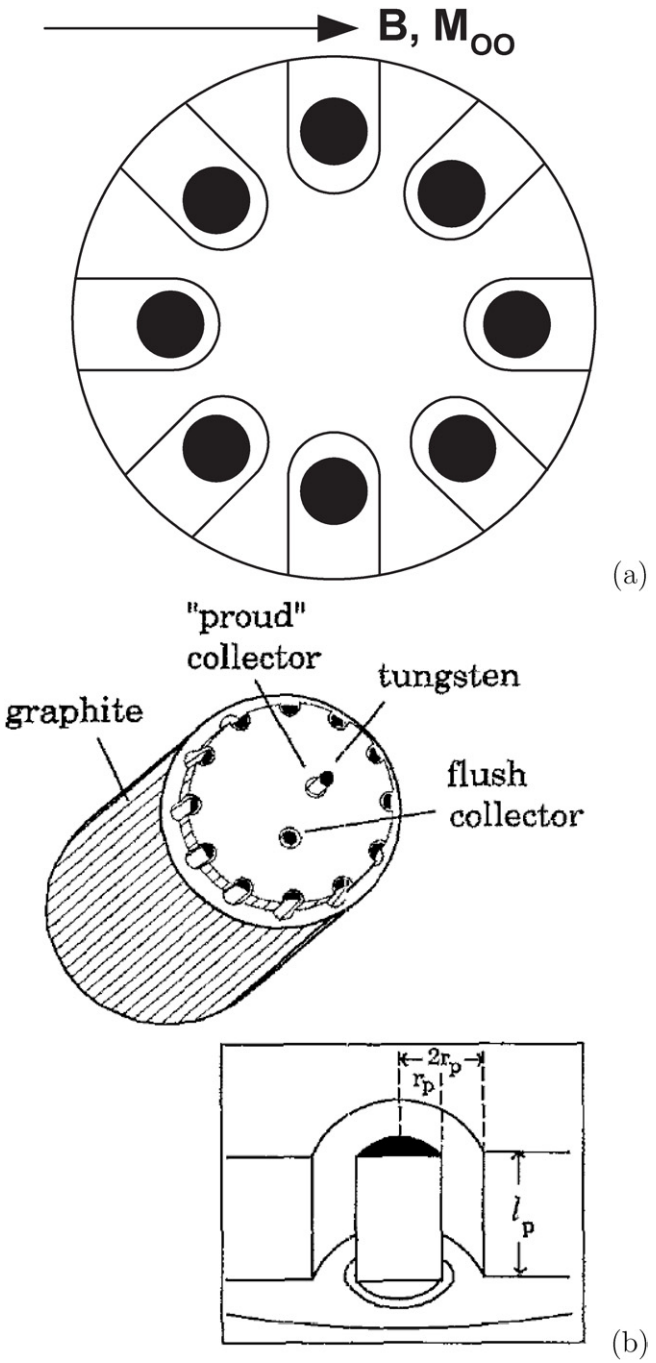

Figure 4. GP. (*a*) Schematic drawing of a GP, (*b*) actual drawing of a GP (TdeV) [130].

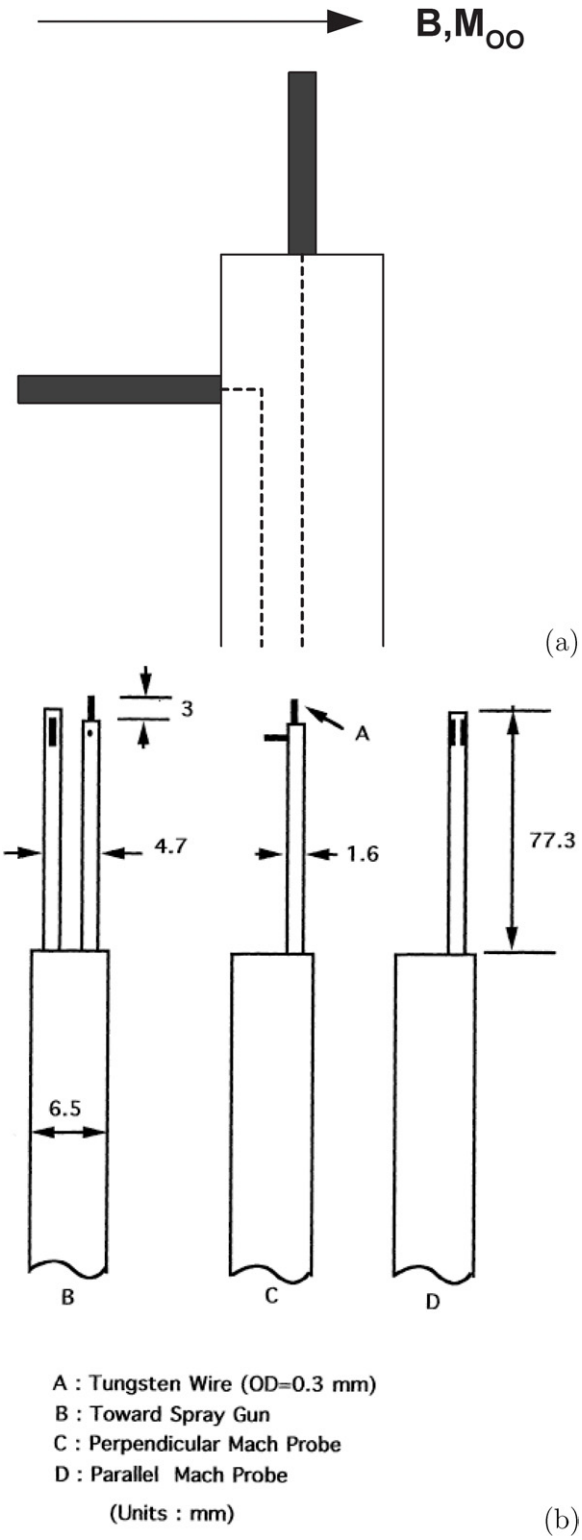

Figure 5. PMP. (*a*) Schematic drawing of a PMP, (*b*) actual drawing of a PMP (plasma torch) [38].

involved in the flows themselves. Planetary objects and spacecraft at high altitudes drift through an unmagnetized plasma ($\rho_i > a$ or $B = 0$, $\rho_i =$ ion gyro-radius), while a space shuttle in low Earth to ionosphere orbits moves through a magnetized plasma ($\rho_i < a$). A consequence of the motion of solid bodies through space plasmas is the formation of a wake, and modification of their electrical charge [2]. When the unmagnetized plasmas undergo plasma processing, the parameters of the processed material may depend on the ratio of ion to electron temperatures and the plasma drift [15].

As a device to measure the local plasma flows, the MP can be used for the following phenomena related to plasma flows. (1) Edge flow in tokamak devices is still an important issue to understand the scrape-off layer (SOL), which includes the problems of non-ideal MHD and plasma–wall interactions. Application of an MP to measure $E \times B$ drift, supersonic flow and flows with various atomic processes still requires new analyzing models, and independent calibration diagnostics

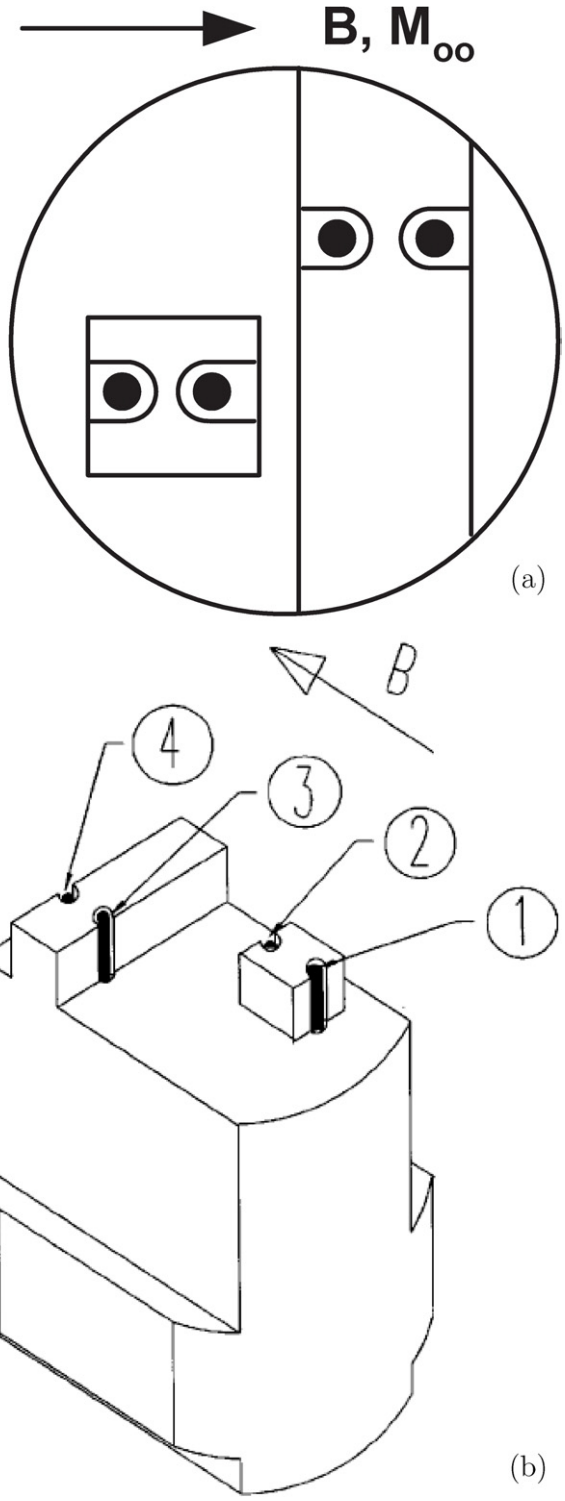

Figure 6. VMP. (*a*) Schematic drawing of a VMP (*b*) actual drawing of a VMP (TEXT-U). 1 = probe pin of SMP for the upstream flow, 2 = probe pin of SMP for the downstream flow, 3 = probe pin of LMP for the upstream flow, 4 = probe pin of LMP for the downstream flow [97].

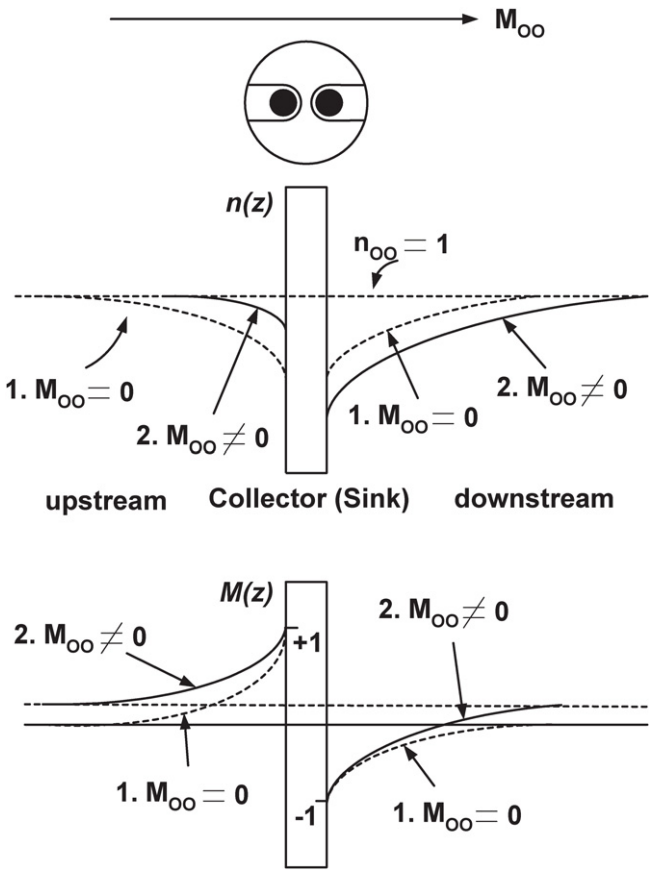

Figure 7. Effect of drift flow on collection at both ram (upstream) and wake (downstream) sides. The curves for 1 are density profiles without drift flow (M_∞) and those for 2 are the flow [13].

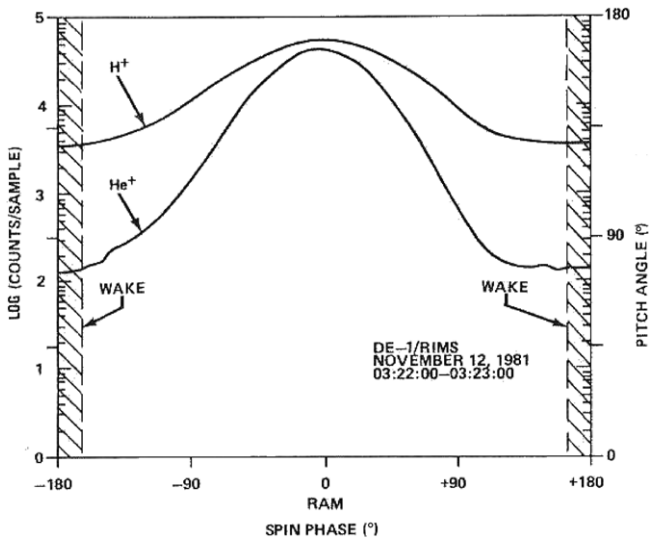

Figure 8. DE 1/RIMS data showing the angular variation of H^+ and He^+ ion currents (spin phase is angle θ in the text) [2].

[19, 20]. (2) The problem of the sheath has a long history as a typical non-linear phenomenon, and it still raises many open questions in terms of collisionality, non-thermal electrons [16], negative and/or multiply charged ions [17], etc. (3) Plasma processing also involves problems with a strong flow during the plasma source ion implantation (or plasma immersed ion implantation) [18]. A radio frequency (RF) sheath is formed to balance ions and electrons when the RF is applied to the substrates of etching, ashing or cleaning devices, which is large enough to pull the ions with a very large velocity. (4) The plasma jet (propulsion) problem includes non-adiabaticity and

plasma–neutral interactions. Plasma propulsion systems are versatile for the micro-positioning of the satellite, propulsion system of the satellites for the study of asteroids passing around the Earth, or deep space exploration such as travel to Mars. For an electrostatic space propulsion system, the measurement of flow is one of the key elements to improve thrust and specific impulse with a magnetic nozzle [21, 22]. (5) Magnetic reconnection in Earth's magnetosphere due to the Earth magnet and solar wind is another interesting problem of strong plasma flows related to non-ideal MHD and field–particle interactions [23]. (6) Simulation of an acoustic black hole with supersonic plasma flow in a complex plasma based on the sonic analog is very closely related to the Hawking radiation. In particular, horizons for sound propagation could be present in dumb holes, i.e. there are similarities among (black hole space-time, light), (flow with sonic point, sound wave) and (plasma flow, ion acoustic wave), which are pioneered by Unruh [24] and Sakagami [25]. (7) The plasma bubble expansion is an extragalatic phenomenon associated with hypersonic plasma flow and magnetic field. Recent observations suggest that such outflow systems could be magnetically dominated and it is an important phenomenon in the evolution of active galaxies [26].

1.4. What has been done on MPs?

There have been attempts to measure the flow velocity in unmagnetized plasmas such as atmospheric torch plasmas [38], in mirror plasmas for rotation [39], in basic plasmas [40], in linear divertor simulators [41] and ion sources [42].

As for the magnetized plasmas, an MP has been used in various fusion devices for the toroidal and $\boldsymbol{E} \times \boldsymbol{B}$ shear flows. In the early 1970–80s, an MP was used to measure the flow velocity in the SOL of JFT-2a as a form of directional RP [43], DITE [1, 44] and T-10 tokamaks [45]. Recently, MPs have been used at various poloidal locations in major tokamak devices or stellarators such as JET, DIII-D, JT60-U, Alcator C-Mod, ASDEX-U, Tore Supra, TEXTOR, Tokamak de Varennes (TdeV) or IMS (Interchangeable Module Stellarator) [46–54].

1.4.1. MP analysis in magnetized plasmas. The mechanism between a plasma and a target in plasma processing such as plasma etching [15], the physics of tokamak edge plasmas [19], and the interaction between a space shuttle and the surrounding plasma in a low-Earth orbit [55] contains similar features such that (i) the plasmas are magnetized (ion gyro-radius, $\rho_i <$ typical object size, a), (ii) the plasmas are flowing toward an object and (iii) the characteristics of the plasmas are not well quantified.

The theory of probe operation in magnetic fields is very difficult. For stationary plasmas, Bohm obtained a criterion for stable sheath formation with mono-energetic ions and inferred a weak dependence of ion current on ion temperature for $T_i < T_e$ [56]. Sanmartin [57] performed an asymptotic analysis of particle collection by spherical probes in the magnetic field for $T_i/T_e \sim 1$ concentrating on electron collection and weakly magnetized ions. Laframboise and Rubinstein [58] developed a theory of a cylindrical probe with an arbitrary angle to the uniform magnetic field for a completely collisionless plasma for arbitrary ion temperatures.

Stangeby [59] applied the kinetic calculation results of Emmert *et al* [60] directly to the theory of magnetized probes by treating the cross-field transport to provide a source in the one-dimensional (1D) parallel equations. He also gave a 1D fluid calculation, which was proven to be analytically integrable even with a plasma flow incorporated into the source [5]. Here, the ion source adopted corresponds to a 'birth' of ions within the collection region considering only the cross-field transport of ions 'into' the flux tube.

Hutchinson [6] introduced a fluid approach that uses a more physically appropriate source, accounting not only for ions moving 'into' the collection region, but also for ions moving 'out'. In the context of a 1D model, this implies a sink of ions within the inner presheath as well as a source of ions in the bulk plasma. This modification corresponds to adopting a realistic value of ion viscosity rather than making it effectively zero, as Stangeby's approach does. In a further study, Hutchinson [9] expanded his theory by adopting different values of viscosity and showed that the inviscid case becomes singular, not relevant to any finite viscosity. In addition, this latter work includes a two-dimensional calculation that shows excellent agreement with the 1D approximation. These fluid analyses offer a substantially more accurate and reliable basis for understanding the interaction of probes with flowing magnetized plasmas. However, they mostly cover only the subsonic regime and approximate the ion energy equation by assuming that the ions are isothermal along the presheath, which they usually are not [8, 45, 111]. In addition, they naturally provide no information on the ion distribution function or related important quantities such as heat flux within the presheath.

Asakura *et al* [61] gave a comprehensive review on the mechanism of flow in the SOL and its effect on the edge transport of tokamak plasmas. Specifically, they raised an issue on the overestimation of Mach number deduction by the MP measurement over those by simulations such as UEDGE2D, B2SOLPS5.0, UEDGE, and plume experiments in Alcator C-Mod and DIII-D, which raised attention on atomic processes. Gravier *et al* [62] performed an experiment in Tore Supra to see the flow modification caused by biasing the toroidal pumped limiter and to check the effect of pumping by using a simple fluid model based on Hutchinson's fluid equation without shear viscosity, i.e. similar to Stangeby's inviscid fluid model. They suggested an optimal pumping by biasing the limiter negatively with adaptation of a toroidally symmetric neutralizer geometry, since the net poloidal flow could be opposite to the polodial projection of the parallel flow due to a strong $\boldsymbol{E} \times \boldsymbol{B}$ drift, even with a large parallel flow.

Although current edge simulation codes such as EDGE2D/Nimbus show a very weak parallel flow in fusion edge plasmas, the MP measured strong flows. From the experiment of Alcator C-Mod, Labombard *et al* [63] observed strong parallel flows in SOL, which could be driven by the asymmetric cross-field transport in SOL. In turn, this might affect either the turbulence or the cross-field transport. This cross-field transport would be the result of a 'self-organized

critical' system rather than a 'simple diffusive transport' system [64].

Erents *et al* [46] tried to explain the overestimation of Mach number by MP measurements as an (atomic process due to) impurity generated at the probe by plasma–surface interactions during the measurement. Hidalgo *et al* [65] maintained that 'there is a dynamical relationship between turbulent transport and parallel flows of tokamak edge plasmas via Reynolds stresses: parallel flows grow with the size of the transport event'. However, an alternative and non-perturbing measurement for the parallel flow to clarify the amplification of Mach numbers by the probes may be needed, or a readjustment of the calibration factor may be necessary.

Simultaneous measurements of the parallel and perpendicular flow velocities are possible if one uses a probe with multiple single probes, which is shown in figure 4 (GP) or by rotating a parallel MP, which is shown in figure 3 (RP). Instead of using the parallel MP, a symmetric double or an asymmetric double probe [86] has been used for the deduction of parallel Mach number and ion temperature by rotating them and by using the kinetic theory of a magnetized Mach probe (MMP) [8]. As for the parallel MP in magnetized plasmas, the existing kinetic and fluid theories of Chung and Hutchinson [8] and Hutchinson [6] have been used. As for the perpendicular flow they adopted the existing kinetic theory [8, 86], a combined fluid theory based on the collection angle and the viscous fluid model [6, 52, 87], or their own fluid theory [88]. In a linear mirror machine, there is $\boldsymbol{E} \times \boldsymbol{B}$ rotation and this poloidal flow velocity was measured by a GP using the kinetic model for unmagnetized flowing plasmas [39]. Hutchinson also developed a general model for oblique ion collection in transversely flowing magnetized plasmas [10, 11] by generalizing his previous simple 2D fluid model for plasma expansion into the vacuum using a self-similar method [4].

Models for probe behavior in the SOL have been devoted mainly to a free presheath [5, 7, 9], which does not come into contact with any object along the field line, although there are situations generating a bounded (connected) presheath, which does touch an object along the field line. A fluid analysis has been given numerically for the bounded presheath in terms of the normalized viscosity (α; the ratio of cross-field viscosity to diffusivity) by Hutchinson, and he showed α to be unity [95] from the previous experiment of Chung *et al* containing data of bounded (connected) presheath, yet claiming $\alpha = 0.5$ [113]. The relevance of the theory applied to interpret the experimental data may be questionable, whether it is kinetic [7, 60] or fluid analysis [5, 9, 45], for free presheath [5, 7, 9, 45] or for bounded [60, 95]. The key point in this debate is that we have to know both the flow Mach number (M_∞) and α simultaneously, i.e. without knowing α, the MP may be just a directional probe, or a flow meter with large uncertainties. To solve the problem above, a VMP is proposed [96], together with an analytic fluid theory, which can measure the normalized viscosity and the flow Mach number simultaneously. Using the analytic fluid model for the bounded and free presheath, Chung and Bengston measured the Mach number and normalized shear viscosity in the TEXT-U tokamak with a VMP [97].

1.4.2. MP analysis in unmagnetized plasmas. Theoretical treatments of the 1D plasma sheath have a long history. For stationary unmagnetized plasmas, 1D collisionless kinetic models were adopted with various ion sources by Tonks and Langmuir [66], Bernstein and Rabinowitz [67], Laframboise [68], Parrot *et al* [69], Harrison and Thompson [70], Emmert *et al* [60] and Bissel and Johnson [71], etc.

For drifting unmagnetized plasmas, Mott-Smith and Langmuir set up conservation equations of energy and momentum near the sheath of a cylindrical probe, by neglecting the electric field effect [72], which was adopted by Harbour and Proudfoot for the empirical exponential formula for the flow measurement of the DITE tokamak [1]. Adopting this idea, Hudis and Lidsky [3] set up a fluid model for a 1D cylindrical probe. Hutchinson [73] demonstrated that this model is neither physical nor consistent. Hershkowitz and Oksuz [14, 74] showed the applicability of the Hudis model through potential measurements in the wake region for very slow drift motion with very low ion temperatures. However, this model seems to be physically incorrect since it cannot be applicable in the case of zero ion temperature.

Grabowski and Fisher [76] analyzed 2D Vlasov–Poisson equations with plasma drift in the wake region for cylindrical geometry. It would be an extension of the model of Laframboise by replacing the stationary Maxwellian distribution with a shifted Maxwellian distribution in the 2D cylindrical geometry. Their data of plasma-sheath densities in the wake area are smaller than those of the 1D particle-in-cell (PIC) code [77] and the 1D kinetic code [78]. Chung [78] developed a self-consistent kinetic model for a planar probe, using a source based on the convection of particle toward the wake, and by taking the size of the perturbation due to the planar disk as that of the disk. Hutchinson [77] provided an extensive and excellent analysis for a spherical probe by developing a PIC model using the specialized-coordinate electrostatic particle and thermals in cell (SCEPTIC) coordination system in unmagnetized flowing plasmas.

A PMP was introduced to measure the flow velocity of unmagnetized plasmas for an atmospheric torch plasma using kinetic and fluid models [3, 78, 90], for high-pressure plasmas ($P_n \sim 1$ Torr, $n_e \sim 10^{13}$ cm^{-3}) using a kinetic model with zero sheath approximation [90, 91], and for plasma gas jets [92, 93] using a fluid model with cold ions [94].

1.4.3. MP analysis in special cases. Along with the magnetized presheath formed by the probes, not only the diffusive ion source in the magnetized presheath with Boltzmann electrons [12], but also other sources such as charge exchange [79], ionization [80, 81] and recombination [82] are important in the SOL of divertor-type tokamaks.

Chung and Hutchinson [7] kinetically analyzed the effect of ionization on the ion collection in magnetized flowing plasmas, and obtained a numerical result on the contribution of ionization to the deduction of flow velocity from MP measurements. Recombination and charge-exchange processes in fusion edge plasmas are important for the reduction of particle and heat fluxes onto the divertor targets.

Molecular-activated recombination (MAR) processes induced by hydrogen or hydrocarbon puffing have shown the capability of contributing to the volume recombination [82, 83], along with electron–ion recombination processes characterized by radiative and three-body recombinations. Hydrogen-MAR process can especially play a major role in cooling the plasma for low electron temperatures of 1–3 eV [84]. The conditions for each process to be effective strongly depend on the electron temperature, electron density and neutrals. Chung *et al* [80, 85] added recombination and ionization terms in the fluid model for MPs, maintaining that ionization makes R smaller while recombination makes R bigger.

1.5. How far can we cover on an MP?

Although there are various phenomena related to plasma flows, such as those in SOL/edge of fusion devices, flows surrounding space vehicles or space propulsion systems, impact of flows on the processing material, flows related to the magnetic reconnection solar system or extragalactic phenomena, which may require totally different and separate review(s), we try to focus on how to measure the plasma flows—techniques and theories, not the details of the mechanism or the cause of the flows. If one adds the effect of atomic processes such as ionization, charge-exchange and recombination, or the effect of negative ions, various species ions and multiply charged ions, non-thermal electrons, or even two-temperature isothermal electrons, theories and experiments are rare.

The goal of this review is (1) to summarize the existing (fluid, kinetic and PIC) theories of MPs in magnetized and unmagnetized plasmas, (2) to introduce related experiments for flow measurements, (3) to make brief comments on both theories and experiments, and (4) to give a new interpretation, not only by referring to the prevailing parallel MP, but also by relating the PMP, RP and GP and VMP. In particular, the effect of atomic processes and other factors on the deduction of Mach numbers by MPs is also added along with calibration and error analysis.

2. MP analyses in magnetized plasmas

The presence of plasma flow along the magnetic field causes large asymmetries in the ion saturation current drawn to the probe faces parallel and anti-parallel to the magnetic field [30, 31]. In using diagnostic edge probes, such flows introduce a complicating factor, which must be taken into account for probe data interpretation. More importantly, the asymmetry can be used to measure the flow velocity using ion collection theories. In particular, in divertor-type tokamaks, an understanding of the SOL plasma including flow reversal [32], the role of heat conduction specific to probes [33, 34] and detached plasmas [35, 36] are still critical issues. All of these problems are linked to the transport of momentum in the SOL. Flow velocity is one of the key parameters in boundary plasmas, since it dominates the physics of recycling and controls the fueling of the core plasma. Physics behind the control of plasma flow may affect the design and optimization of the divertor structures [37].

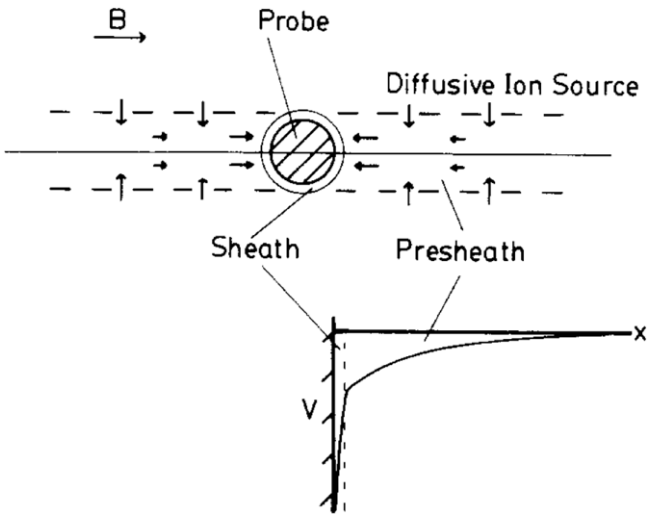

Figure 9. Schematic illustration of the geometry of ion collection in a strong magnetic field [6].

When the magnetic field is strong enough the ion gyro-radius is substantially smaller than the probing object. In this case ion collection across the field is diffusive even if the parallel flow is dominated by inertial effects. As a result, the quasi-neutral presheath region, where the acceleration of ions occurs into the sheath, becomes highly elongated along the field until the cross-field diffusion is able to balance the parallel collection flow, as shown in figure 9 [6]. Since the perpendicular momentum is unimportant in this process, it appears attractive to attempt to simplify the problem by treating the presheath as effectively 1D. One can then seek solutions satisfying Poisson's equation and the Boltzmann equation in the parallel direction, treating the perpendicular diffusion equation as a source term in the parallel equations.

Models on the MP in strongly magnetized plasmas is briefly summarized by Stangeby [99, 100] and Hutchinson [4, 98] debating the mechanism of cross-field transport as either convection or diffusion. In addition to the toroidal and $\boldsymbol{E} \times \boldsymbol{B}$ shear flows in toroidal fusion devices [47, 49, 50, 52–54], other experiments have shown to measure the Mach numbers using the existing collisionless theories excluding the atomic processes [46, 64, 101]. Discussions among Hutchinson, Stangeby and Chung provide some insights on the MP theories in magnetized plasmas along with experimental backgrounds [4, 100, 102, 103], leading to the importance of inclusion of strong shear viscosity and reasonable fluid approximation.

Hutchinson extended the 1D or 2D fluid model for parallel ion collection to oblique collection using self-similar methods [10, 11] to confirm the model of Van Goubergen for the Gundestrup or RPs [52]

2.1. Kinetic theory of MPs in magnetized plasmas

2.1.1. Ion flux tube. Referring to figure 10, consider a probe flux tube of force with volume $\pi a^2\,\mathrm{d}z$ defined by a probe of circular cross-section with radius (a), there are

$$N_{\mathrm{in}}/\mathrm{s} \approx \pi a^2\,\mathrm{d}z \int W(z, v)\, f_{\mathrm{i}\infty}(v)\,\mathrm{d}v, \qquad (1)$$

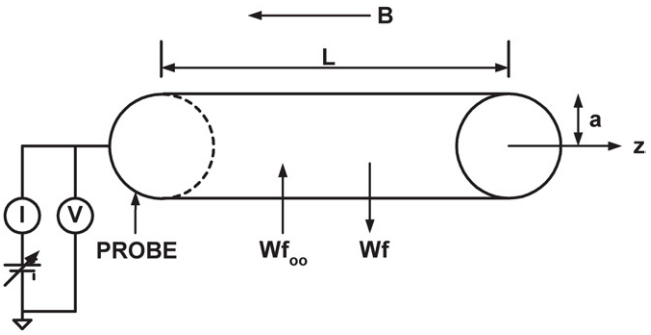

Figure 10. Ions are exchanged between 'inside' and 'outside' of the ion flux tube with rate W [109].

particles per second transported from outside to inside of the tube and there are

$$N_{\text{out}}/\text{s} \approx \pi a^2 \,\text{d}z \int W(z, v) f_{\text{i}}(z, v)\,\text{d}v, \tag{2}$$

particles per second transported out of this volume. Then the net flux transferred through the surface $2\pi a\,\text{d}z$ is found by

$$J_{\text{net}} = \frac{N_{\text{in}}/\text{s} - N_{\text{in}}/\text{s}}{2\pi a\,\text{d}z} \sim a \int W(z, v)[f_{\text{i}\infty}(v) - f_{\text{i}}(z, v)]\,\text{d}v. \tag{3}$$

The frequency $W(z, v)$ can be related to a transverse transport coefficient, which is expressed by $D_\perp(z, v)$. It is assumed that the probe dimension a is small compared with any cross-field density gradient existing in the absence of the probe. In this case, the probe induces a cross-field density gradient ($\sim(\partial/\partial r)\int f_{\text{i}}(z, v)\,\text{d}v \sim 1/a \int f_{\text{i}}(z, v)\,\text{d}v$), drawing the plasma into the flux tube, which terminates in the longitudinal direction. Then the transverse flux is obtained by

$$\begin{aligned} J_r &= -\frac{\partial}{\partial r} \int D_\perp(z, v) f_{\text{i}}(z, v)\,\text{d}v \\ &= -\frac{1}{a} \int D_\perp(z, v)[f_{\text{i}}(z, v) - f_{\text{i}\infty}(v)]\,\text{d}v. \end{aligned} \tag{4}$$

From equations (3) and (4)

$$D_\perp(z, v) = a^2 W(z, v). \tag{5}$$

Therefore, the frequency, $W(z, v)$, has the form

$$W(z, v) = \frac{D_\perp(z, v)}{a^2}. \tag{6}$$

$D_\perp(z, v)$ is a type of diffusion coefficient and may be a function of position and velocity, i.e. $D_\perp(z, v) \equiv D_\perp(z)F(v)$, where $D_\perp(z)$ is an anomalous vertical diffusion coefficient and $F(v)$ is a normalized function as $\int F(v) f(z, v)\,\text{d}v / \int f(z, v)\,\text{d}v = 1$. So the source due to transverse transport becomes

$$S_{\text{t}} = W(z, v)[f_\infty(v) - f(z, v)] = \frac{D_\perp(z, v)}{a^2}[f_\infty(v) - f(z, v)]. \tag{7}$$

In order to determine the characteristic length of this problem, we take the characteristic speed of ions as

$$v_\parallel \approx C_{\text{s}}, \qquad v_\perp \approx \frac{D_\perp}{a}, \tag{8}$$

where $C_{\text{s}} \equiv \sqrt{(T_{\text{e}} + T_{\text{i}})/m_{\text{i}}}$ is the ion acoustic speed. Taking the cross-sectional area of the flux tube to be $\sim a^2$ and the side area of the flux tube to be $\sim L_\parallel a$, where $L_\parallel$ is the natural collection length of the probe for ions, then we have the form from the particle balance between z and $z + \text{d}z$ as

$$\int f_{\text{i}}(z, v) a^2 v_\parallel \,\text{d}v\,\text{d}z \approx \int f_{\text{i}}(z, v) a L_\parallel v_\perp \,\text{d}v\,\text{d}z. \tag{9}$$

Hence, if the diffusion coefficient is of Bohm type, the ion collection length is obtained as

$$L_\parallel \approx \frac{a v_\parallel}{v_\perp} \approx \frac{a^2 V_{\text{s}}}{D_\perp} \sim \frac{a^2 B}{\sqrt{T_{\text{e}}}}, \tag{10}$$

where $V_{\text{s}} \equiv \sqrt{T_{\text{e}}/m_{\text{i}}}$. Depending on the definition of the ion acoustic speed and geometry of the ion flux tube, cylindrical or rectangular, the collection length becomes

$$L_\parallel = \frac{a^2 V_{\text{s}}}{\xi D_\perp}, \tag{11}$$

where $\xi = 1, \sqrt{T_{\text{e}}/(T_{\text{e}} + T_{\text{i}})}, 2\sqrt{T_{\text{e}}/(T_{\text{e}} + T_{\text{i}})}, \sqrt{2T_{\text{e}}/T_{\text{i}}}$ depending on different authors, such as Chung and Hutchinson [8], Hutchinson [6], Stangeby [5, 104], Harbour and Proudfoot [1], Matthews *et al* [105] and Cohen [106], respectively.

However, using a general cross-field transport with the self-similarity of Hutchinson [10, 11], the parallel length of the presheath is given as $a(M_\parallel + 1)/M_\perp$, which is much smaller than $L_\parallel$ for $0 \leqslant M_\infty \leqslant 1$, where $M_\parallel = M_\infty$, $M_\perp =$ perpendicular Mach number to B.

2.1.2. Kinetic model. Chung and Hutchinson [8] considered a cross-field transport governed by a frequency $W(z, v)$, which gives the rate at which particles are exchanged between the presheath and the outer plasma, so the Boltzmann transport equation with the vertical transport source becomes

$$\begin{aligned} &\left[v\frac{\partial}{\partial z} - \frac{q}{m_{\text{i}}}\frac{\text{d}\phi}{\text{d}z}\frac{\partial}{\partial v}\right] f_{\text{i}}(z, v) = S_{\text{t}} \\ &\quad = W(z, v)\Bigg[\alpha\{f_{\text{i}\infty}(v) - f_{\text{i}}(z, v)\} \\ &\qquad + (1 - \alpha)\left(1 - \frac{n_{\text{i}}(z)}{n_\infty}\right) f_{\text{i}\infty}(v)\Bigg], \end{aligned} \tag{12}$$

where α is the equivalent ratio of viscosity to diffusivity ($\equiv \eta/n_{\text{i}}m_{\text{i}}D_\perp$: normalized shear viscosity), and $f_{\text{i}}, m_{\text{i}}, z, n_{\text{i}}, q$, ϕ and v are the ion distribution function, ion mass, direction of particle stream to the planar probe, ion density, the probe size, ion charge, electric potential and ion velocity along the phase space of the energy orbit, respectively. Here the subscript ∞ means outside of the transition region.

The idea here is that there is a certain amount of particle exchange in position–velocity space, represented by the first term, plus a certain amount of particle inflow, represented by the second term. The first term of particle exchange indicates the ions entering the flux tube from outside, the second one is a new term and it represents the ions coming out of the flux tube. The inflow is presumably driven by the density difference between inside and outside of the collection tube and

is therefore taken to be proportional to the density difference. The distribution of the inflowing particles is that of the external plasma. Obviously, $\alpha = 0$ corresponds to pure inflow (no viscosity) and $\alpha = 1$ to pure exchange. The rate of particle and momentum exchange between outside and inside of the flux tube is taken to be equal, representing random migration of ions in either direction. The rate is related via

$$W(z, v) \sim \frac{D_\perp(z, v)}{a^2}$$

to $D_\perp$, the anomalous cross-field diffusion coefficient, and to a, the characteristic size of the probing object.

The energy equation of ions, governing the phase space orbits, is

$$\tfrac{1}{2}mv^2 + q\phi(z) = \mathcal{E}, \tag{13}$$

where $\mathcal{E}$ is the constant total energy. The electrons are assumed to be isothermal, described by the Boltzmann relation:

$$n_e(z) = n_\infty \exp\left[\frac{e\phi(z)}{T_e}\right], \tag{14}$$

where n_e and T_e are the electron density and temperature. The electron and ion densities are related by Poisson's equation, i.e.

$$\frac{d\phi^2}{dz^2} = -4\pi[q\int f_i(z, v)\,dv - en_e(z)]. \tag{15}$$

If we assume that $W(z, v)$ is independent of v, the equations can be non-dimensionalized by using the following transformations:

$$Z = \frac{q}{e}, \qquad y \equiv \frac{z}{L_{||}}, \qquad u \equiv \frac{v}{V_s}, \qquad \lambda(y) \equiv \frac{\lambda_D}{L_{||}(y)},$$
$$n \equiv \frac{n_i}{n_\infty}, \qquad \psi \equiv -\frac{e\phi}{T_e}, \qquad \tau \equiv \frac{T_{i\infty}}{T_e},$$
$$\epsilon \equiv \frac{\mathcal{E}}{ZT_e}, \qquad g(y, u) \equiv \frac{V_s}{n_\infty} f(z, v),$$

where λ_D is the Debye length and y is the non-dimensional distance. In terms of these parameters, equations (12), (13) and (15) become

$$\left[u\frac{\partial}{\partial y} + \frac{d\psi}{dy}\frac{\partial}{\partial u}\right] g(y, u) = [\alpha\{g_{i\infty}(u) - g(y, u)\} + (1 - \alpha)(1 - n)g_{i\infty}(u), \tag{16}$$

$$\epsilon = \frac{u^2}{2} - \psi, \tag{17}$$

$$\lambda^2\frac{d^2\psi}{dy^2} = Z\int g_i(y, u)\,du - \exp[-\psi(y)]. \tag{18}$$

If the external ion distribution is Maxwellian with temperature $T_{i\infty}$, shifted by a drift velocity v_d, then

$$g_{i\infty}(u) = \left(\frac{ZT_e}{2\pi T_{i\infty}}\right)^{0.5} \exp\left[-\frac{ZT_e(u - M_\infty)^2}{2T_{i\infty}}\right],$$

where $M_\infty = v_d/V_s$.

The boundary conditions on the distribution function are $g_i(y, M \geqslant 0) = 0$, $g_i(y = \infty, M) = g_{i\infty}(u)$, which means that the probe has a perfectly absorbing surface and the ion distribution has a Maxwellian form outside the perturbation.

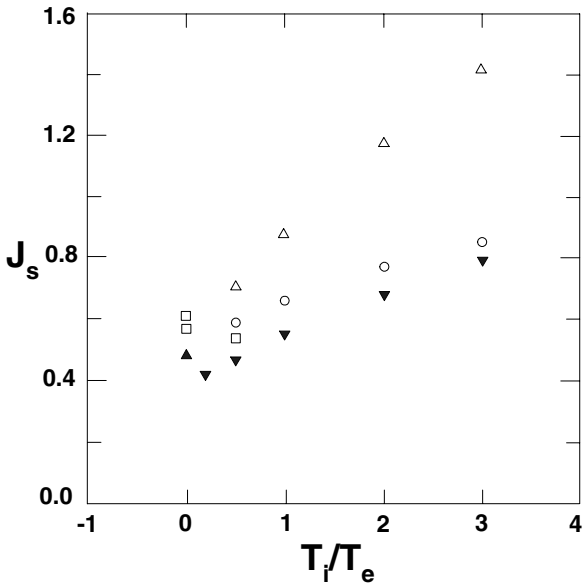

Figure 11. Sheath current variations with zero drift ($M = 0$) for $0 < T_{i\infty}/T_e < 3$ from various theories. ▼: Chung and Hutchinson [8, 109], ○: Bissel and Johnson [71], △: Emmert *et al* [60], □: Bohm *et al* [56], ▲: Harrison and Thomson [70].

Those on the potential are $\psi(y = 0) = \psi_w$, $\psi(y = \infty) = 0$, where the first equation indicates that the probe is biased by the applied voltage ϕ_w, which should be bigger than the sheath potential in magnitude. Far from the probe surface the potential is set to be zero, since there is no perturbation due to a probe. Here we subtract the potentials along the perturbation by the plasma (space) potential. By taking the moments of the ion distribution, we can get the ion density, current, fluid velocity, temperature and power flux.

To solve the preceding equations, we assume an initial potential variation along the presheath (ψ). Then along each energy orbit (ϵ), velocity sets are obtained (M). We calculate the ion distribution function along the orbits by solving the kinetic equation, equation (77), with a semi-implicit method. After this, the ion density is obtained by integrating the ion distribution functions over velocity space at each position using a modified Simpson rule for uneven meshing in velocity space. To solve the Poisson equation, equation (18), we use the successive over-relaxation method for the plasma-sheath equation ($\lambda \neq 0$), or a simple relaxation method for the plasma equation ($\lambda = 0$) with uneven meshing in position space. The final self-consistent solutions for the potential and ion distribution are obtained by iterating these procedures until they reach a convergence criterion.

For magnetized plasmas, the perturbation due to a probe is much longer than that for the unmagnetized case, i.e. $L_{||} \gg a$. So it would be much better to use the non-uniform meshing along the field direction as $y = s^\delta$, $\delta > 1$. Since the ratio of the Debye length to the length of the ion flux tube is so small, the Poisson equation is best written as

$$\psi(y) = -\ln[Z\int du g(y, u) - \lambda^2\frac{d^2\psi}{dy^2}]. \tag{19}$$

Figure 11 shows a comparison of the results of different kinetic analyses [45, 60, 70, 71]. With the exception of Bohm's

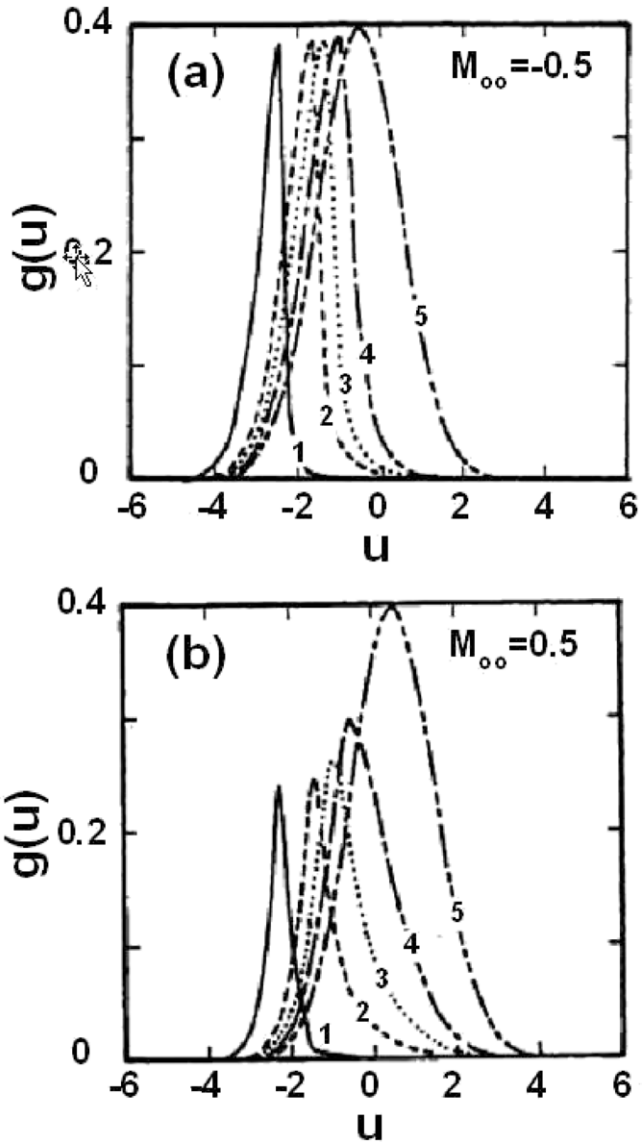

Figure 12. Ion density distribution functions for different ion drift velocities $M_\infty = 0.5$. $M_\infty > 0$ (upstream) and $M_\infty < 0$ (downstream) [8, 109].

finite ion energy calculation, which is for a spherical probe, the models are 1D plane geometry cases. As anticipated, Chung and Hutchinson's [8] model gives lower currents than the other models, because they have included the ion momentum loss due to particle exchange. (Note: in the original papers of Emmert *et al* [60], and Bissel and Johnson [71], the current was normalized by $n_\infty\sqrt{2T_{i\infty}/\pi m_i}$ and $n_\infty\sqrt{(T_{i\infty}+T_e)/m_i}$, respectively.) In their normalization their results show a decrease in current with $T_{i\infty}$. However, the currents increase with $T_{i\infty}$ when they are normalized by our definition of ion sound speed ($V_s = \sqrt{T_e/m_i}$).

Figure 12 shows the ion distributions along the presheath for $M_\infty = -0.5$ (upstream) and 0.5 (downstream). The reduction in ion density and ion temperature is clearly shown. Figure 13 shows the sheath currents calculated here with those of fluid models [5, 6], which give results with a finite ion drift. The fluid results are expressed in units normalized by the 'acoustic speed', C_s ($\equiv\sqrt{(T_e+T_i)/m_i}$), which is not

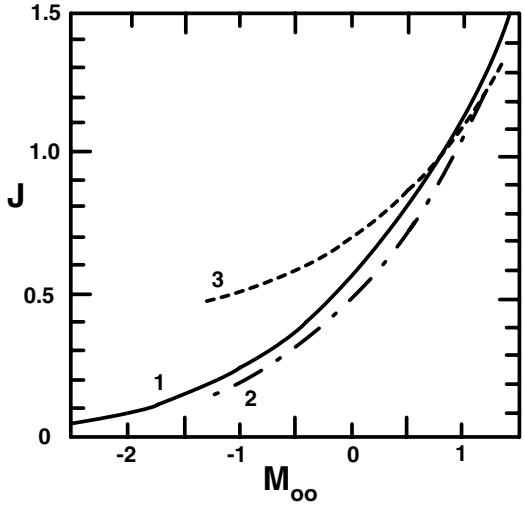

Figure 13. Sheath current variations with drift ($-2.5 \leqslant M_\infty \leqslant 1.4$) for $T_i = T_e$. curve 1: Chung and Hutchinson [8, 109], curve 2: fluid model of Hutchinson [6], curve 3: fluid model of Stangeby [104].

the same as the ion sound speed V_s ($\equiv\sqrt{T_e/m_i}$) used in the kinetic model. Thus, there is a degree of ambiguity in the comparison, since the effective acoustic velocity in the fluid treatments is $C_s \equiv \sqrt{(ZT_e+\gamma_i T_i)/m_i}$ and it is not obvious what to take for either γ_i or T_i, although there are experimental determinations of γ_i as Ando *et al* [93] and Woo *et al* [107] tried. For the purposes of comparison, they show kinetic results when $T_{i\infty} = T_e$ and scale the fluid results by taking $C_s = \sqrt{2}V_s$. This means that the fluid results, which are limited to $|v| < C_s$, range over $-\sqrt{2} < M < \sqrt{2}$. One can think of this assumption as being that $\gamma_i = 1$ and the relevant ion temperature is the external value. Hence a smaller sheath ion temperature than the unperturbed ion temperature and a smaller value of the heat specific ratio of ions make the absolute speed at the sheath smaller, so does the deduced drift speed. However, actual γ_i and T_{is} should be applied.

On this basis, the kinetic results of Chung and Hutchinson [8] agree well with those from the fluid calculation of Hutchinson [6] (and disagree with those of Stangeby [5]), as shown in figure 13. This is perhaps not surprising since Hutchinson's assumptions are essentially the fluid equivalents of the present kinetic model. The kinetic calculation gives a slightly larger current, although not very significantly, in view of the uncertainties in the comparison. The present results extend to the supersonic case, while the fluid treatments do not.

In figure 14 Chung and Hutchinson compared the ratio of upstream/downstream ion sheath current versus flow velocity with several other theories. They included the fluid theories of Hutchinson and Stangeby and also the naive particle model of Harbour and Proudfoot [1] (essentially equivalent to that of Mott-Smith and Langmuir [72], which takes the ion distributions at the probe to be drifted Maxwellians and ignores the presheath field effects). Also shown is the *ad hoc* empirical model of Proudfoot *et al* [30], which in their present normalization is $R = \exp(1.2M_\infty)$. The ion temperature is taken equal to the electron temperature. Early data of ion currents collected by satellites on ionosphere

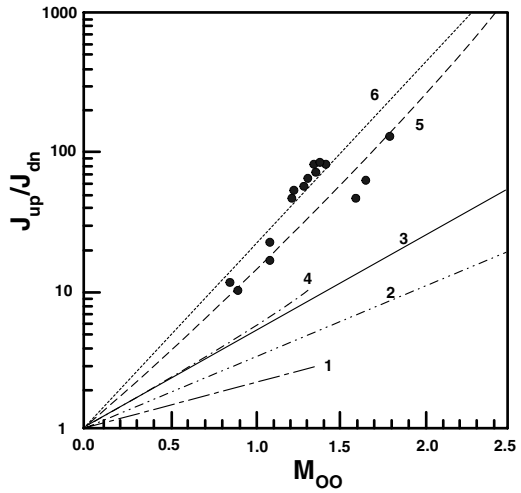

Figure 14. Comparison of the up/downstream ratio of sheath currents from various models, for $T_i = T_e$. curve 1: Stangeby ($K \approx 0.75$) [104], curve 2: Proudfoot *et al* ($K \approx 1.2$) [30], curve 3: Chung and Hutchinson ($K \approx 1.66$) [8, 109], curve 4: Hutchinson ($K \approx 1.7$) [6], curve 5: Mott-Smith and Langmuir ($K \approx 2.7$) [72], curve 6 and •; Samir ($K \approx 2.5$–3.1) [2].

(supersonic/hypersonic) or plasma sphere (subsonic/transonic) flow region are fitted as exponential forms. Samir *et al* [2] measured the low-energy ions such as hydrogen and helium by the RIMS onboard the Dynamic Explorer 1 (DE 1) satellite covering the geocentric altitude range $1.37 < R_E < 3.01$, and compared them with those of Explore 31. Since the gyro-radii of hydrogen ions with temperatures of ~0.2–0.7 eV $\approx$ 2–7T_e are about 90–160 cm comparing the size of the DE 1 satellite, which is $100 \times 130\,\mathrm{cm}^2$, hydrogen ions could be treated either as weakly magnetized or unmagnetized. These data are plotted in figure 14 comparing with those by other theories.

All these results give remarkably straight lines on a log-linear plot, as figure 14 shows. Therefore, they may be summarized in the form of an exponential, $R = \exp(K M_\infty) = \exp[K v_d/\sqrt{T_e/m_i}]$, where the calibration factor K is given as follows: Samir $\approx$ 2.5–3.1, Mott–Smith and Langmuir $\approx$ 2.7, Proudfoot *et al* $\approx$ 1.2, Stangeby $\approx$ 0.75, Hutchinson $\approx$ 1.7, and our present calculation $\approx$1.66.

2.2. Fluid theory of MPs in magnetized plasmas

2.2.1. The 1D fluid model from the 3D fluid model. Assuming that (i) the phenomenological cross-field flux of ions is $n_i \vec{V}_\perp = -D\nabla_\perp n_i$; (ii) electrons are isothermal, $n_e = n_\infty \exp[e\phi/T_e]$; (iii) cross-field diffusivity D is constant, (iv) parallel viscosity is classical; (v) ion temperature is constant along the presheath and (vi) θ-component is neglected, then the three-dimensional (3D) steady-state fluid equations for ions without volume source and collisional friction become

$$\frac{\partial}{\partial z}(n_i V) = D\nabla_\perp^2 n_i, \tag{20}$$

$$\frac{\partial}{\partial z}(n_i V^2) + C_s^2 \frac{\partial n_i}{\partial z} = D\nabla_\perp \cdot (V\nabla_\perp n_i) + \nabla_\perp \cdot \left(\frac{\eta}{m_i}\nabla_\perp V\right), \tag{21}$$

where $C_s^2 \equiv (ZT_e + T_i)/m_i$ and T_i and T_e are assumed to be constants. Here we focus on the parallel component of the momentum equations, treating these cross-field diffusion equations as a source term in the parallel equations, which is shown in figure 9. Equation (21) indicates that the parallel momentum transfer and pressure gradient are balanced by the perpendicular momentum transfer, which is composed of diffusion and viscosity terms.

We use the following non-dimensional variables and approximations in the cross-field direction including $n \equiv n_i/n_\infty$, $M^* \equiv V/C_s$, $L_{||} \equiv zD/a^2C_s$, $y \equiv z/L_{||}$, $\nabla \equiv a\nabla_\perp$, where a is the half-size of a perturbing object or an effective probe radius, and L_p is the characteristic length of the presheath. Equations (20) and (21) are expressed non-dimensionally as

$$\frac{\partial}{\partial y}(nM^*) = \nabla^2 n, \tag{22}$$

$$\frac{\partial}{\partial y}(nM^{*2}) + \frac{\partial n}{\partial y} = \nabla \cdot (M^*\nabla n) + \nabla \cdot \left(\frac{\eta}{m_i n_\infty D}\nabla M^*\right). \tag{23}$$

Here the viscosity contribution of equation (23)

$$S_v \equiv \nabla \cdot \left(\frac{\eta}{m_i n_\infty D}\nabla M^*\right) \tag{24}$$

is a very important term debated by several researchers [5, 7, 9, 12], and can be approximated by using either $\nabla Q \sim Q_\infty - Q$ or $\nabla^2 Q \sim Q_\infty - Q$ [103] as (i) $\alpha(M_\infty^* - M^*)$; (ii) $\alpha n(M_\infty^* - M^*)$; (iii) $\alpha(1-n)(M_\infty^* - M^*)$; (iv) $\alpha(1-2n)(M_\infty^* - M^*)$.

Term (i) is obtained by assuming either (a) $\eta \equiv \alpha m_i n_i D$ or (b) $\eta \equiv \alpha m_i n_\infty D$. Other terms are based on $\eta \equiv \alpha m_i n_i D$. Term (ii) can be derived either (c) by neglecting $\alpha(\nabla n)\cdot(\nabla M^*)$ as Hutchinson's [6] or (d) by manipulation of $\alpha\nabla \cdot (M^*\nabla n)$. Although terms (i) and (ii) are obtained using the exact same assumption of $\eta \equiv \alpha m_i n_i D$ without neglecting any term, term (i) results in a larger momentum by $\alpha(M_\infty^* - M^*)(1-n)$ when n is small. This is only due to the different procedures of approximation. Term (iii), which is used by Chung [12], can be obtained either (e) by neglecting $\alpha\nabla^2 M^*$ or (f) by taking the average of (i) and (iv). Term (iv) is derived (g) using only $\nabla Q \approx Q_\infty - Q$. It should be noted that $\nabla^2 M^*$ has the same form as ∇M^* in one- and non-dimensional approximations.

So far one can obtain four different approximations, (i)–(iv), of viscosity contribution by seven different approaches (a)–(g) in fluid equations. Although any approximation among them is as mathematically valid as the others, the physical validity would be quite different.

A. The Hutchinson model

A combination of equation (24) and approximation (ii) leads to

$$M^*\frac{dn}{dy} + n\frac{dM^*}{dy} = 1 - n, \tag{25}$$

$$\frac{dn}{dy} + nM^*\frac{dM^*}{dy} = (M_\infty^* - M^*)[1 - (1-\alpha)n]. \tag{26}$$

After some arrangements, one can get the following equations for $\mathrm{d}n/\mathrm{d}y$ and $\mathrm{d}M^*/\mathrm{d}y$:

$$\frac{\mathrm{d}n}{\mathrm{d}y} = \frac{M^*_\infty - 2M^* - (M^*_\infty - M^*)(1-\alpha)n + nM^*}{1 - M^{*2}}, \quad (27)$$

$$\frac{\mathrm{d}M^*}{\mathrm{d}y} = \frac{1 - n - M^*(M^*_\infty - M^*)[1-(1-\alpha)n]}{n(1-M^{*2})}, \quad (28)$$

Dividing equation (27) by equation (28) leads to

$$\frac{1}{n}\frac{\mathrm{d}n}{\mathrm{d}M^*} = \frac{M^*_\infty - 2M^* - (M^*_\infty - M^*)(1-\alpha)n + nM^*}{1 - n - M^*(M^*_\infty - M^*)[1-(1-\alpha)n]}. \quad (29)$$

For $\alpha = 0$, equation (29) recovers the same equations of Stangeby [5], and the density is analytically given as

$$n(M^*) = \frac{1}{1 - M^*_\infty M^* + M^{*2}}. \quad (30)$$

Then the relation between the ratio and the Mach number is given as

$$R(M^*_\infty) = \frac{n(M^* = +1)}{n(M^* = -1)} = \frac{1/(2 - M^*_\infty)}{1/(2 + M^*_\infty)} = \frac{2 + M^*_\infty}{2 - M^*_\infty} \approx \exp[M^*_\infty], \quad (31)$$

where the approximation is made for $0 \leqslant M^*_\infty \leqslant 0.5$.

For $0 \leqslant \alpha \leqslant 1$, equation (29) is the same equation as Hutchinson [9], and he solved them numerically. Hutchinson also provided an analytical solution for the density in terms of M^* for the case of $\alpha = 1$, approximately [6]:

$$n(M^*) = p^\beta \exp[(-\Omega)], \quad (32)$$

where $\beta = (M^*_\infty + 1)(M^*_\infty + 3)({M^*_\infty}^3 + 3{M^*_\infty}^2 + 7M^*_\infty + 5)/8$, $p = 1 + 2(M^* - M^*_\infty)/(M^*_\infty + 1)(M^*_\infty + 3)$, $\Omega = [({M^*_\infty}^3 + 3{M^*_\infty}^2 + 7M^*_\infty + 9)(M^* - M^*_\infty) - (M^*_\infty + 1)(M^* - M^*_\infty)^2]/4$. From this analytical form, the ratio is derived as

$$R(M^*_\infty) = \left(\frac{{M^*_\infty}^2 + 2M^*_\infty + 5}{{M^*_\infty}^2 + 2M^*_\infty + 1}\right)^\beta \times \exp[-({M^*_\infty}^3 + {M^*_\infty}^2 + 5M^*_\infty + 9)/2]. \quad (33)$$

He developed a 2D fluid model to check the validity of his 1D fluid model, which proved that the 1D approximation is valid within 10% difference in velocities, i.e. $K^* \approx 2.4$ for 1D approximation and 2.2 for 2D [9]. Here from $R = \exp[K v_\mathrm{d}/\sqrt{T_\mathrm{e}/m_\mathrm{i}}] = \exp[K^* v_\mathrm{d}/\sqrt{(T_\mathrm{e} + T_\mathrm{i})/m_\mathrm{i}}]$, $K = K^*/\sqrt{1+\tau} = 1.7$ for 1D, $=1.6$ for 2D. Figure 15 shows the ratios of current densities calculated by the 1D and 2D fluid models. He also fitted his numerical results into the following simple form:

$$n_\mathrm{s}(M^*_\infty, \alpha) = \exp[-1 - 1.1M^*_\infty + (1 - \sqrt{\alpha})(0.31 + 0.6M^*_\infty)], \quad (34)$$

which leads to the following ratio for $0 \leqslant \alpha \leqslant 1$:

$$R(M^*_\infty, \alpha) = \exp[(1 + 1.2\sqrt{\alpha})M^*_\infty], \quad (35)$$

which is remarkably simple and well fitted. For for $\alpha = 1$, this becomes $R(M^*_\infty) = \exp[2.2M^*_\infty]$, which is the same as the 2D isothermal and viscous case.

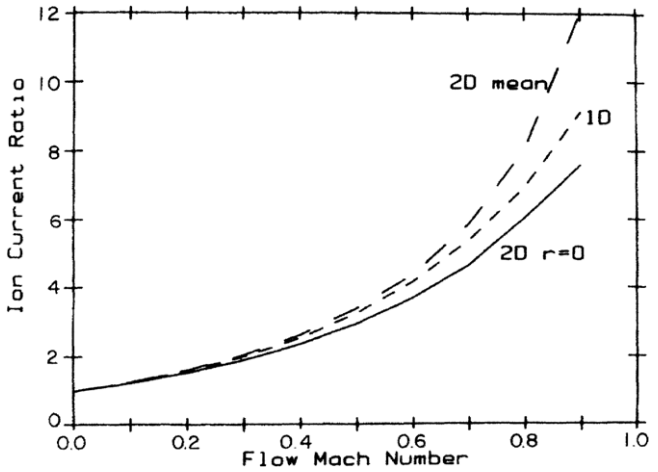

Figure 15. Current ratios in terms of flow Mach number ($\equiv v_\mathrm{d}/\sqrt{(T_\mathrm{e} + T_\mathrm{i})/m_\mathrm{i}}$) by Hutchinson's 1D and 2D viscid fluid models. Fitting to $R = \exp[K^* v_\mathrm{d}/\sqrt{(T_\mathrm{e} + T_\mathrm{i})/m_\mathrm{i}}] = \exp[K v_\mathrm{d}/\sqrt{T_\mathrm{e}/m_\mathrm{i}}]$ produces $K(2 - D) = 1.6$, $K(1 - D) = 1.7$, $K^*(2 - D) = 2.2$, $K^*(1 - D) = 2.4$ [9].

Hutchinson developed a general model for the arbitrary incident angle toward the multifaced probe, which will be discussed in the RP section, and he approximately recovers this for $\alpha = 1$ [10, 11]. Hutchinson mentioned the singularity with $\alpha = 0$ indicating the necessity of inclusion of the shear viscosity to avoid the singularity, even with the smallest value [9]. This argument seemed to be settled down in favor of Hutchinson through the open discussion between Stangeby and Hutchinson [4, 100], although there have been data supporting each side [112, 113]. Later, Chung showed the experimental evidence of the necessity of shear viscosity in TEXT-U tokamak experiments by measuring the shear viscosity and flow velocity simultaneously by introducing a VMP, which can measure the Mach number and shear viscosity simultaneously [97]. Independent experiments by laser induced fluorescence (LIF) [153] and 2D kinetic analysis [87] also seem to support the inclusion of the strong viscosity.

B. Chung's approximation

As an another approximation, a combination of equation (24) and approximation (iii) leads to

$$\frac{\mathrm{d}n}{\mathrm{d}y} = (1-n)\frac{(1+\alpha)M^*_\infty - (2+\alpha)M^*}{1 - M^{*2}}, \quad (36)$$

$$\frac{\mathrm{d}M^*}{\mathrm{d}y} = \frac{(1-n)}{n}\frac{1 - (1+\alpha)M^*_\infty M^* + (1+\alpha)M^{*2}}{1 - M^{*2}}. \quad (37)$$

Dividing equation (36) by equation (37) leads to

$$\frac{\mathrm{d}n}{\mathrm{d}M^*} + F(M^*)n(M^*) = 0,$$
$$F(M^*) = \frac{(2+\alpha)M^* - (1+\alpha)M^*_\infty}{1 - (1+\alpha)M^*_\infty M^* + (1+\alpha)M^{*2}}. \quad (38)$$

This is a first-order homogeneous differential equation, and we can apply either a Dirichlet ($n = n_\infty = 1$) or a Neumann ($\mathrm{d}n/\mathrm{d}M^* = 0$) boundary condition at the boundaries

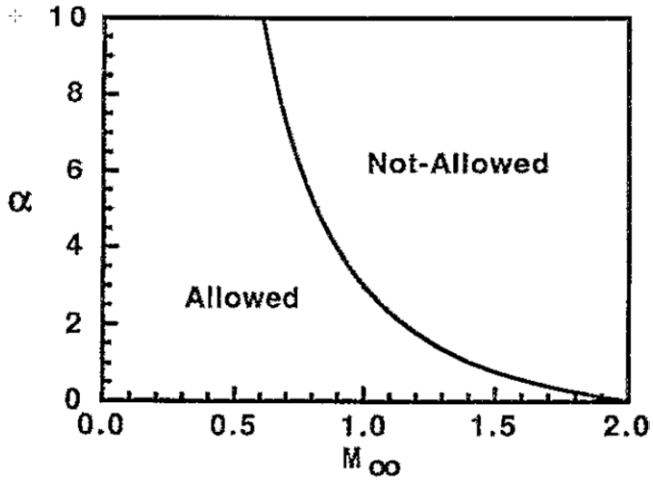

Figure 16. Allowed range of the normalized viscosity (α) in terms of the external flow velocity (M^*_∞). α can be negative for $M^*_\infty > 2$, $M^* \equiv v_\mathrm{d}/\sqrt{(T_\mathrm{e}+T_\mathrm{i})/m_\mathrm{i}}$ [12].

($M^* = M^*_\infty$) [110]. The choice of either condition is mathematically arbitrary although feasibility of the physical model would be different: for $M^*_\infty > 0$, the Neumann condition ($\mathrm{d}n/\mathrm{d}M^* = 0$) cannot be applied because it produces $n = 0.81$ for $M^*_\infty = 1$, which is unphysical, instead $n(M^*_\infty = 1)$ should be 1. So only the Dirichlet condition is applied. For $M^*_\infty < 0$, both conditions can be applied, and results with Neumann condition are smaller than those with Dirichlet.

Application of the Dirichlet conditions for all M^*_∞ leads to the ratio of up- to down-sheath current densities for $0 < M^*_\infty < 1$ as

$$\begin{aligned} R(M^*_\infty) \equiv \frac{n_\mathrm{s}(M^*_\infty > 0)}{n_\mathrm{s}(M^*_\infty < 0)} &= \left[\frac{1+\gamma M^*_\infty}{1-\gamma M^*_\infty}\right]^\delta \times \exp\left[\frac{\alpha M^*_\infty}{\sqrt{\omega}}\right. \\ &\times \left.\left\{\tan^{-1}\frac{(1+\alpha)(2-M^*_\infty)}{\sqrt{\omega}} + \tan^{-1}\frac{(1+\alpha)(2+M^*_\infty)}{\sqrt{\omega}}\right\}\right]. \\ &\approx \left(1+\gamma M^*_\infty\right)^{2\delta} \exp\left(\frac{\alpha M^*_\infty \tan^{-1}\sqrt{1+\alpha}}{\sqrt{1+\alpha}}\right) \\ &\approx \exp\left\{\left[1+\sqrt{\frac{\alpha^2}{(1+\alpha)}}\tan^{-1}\sqrt{1+\alpha}\right] M^*_\infty\right\} \end{aligned} \tag{39}$$

where n_∞ is the normalized unperturbed plasma density, M^*_∞ is the normalized flow Mach number outside the free presheath, $\gamma = (1+\alpha)/(2+\alpha)$, $\delta = (2+\alpha)/(2+2\alpha)$, $\omega = 4(1+\alpha) - (1+\alpha)^2 {M^*_\infty}^2$ and $G(M^*) = (1+\alpha)M^{*2} - (1+\alpha)M^*_\infty M^* + 1$. This recovers the simple exponential form as in other models [1, 7, 8]. The maximum difference between the first and the last is less than 5% for $0 < M^*_\infty \leqslant 0.5$.

In order for $n(M^*)$ to be real, ω should be positive, i.e. $\omega = 4(1+\alpha) - (1+\alpha)^2 {M^*_\infty}^2 > 0$, and figure 16 shows the relation of the normalized viscosity (α) to the external flow velocity (M^*_∞). Although α is an arbitrary number, it has an allowed range in terms of plasma flow velocity, e.g. $0 \leqslant \alpha \leqslant 3$ for M^*_∞=l. For positive viscosity, the plasma flow velocity cannot exceed the Mach number $2[v_\mathrm{d} = 2\sqrt{(ZT_\mathrm{e}+T_\mathrm{i})/m_\mathrm{i}}]$. For hypersonic flow ($M^*_\infty > 2$), there is the possibility that viscosity could be negative, although the possible physical meaning of this is not clear.

The ratio applied for the mixed boundary condition, Dirichlet for $M^*_\infty > 0$, and Neumann for $M^*_\infty < 0$, is calculated as

$$\begin{aligned} R(M^*_\infty) = \frac{1}{(1-\gamma^2 {M^*_\infty}^2)^\delta}&\left[\frac{1+\gamma M^*_\infty}{1-\gamma M^*_\infty}\right]^\delta \times \exp\left[\frac{\alpha M^*_\infty}{\sqrt{\omega}}\right. \\ &\times \left\{\tan^{-1}\frac{(1+\alpha)(2-M^*_\infty)}{\sqrt{\omega}} + \tan^{-1}\frac{(1+\alpha)(2+M^*_\infty)}{\sqrt{\omega}}\right. \\ &\left.\left. - \tan^{-1}\frac{(1+\alpha)M^*_\infty}{\sqrt{\omega}} + \tan^{-1}\frac{(1+\alpha)(2\gamma-1)M^*_\infty}{\sqrt{\omega}}\right\}\right]. \end{aligned} \tag{40}$$

The ratio of current densities will be given later along with those of other models. The present analytic treatment with mixed boundary conditions (for $M^*_\infty > 0$, Dirichlet, and for $M^*_\infty < 0$, Neumann condition) produces ratios closer to those from the kinetic model than those with Dirichlet only. The application of the Neumann boundary condition produces a lower sheath current density and a larger current density ratio. Although this approximation is mathematically valid, it is inconsistent since it has limitation in applying boundary conditions to produce physically incorrect result: mismatch of the lengths of density perturbation and velocity perturbation. However, it produces a similar result to those of Hutchinson's and the kinetic model within 20% or so, [102, 103], which is to be shown in figure 22 and it has a merit to have analyticity in recovering the spatial dependence and to apply for measuring the normalized viscosity.

2.2.2. The 1D fluid model from the 1D kinetic model. After assuming that the cross-field frequency, $W(z, v)$, is only a function of position and electrons are governed by the Boltzmann relation, and taking moments (1, v, and $v^2/2$) of the Boltzmann equation, equation (12), Chung [109] obtained the following:

$$\frac{\mathrm{d}}{\mathrm{d}z}[n_\mathrm{i}V] = W(z)[n_\infty - n_\mathrm{i}(z)], \tag{41}$$

$$\begin{aligned} n_\mathrm{i}V\frac{\mathrm{d}V}{\mathrm{d}z} + \frac{\mathrm{d}}{\mathrm{d}z}\left[\left(\frac{ZT_\mathrm{e}}{m_\mathrm{i}} + \frac{T_\mathrm{i}}{m_\mathrm{i}}\right)n_\mathrm{i}\right] &= W(z)(v_\mathrm{d} - V) \\ &\times [n_\infty - (1-\alpha)n_\mathrm{i}], \end{aligned} \tag{42}$$

$$\begin{aligned} \frac{\mathrm{d}}{\mathrm{d}z}\left[n_\mathrm{i}V\left(\frac{v^2}{2} + \frac{3T_\mathrm{i}}{2m_\mathrm{i}}\right) + \frac{H}{m_\mathrm{i}}\right] + ZVT_\mathrm{e}\frac{\mathrm{d}n_\mathrm{i}}{\mathrm{d}z} \\ = W(z)\left[\alpha + (1-\alpha)\frac{n_\mathrm{i}}{n_\infty}\right]\left[\frac{n_\infty T_{\mathrm{i}\infty}}{2m_\mathrm{i}} + \frac{n_\infty v^2_\infty}{2}\right] \\ - \alpha W(z)\left[\frac{n_\mathrm{i}V^2}{2} + \frac{n_\mathrm{i}T_\mathrm{i}}{2m_\mathrm{i}}\right], \end{aligned} \tag{43}$$

where $n_\mathrm{i}(z) \equiv \int f_\mathrm{i}(z, v)\,\mathrm{d}v$, $V(z) \equiv \int v f_\mathrm{i}(z, v)\,\mathrm{d}v/n_\mathrm{i}$, $T_\mathrm{i}(z) \equiv \int m(v-V)^2\,\mathrm{d}v/n_\mathrm{i}$, $H(z) \equiv \int m(v-V)^3/2\,\mathrm{d}v$. Defining the non-dimensional variables as $y \equiv \int W(z)/V_\mathrm{s}\,\mathrm{d}z$, $n \equiv n_\mathrm{i}/n_\infty$, $M \equiv V/V_\mathrm{s}$, $\tau \equiv T_\mathrm{i}/ZT_\mathrm{e}$, after neglecting the parallel heat flux(H), we get the following:

$$M\frac{\mathrm{d}n}{\mathrm{d}y} + n\frac{\mathrm{d}M}{\mathrm{d}y} = A(n), \tag{44}$$

$$(1+\tau)\frac{\mathrm{d}n}{\mathrm{d}y} + nM\frac{\mathrm{d}M}{\mathrm{d}y} + n\frac{\mathrm{d}\tau}{\mathrm{d}y} = B(n, M), \tag{45}$$

$$M\frac{\mathrm{d}n}{\mathrm{d}y} + nM^2\frac{\mathrm{d}M}{\mathrm{d}y} + \frac{3}{2}nM\frac{\mathrm{d}\tau}{\mathrm{d}y} = C(n, M, \tau), \tag{46}$$

where $A(n) \equiv 1-n$, $B(n, M) \equiv (M_\infty - M)[1-(1-\alpha)n]$, $C(n, M, \tau) \equiv [\alpha + (1-\alpha)n](\tau_\infty/2 + M_\infty^2/2) - \alpha(nM^2/2 + n\tau/2) - (1-n)(M^2/2 + 3\tau/2)$, with $V_\mathrm{s} \equiv (ZT_\mathrm{e}/m)^{1/2}$.

These equations can be expressed in a matrix form:

$$\vec{\boldsymbol{R}} \cdot \frac{\mathrm{d}}{\mathrm{d}y}\vec{\Phi} = \vec{\boldsymbol{S}}, \tag{47}$$

where

$$\vec{\boldsymbol{R}} = \begin{pmatrix} M & n & 0 \\ 1+\tau & nM & n \\ M & nM^2 & 1.5nM \end{pmatrix}, \qquad \vec{\Phi} = \begin{pmatrix} n \\ M \\ \tau \end{pmatrix},$$

$$\vec{\boldsymbol{S}} = \begin{pmatrix} A \\ B \\ C \end{pmatrix}. \tag{48}$$

In order to have the non-trivial solutions of n, M and T, the determinant of $\boldsymbol{R}$ should not be zero [110], while the above fluid equations break down (i.e., become singular) at the point where

$$D(\boldsymbol{R}) = \tfrac{1}{2}n^2M(M^2 - 3\tau - 1) = 0 \tag{49}$$

is satisfied, i.e. $M_*^2 = 1 + 3\tau_*^*$, which is equivalent to

$$V_*^2 = \frac{ZT_\mathrm{e} + 3T_{i*}}{m}. \tag{50}$$

This is the Bohm criterion for the warm ion plasma (Bohm–Chodura condition). We can replace V_* with the ion acoustic velocity C_s and T_{i*} with the sheath ion temperature T_is. This indicates that the specific heat ratio of ion (γ_i) becomes 3 for the 1D case. If we assume that τ is constant, we do not need the energy equation. For an arbitrary α without energy equation, we recover Hutchinson's case, which introduces the viscosity variations for the 1D continuity and momentum equations.

Here it might be quite interesting to compare this with the results of Laux *et al* [45]. For $\alpha = 1$, Chung can recover their case. They have the same continuity and momentum equations; however, they choose the energy equation from the 3D fluid equation. Hence the heat specific ratio was 5/3 in their case, while it was 3 in Chung's case. The difference from Chung's in the energy equation is that they have $2.5\,n\mathrm{M}\,\mathrm{d}T/\mathrm{d}y$ instead of $1.5\,n\mathrm{M}\,\mathrm{d}T/\mathrm{d}y$ on the left-hand side and $1.5(\tau_\infty - n\tau)$ instead of $0.5(\tau_\infty - n\tau)$ on the right-hand side. This causes some difference in ion temperature variations, hence in ion temperatures at the sheath, as shown in figure 17.

Gunn used the kinetic model of Chung and Hutchinson, and set up a kinetic model to clarify the overall SOL behavior [111] by replacing the perpendicular transport source with a poloidal momentum and by choosing the poloidal velocity toward the surface as the sum of the poloidal projection of the parallel velocity and a perpendicular velocity, i.e. $v_\mathrm{p} = v_{||}\sin\theta + V_\perp\cos\theta$, with θ being the angle between the magnetic field and the surface. By taking moments of the kinetic equation, he solved the fluid equations for the ion density, velocity and kinetic temperature (T), and showed consistency of density and velocity with those by the kinetic model of Chung and Hutchinson, except for the ion temperature in the wake region (downstream), comparing the results of kinetic and fluid models.

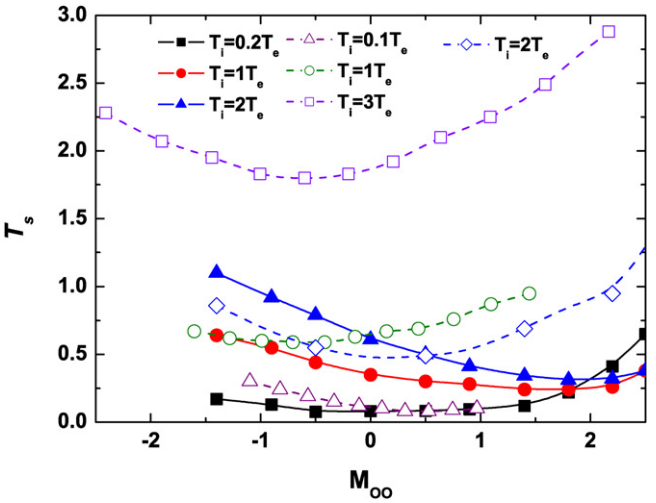

Figure 17. Sheath temperature versus flow velocity for different temperature ratios ($T_\mathrm{i}/T_\mathrm{e}$) by Chung (●, ■, ▲) [113], Laux *et al* (○, □, △) [45], and Gunn (◇) [111].

If one rearranges three 1D fluid equations derived from the 1D kinetic equation, one can get the following as Gunn derived:

$$\frac{\mathrm{d}n}{\mathrm{d}y} = \frac{A^*(n, M, \tau)}{M\mathbb{D}}, \qquad \frac{\mathrm{d}M}{\mathrm{d}y} = \frac{B^*(n, M, \tau)}{n\mathbb{D}}, \qquad \frac{\mathrm{d}\tau}{\mathrm{d}y} = \frac{C^*(n, M, \tau)}{nM\mathbb{D}}, \tag{51}$$

where $A^*(n, M, \tau) \equiv 3M^2 - 3M_\infty M + M_\infty^2 - 3\tau + \tau_\infty + n(2\tau - M^2)$, $B^*(n, M, \tau) \equiv n(1+\tau) - (1+\tau_\infty) - (2M - M_\infty)(M - M_\infty)$, $C^*(n, M, \tau) \equiv \tau_\infty + (M - M_\infty)^2](M^2 - 1) + [(3-2n)(1+\tau) - M_\infty^2 - \tau_\infty)\tau$ and $\mathbb{D} \equiv M^2 - 1 - 3\tau$. Here the cross-field diffusive source and the parallel velocity are replaced by the poloidal momentum source and the poloidal velocity. These equations have singularity at either $M = \sqrt{1+3\tau}$ or $M = 0$, since $n > 0$. One singularity as the Bohm–Chodura condition ($M = \sqrt{1+3\tau}$) is to be used as a boundary condition at the probe surface, while the other singularity problem ($M = 0$) should be solved. Division of the continuity equations (for n) and ion energy equation (for τ) by the momentum equation (for M) leads to the elimination of the (normalized) position variable (y) as follows:

$$\frac{\mathrm{d}n}{\mathrm{d}M} = \frac{nA^*(n, M, \tau)}{MB^*(n, M, \tau)}, \qquad \frac{\mathrm{d}\tau}{\mathrm{d}M} = \frac{C^*(n, M, \tau)}{MB^*(n, M, \tau)}. \tag{52}$$

These two equations have singularities at $M = 0$, and the following is the method to overcome this problem by Gunn. For the upstream flow, this does not cause any mathematical problem, since M is always positive. However, for the downstream flow, this causes singularity along the presheath, as shown in figure 7, i.e. during the change of M from $M = M_\infty > 0$ (moving away from the surface of the downstream side) to $M = -\sqrt{1+3\tau}$ (moving toward the surface with

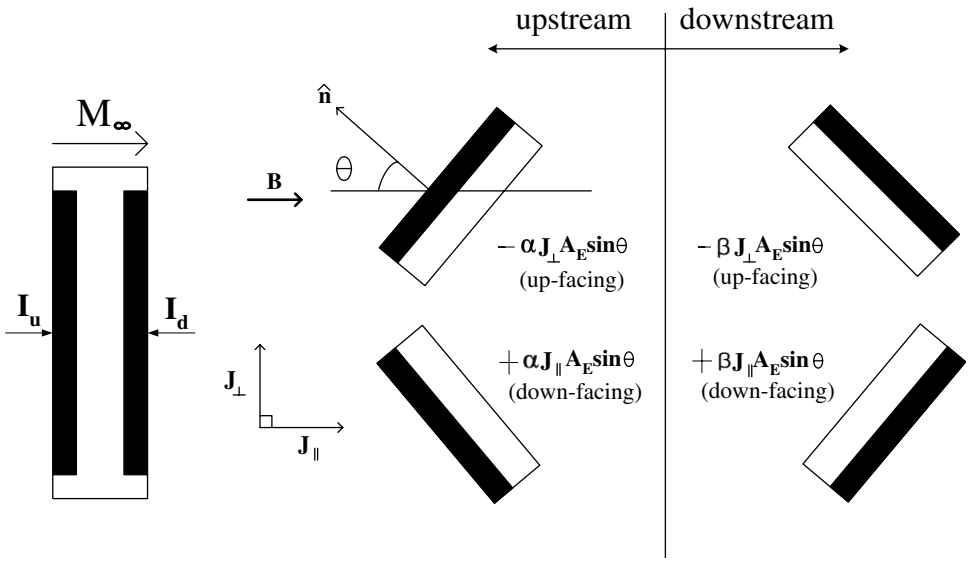

Figure 18. Schematic drawings of the GP and its pin's rotation. $I_{u,d}$ are the ion saturation currents on the upstream and downstream sides normal to the probe surfaces. On each upstream or downstream side there are up-facing and down-facing probe tips collecting (or blocking) extra current due to $J_\perp$ [159].

the Bohm speed), the value of M reaches zero, causing the singularity mathematically (or reaching a stagnation point physically) as Gunn indicated. To avoid the singularity at $M = 0$, using l'Hôpital's rule, the numerator of $\mathrm{d}n/\mathrm{d}M$ should be zero: $B^*(n, M, \tau) = 0 \rightarrow n^{(1)}(M, \tau) = [3M^2 - 3M_\infty M + M_\infty^2 - 3\tau + \tau_\infty]/(M^2 - 2\tau)$. Put this initial density into the zero of the energy equation: $C^*(n^{(1)}, M, \tau) = 0$, to avoid the singularity in $\mathrm{d}\tau/\mathrm{d}M$, then τ is calculated from the quadratic equation of only M: $\tau = \tau(n^{(1)}, M) = \tau^{(1)}(M)$. Again, put this initial ion temperature into the initial density, to make it a function of only one variable, M: $n^{(1)}(M, \tau^{(1)}(M)) = n^{(1)}(M)$. In turn, put these initial density and temperature to the original equation for $\mathrm{d}n/\mathrm{d}M$ and $\mathrm{d}\tau/\mathrm{d}M$: $\mathrm{d}n/\mathrm{d}M = n^{(1)}A^*(n^{(1)}, M, \tau^{(1)})/MB^*(n^{(1)}, M, \tau^{(1)}) \equiv G^*(M)$ and $\mathrm{d}\tau/\mathrm{d}M = C^*(n^{(1)}, M, \tau^{(1)})/MB^*(n^{(1)}, M, \tau^{(1)}) \equiv H^*(M)$. Integrate these equations toward the sheath until $M = \sqrt{1 + 3\tau}$. From these initially iterated equations, the first guessed density and temperature can be calculated in terms of M. Finally, put these first guessed density and temperature into the unused equation of $\mathrm{d}M/\mathrm{d}y$, which becomes a function only of variable M. From this $\mathrm{d}M/\mathrm{d}y = F^*(M)$, the position along the field line can be easily obtained by the direct integration: $y(M) = \int_{M=1}^{M}[\mathrm{d}M/F^*(M)]$, where the Bohm–Chodura condition is applied at the surface. The initial n and τ must be chosen such that the maximum of $y(M)$ meets 'the connection length for the presheath for the bounded presheath' or the presheath length for the free-presheath. The solution procedure involves iterating to find the correct size of the presheaths.

Figure 17 shows the ion temperatures at the sheath calculated by Laux (the 1D fluid model from 3D fluid equations), Gunn (the 1D fluid model from kinetic model) and Chung and Hutchinson (the kinetic model) in terms of the Mach number. The Laux model seems to produce larger values than those by Chung and Hutchinson, while Gunn's gives smaller values. For any case, sheath ion temperatures are smaller than the unperturbed ion temperature, so that the application of the sheath ion temperature would decrease the absolute flow speed.

2.3. Analyses of GP and RP

If there is an additional flow(s) with a different direction to the parallel flow, it generates angular asymmetries of the ion current density to the probe surface. With such a flow in unmagnetized plasmas ($\rho_\mathrm{i} > a$), a polar diagram of ion saturation current appears roughly like a displaced circle, with the maximum current coinciding with the angle of the flow vector in the plane perpendicular to the axis of the probe. In strongly magnetized plasmas ($\rho_\mathrm{i} < a$), there is a strong reduction in ion current on the surfaces that are nearly parallel to the magnetic field. The polar diagram in this case has a 'double lobe' structure. If perpendicular ($\boldsymbol{E} \times \boldsymbol{B}$) or diamagnetic drift flows are present in addition to the parallel component, there are asymmetries in the perpendicular direction as well as the parallel direction. Rotating MPs, consisting of two planar collectors separated by an insulator as used in CASTOR [87], can map out the polar diagram, or alternatively, GP, consisting of several collectors mounted around an insulating cylindrical housing as used in TdeV, measures the polar distribution at several angles simultaneously.

A. Gundestrup probe

GP was first introduced by MacLatchy *et al* to measure the flows in the SOL of TdeV, which is shown in figure 4. Referring to figure 18, the currents collected by the upstream-facing probe (I_u) and the downstream-facing probe (I_d) are given as

$$I_\mathrm{u} = \alpha_\mathrm{s} A_\mathrm{p} n_\mathrm{e} e C_\mathrm{s}, \qquad \text{and} \qquad I_\mathrm{d} = \beta_\mathrm{s} A_\mathrm{p} n_\mathrm{e} e C_\mathrm{s}$$

where $C_s \equiv \sqrt{(T_e + T_i)/m_i}$, A_p is the area of the probe normal to the magnetic field, n_e is the unperturbed electron density and e = electron charge. α_s and β_s are the normalized sheath densities, given by the parallel MP model (e.g. that of Hutchinson). Due to the azimuthally angular position of the probe, each probe tip (pin) and vacant space between the probe tip and the holder (housing), the effective collecting area A_E is different from the cross-sectional area of the probe $A_p(\equiv 2r_p l_p$, see figure 4), and it is calculated as $1.4A_p$ via the Monte Carlo model based on ion dynamics. This was approximately confirmed by the Larmor technique, given as $A_E \cos\theta \approx 1.5A_p \cos\theta$, and is given with $\theta \equiv$ angle between the normal to A_p and the magnetic field. Again, from figure 18, setting the parallel and perpendicular current densities as

$$J_\parallel = n_e e C_s, \qquad \text{and} \qquad J_\perp = n_e e \upsilon_\perp, \tag{53}$$

there are up-facing and down-facing probe tips collecting (down-facing) or blocking (up-facing) at each upstream or downstream side. So the current collected by the up-facing pin is given as

$$I_p^* = \alpha_s J_\parallel A_E \cos\theta - \alpha_s J_\perp A_E \sin\theta$$

and the current collected by the down-facing pin, gaining charge due to $J_\perp$, is given by

$$I_p^* = \alpha_s J_\parallel A_E \cos\theta + \alpha_s J_\perp A_E \sin\theta.$$

Hence the total current to an upstream-facing pin is given as

$$I_{pu} = \alpha_s A_E (J_\parallel \cos\theta \pm J_\perp \sin\theta) + k^*(1-\alpha_s) J_\parallel A_E \sin\theta$$

and the total current to a downstream-facing pin is calculated as

$$I_{pd} = \beta_s A_E (J_\parallel \cos\theta \pm J_\perp \sin\theta) + k^*(1-\beta_s) J_\parallel A_E \sin\theta,$$

which contains three adjustable parameters $J_\parallel$, $J_\perp$, $k^*(\equiv a/L_p)$. Usually the value of $k^*(0.05 < k^* < 0.1)$ is obtained by obtaining a best fit for the full range of flows, and k^* was 0.075 for their experiment. Since α, β are given by the parallel flow model, θ is known from the experiment, for any θ, two values of $R(\theta = \theta_1)$ and $R(\theta = \theta_1 + \pi/2)$ can produce $J_\perp$ and $J_\parallel$ from the 10 saturation currents out of 12 collections.

Note that in their experiments the two pins located on the y-axis are not used in the analysis because of the grazing incidence ($\theta = \pm\pi/2$) of the magnetic field.

GPs were also used to check the flow reversal near the separatrix and to observe the asymmetries between top and bottom divertors in double null configurations of TdeV [150].

Back and Bengtson measured flow velocities using a fast-scanning GP with 12 pins [158]. They fitted their data according to MacLatahy's method, but added one more parameter (angle between the magnetic field and the normal of the probe) pin order to compensate for the misalignment of the probe array. They adopted the normalized shear viscosity α as 0.5 (middle value between those of Hutchinson and Stangeby). Chung *et al* also used a GP along with an emissive and a triple probe to measure the rotational velocity, plasma potential, electron temperature and plasma density profiles simultaneously in a Hanbit mirror device [39], but they tried to use the probes at grazing angles with models of unmagnetized plasmas. Guun *et al* [87] analyzed the GP data for CASTOR using a 2D-PIC code and compared with those by Hutchinson [6] and Chung and Hutchinson [8]. They found that the kinetic temperature in the presheath drops substantially toward the probe surface, contrary to the isothermal assumption adopted in fluid models, which was also mentioned by Chung and Hutchinson [8]. They also avoided $\pm 30^\circ$ in the perpendicular direction, which has been shown to be the inapplicability of Van Goubergen (VG) [52] model in Dyabillin's analysis [88]. Since MacLachy's original method is very complicated and requires several assumed values, it would be better to use the following VG model.

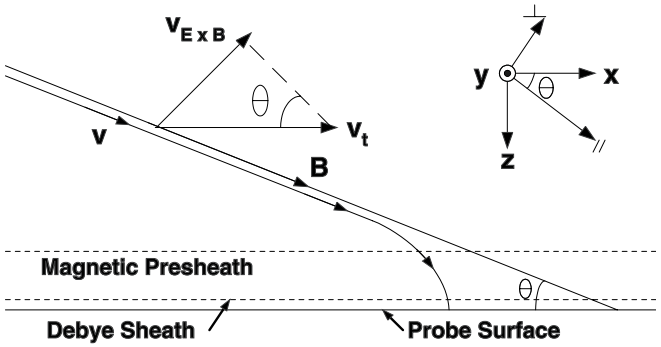

Figure 19. Oblique incidence of ion flux for the Gundestrup/RP. v_t is the tangential flow (grazing angle) to the probe surface and $v_{E\times B}$ is a typical perpendicular flow to the magnetic field (referring to [98]).

Van Goubergen *et al* [52] generalized the 1D fluid model of Hutchinson [6] for $M_{||}^* \cot\theta > M_{||\perp}^*$ to include a finite perpendicular drift as follows:

$$\frac{\partial n}{\partial z} = \big[-[M_{||}^* - M_\perp^* \cot\theta](1-n) + (M_{||\perp}^* - M_{||}^*) \times [1 - n(1-\alpha)]\big]\big[1 - [M_{||}^* - M_\perp^* \cot\theta]^2\big]^{-1}, \tag{54}$$

$$\frac{\partial M_{||}^*}{\partial z} = \big[(1-n) - [M_{||}^* - M_\perp^* \cot\theta](M_{||\perp}^* - M_{||}^*) \times [1 - n(1-\alpha)]\big]\big[n(1 - [M_{||}^* - M_\perp^* \cot\theta]^2)\big]^{-1}, \tag{55}$$

where θ is the angle between the magnetic field and the probe surface: if $\theta = \pi/2$, the probe only collects the parallel flow, and if $\theta = 0$, the probe only collects the perpendicular (cross-field) flow (see figure 19). These equations can be obtained directly from Hutchinson's governing equations (equations (27) and (28)) by substituting the parallel flow along the presheath ($M_{||}^*$) and the unperturbed drift flow ($M_{||\perp}^*$) by $M_{||}^* - M_\perp^* \cot\theta$ and $M_{||\perp}^* - M_\perp^* \cot\theta$, respectively, indicating that ions gain an additional parallel velocity of $-v_t \cos\theta$ with respect to the laboratory frame, where v_t is the speed of the reference frame moving in the tangential direction of the probe surface, which is given by $\vec{v}_t = \hat{x} E_y/B_z = \hat{x} E_y/B \sin\theta = \hat{x} v_d/\sin\theta$ and θ is the angle of the magnetic field to the probe surface, figure 19 [98]. The model equations are characterized by a singularity that determines the maximum parallel speed in the presheath; the singularity is assumed to occur at the

magnetic presheath edge (MPSE), as suggested by Stangeby and Chankin [148]:

$$M^*_{||,\mathrm{MPSE}} = M^*_{\perp} \cot\theta + 1. \tag{56}$$

Then the ratio is given as

$$R = \exp[K(M^*_{||} - M^*_{\perp} \cot\theta)], \tag{57}$$

where the constant is well fitted by the expression $K = 2[1 + 0.14\exp(M^*_{||}/0.862)] \approx 2.3$–$2.5$, which is independent of $M^*_{\perp}$ and θ, and is weakly dependent on $M^*_{||}$. From the two measurements of the ratios (R_1) at the normal angle ($\theta_1 = 90^\circ, \cot\theta_1 = 0$) and R_2 at an arbitrary angle for $0^\circ < \theta_2 < 90^\circ$), one can deduce the parallel Mach number from R_1 as the usual case of MP, and the perpendicular Mach number as $M^*_{\perp} = \ln(R_1/R_2)/K \cot\theta_2$.

B. Rotating probes

Dyabilin *et al* developed a 1D fluid model to analyze the rotating MP, similar to that of Hoethker [89], for parallel and for perpendicular directions [88]. They expressed the velocity in terms of velocity potential such as $\vec{v} = \vec{v_\infty} + \nabla\varphi$, which is similar to that of Stangeby and Allen for the PMP [94], where they used a different form as $\vec{v} = -\nabla\varphi$. This approximation leads to the solution for the flux tube density of exactly the same form as in Hutchinson [6], but allowing the deduction of not only parallel but also the perpendicular Mach numbers. A comparison of the model with experiments on the CASTOR tokamak shows that his model is valid at least for the Mach numbers $|M_{||,\perp}| \leqslant 0.3$. For the estimate of the parallel Mach number one can use Hutchinson's approximation for the ratio R at the inclination angle $\theta = \pi/2$. They used a similar expression to estimate the perpendicular Mach number from the ratio $R(\theta = 0)$:

$$R(\theta = 0) \approx \exp(K M_{\perp}), \quad K \approx 2.2. \tag{58}$$

This seems to be contradicting to those of VG and Hutchinson: $R(VG, \theta \to 0) \to \exp[-2.2 M_{\perp} \cot\theta] \to 0$, yet justifies that the fluid models of Van Goubergen should be applicable only for $30^\circ < \theta < 150^\circ$, and are not adequate for explaining the collection of weakly ionized plasmas with a narrow angle, i.e. $\Delta_{\mathrm{MPSE}} \sim \rho_i \cos\theta$, characterized by unmagnetized ions but still magnetized electrons, which is consistent with the limited applicability of the model of Van Goubergen *et al* [52]. To avoid the unphysical result of the VG model, or expand their applicability, they adopted the normalized density at the MPSE as

$$n_b = 1 + \int_{M_\infty}^{M_b} M_\infty \frac{\mathrm{d}n}{\mathrm{d}M}\,\mathrm{d}M, \tag{59}$$

where the upper limit of the flow speed M_b should be determined from the phenomenological boundary condition:

$$M_b = 1 - \gamma_m |\cos\theta|, \tag{60}$$

where γ_m is a free parameter (0.73–0.77) to calculate the following ion saturation current and satisfies the Bohm–Chodura condition:

$$I_s(\theta)/en_\infty C_s S_p = n_b M_b, \qquad M_{||,b} + M_{\perp,b} \cot\theta = 1, \tag{61}$$

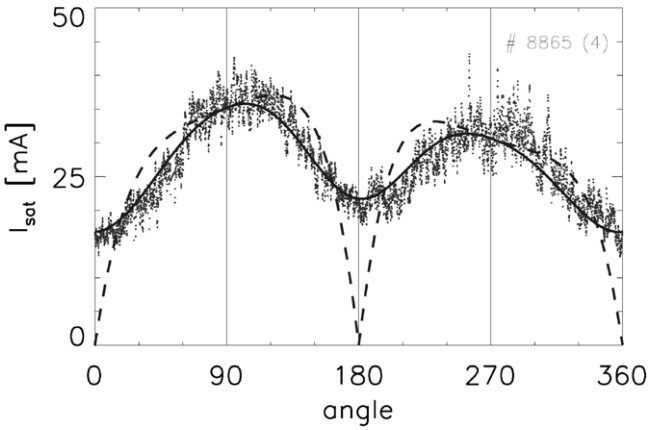

Figure 20. Angular variation of the ion saturation current on the plate. The dashed line is an approximation using the Bohm–Chodura boundary condition (with the Van Goubergen model [52]). The solid line represents calculation using the phenomenological boundary condition [88].

where S_p is the geometrical area of the probe. It is interesting to recover the equations of Hutchinson even with a different approximation: $\partial^2 Q/\partial r^2 \approx 2(Q_\infty - Q)/a^2$ (Dyabilin) versus $\partial^2 Q/\partial r^2 \approx (Q_\infty - Q)/a^2$ (Hutchinson). Figure 20 shows the angular variation of the ion saturation currents and the fitting with their model, and the deduced Mach number as $M_{||} = 0.06$, $M_\perp = -0.12$. Without going into the detailed physics of the magnetic presheath, they seemed to succeed in fitting their angular distribution of ion saturation current, even for the case of $\theta \sim 0, 180^\circ$. However, it is not so clear as to how to implement their model to other machines, since they use a free fitting parameter γ_m. Although they adopted the diffusive approximation for the radial flux, the difference with the convective term is about 10% in deducing the Mach numbers, which is quite different from those of Hutchinson and Stangeby. Since their deduced Mach number is very small, it is too early to say that there is not much difference between the convective and diffusive models, while Hutchinson's argument predicts that the difference is 100% (twice or half).

Ohtsuka *et al* [43] used a RP to deduce the divertor efficiency by measuring the flux to the divertor and the flux to the vacuum shield tokamak. They could deduce the flow velocity (v_d) implicitly by deleting the parallel flux ($J_0 = n_0 C_s/2$) from the perpendicular flux to the probe surface ($J_+ = n_0 C_s/2 + n_0 v_d$). However, the expression of the perpendicular flux does not have such a simple form, rather it could be expressed as $J_+ = k_1 n_0 C_s/2 + k_2 n_0 v_d$ even if random thermal motion would be separated from the drift motion, and the parallel flux is a function of the drift flow, so that there should be an additional scaling factor such that $J_0 = k_3 n_0 C_s/2$, where $0 < k_{1,2,3} < 1$.

Although they did not show the experimental data, Cosler *et al* [149] developed a rotating and sapping (radially fast moving) electrical double probe for implementation at the tokamak TEXTOR94. This new diagnostic system allows one to measure a large number of parameters in the edge plasma. Uehara *et al* [86] measured the radial profiles of the ion temperature as well as the flow velocity by using rotatable symmetric and asymmetric double probes in the boundary

plasma of the JFT-2M tokamak. They deduced the flow velocity as 0.2–0.3 of the ion sound velocity in the SOL for both ohmic and neutral beam injection heating by assuming the shifted Maxwellian ion distribution at the sheath as Mott-Smith and Langmuir did [72]. Here the assumption of the shifted Maxwellian distribution at the sheath is not physically correct, since the ions are influenced by the electric field around the sheath.

C. Oblique ion collection

Gunn [111] replaced the cross-field diffusive source and parallel velocity by the poloidal momentum source and poloidal velocity, respectively. He recovered the same fluid equations of Chung and Hutchinson with the cross-field diffusive source. Dyabilin *et al* [88] could not find a big difference between the cross-field diffusive and convective sources: the difference in deducing Mach numbers between the diffusive and convective terms is about 10%, although their deduced numbers are very small. Considering a general cross-field transport source, not necessarily diffusive, the quasi-neutral steady-state fluid equations in the wake region are given as

$$\frac{\partial}{\partial y} n_\mathrm{i} V_y + \frac{\partial}{\partial z} n_\mathrm{i} V_z = 0, \tag{62}$$

$$\left(V_y \frac{\partial}{\partial y} + V_z \frac{\partial}{\partial z} \right) V_y = -\frac{e}{m} \frac{\partial \phi}{\partial y}, \tag{63}$$

$$\left(V_y \frac{\partial}{\partial y} + V_z \frac{\partial}{\partial z} \right) V_z = -\frac{e}{m} \frac{\partial \phi}{\partial z}, \tag{64}$$

$$n_\mathrm{i} = n_\mathrm{e} = n_\infty \exp\left[\frac{e\phi}{T_\mathrm{e}} \right]. \tag{65}$$

These equations can be analyzed in terms of the self-similar variable $\zeta = z/y$ as in problems of the rarefaction shock in near wake [119] or plasma-free expansion into the vacuum [120]. If V_y = constant, from the second equation, $e[\phi(y_\infty) - \phi(y)]$ = constant, indicating the potential difference to draw particles from outside to the wake area, as a way of plasma expansion. Then the first and third equations are reduced into the following equations as shown by Hutchinson [10, 11]:

$$M_\perp \frac{\partial n}{\partial y} + \frac{\partial}{\partial z} nM = 0, \tag{66}$$

$$nM_\perp \frac{\partial M}{\partial y} + nM \frac{\partial M}{\partial z} + \frac{\partial n}{\partial z} = 0, \tag{67}$$

where n, M and $M_\perp$ are the normalized variables of ion density (n_i/n_∞), parallel flow velocity (V_z/V_s) and perpendicular flow velocity (V_y/V_s), respectively. This is mathematically equivalent to free expansion of a plasma into a vacuum. With $M_\perp = 1$, he solved these equations for n and M in terms of the self-similar variable ζ [4]:

$$n = n_\infty \exp[\zeta - M_\infty - 1], \quad M = \zeta - 1, \text{ for } \zeta < M_\infty + 1,$$
$$n = n_\infty, \quad M = M_\infty \text{ for } \zeta > M_\infty (v_z/V_\mathrm{s}). \tag{68}$$

Then the formula for the Mach number was given by

$$R = \exp[2M_\infty] = \exp[KM_\infty], \tag{69}$$

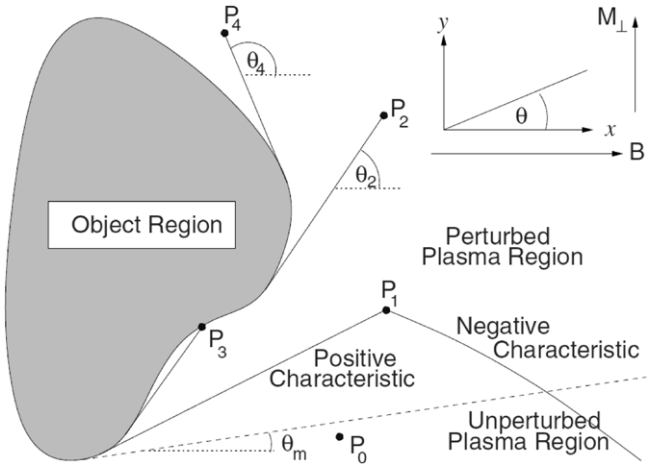

Figure 21. Schematic geometry for the oblique ion collection to the arbitrarily shaped object, especially in the wake region. P_0 is in the unperturbed region. For P_1, the characteristics are shown. P_3 is in a concave region and so its positive characteristic is not tangent at P_3. A value $\theta > \pi/2$ such as for P_4 is not problematic [10].

where $K = 2$ seems to be very similar to the results of his 1D ($K = 1.7$, $K^* = 2.4$ for $\alpha = 1$) and 2D ($K = 1.6$, $K^* = 2.2$) models. Here K^* is the calibration factor based on M^*_∞ (normalized by C_s, $R = \exp[K v_\mathrm{d}/\sqrt{T_\mathrm{e}/m_\mathrm{i}}] = \exp[K^* v_\mathrm{d}/\sqrt{(T_\mathrm{e} + T_\mathrm{i})/m_\mathrm{i}}]$. So K^* from the self-similar model is not 2, as mentioned by Hutchinson, but $2 \times \sqrt{(T_\mathrm{e} + T_\mathrm{i})/T_\mathrm{e}} = 2.8$ for $T_\mathrm{e} = T_\mathrm{i}$. To get a similar result to those by the 1D and 2D viscid fluid models, one should add the ion pressure gradient term along the z-direction (normal to probe surface) to the momentum equation. The force to draw ions into the wake region is not only the electric force but also the pressure gradient, which have the same magnitude as the Boltzmann electron, so that the resultant force of the Hutchinson fluid model becomes double compared with the present case (same as the plasma expansion).

Hutchinson also solved these equations for ion collection by oblique surfaces of an object in a transversely flowing magnetized plasma [10], as shown in figure 21, and obtained the flux density perpendicular to the magnetic field as

$$\Gamma_\parallel = n_\infty C_\mathrm{s} \exp[-1 - K(M_\parallel - M_\perp \cot\theta)], \tag{70}$$

where $K = 1$, which is very close to his previous diffusive solution given as $K = 1.1$, i.e. the deduced value of M_∞ would be different from each other by 10%, indicating that the calibration factor of the MP in the exponential form is almost independent of the type of cross-field transport: $R = \exp[2(M_{||} - M_\perp \cot\theta)]$. Although the detailed mechanisms of the cross-field transport would be different, there seems to be no difference between the cross-field transport in magnetized plasmas and plasma expansion into the vacuum in unmagnetized plasmas. Hutchinson also obtained the analytic solution for perpendicular velocity from the general 3D fluid equations assuming the quasi-neutral drift approximation (included only $E \times B$ and diamagnetic drifts neglecting the polarization drift) and neglecting parallel temperature gradients [11]. He specifies the perpendicular

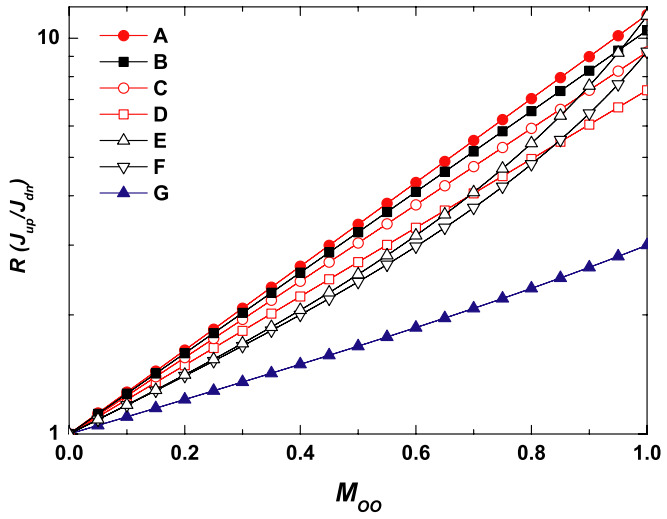

Figure 22. Ratio of up- and downstream currents of the MMP for $T_i = T_e$. A = Hutchinson (1D fluid, $K^* = 2.4$), B = Chung (kinetic, $K^* = 2.3$), C = Hutchinson (2D fluid, $K^* = 2.2$), D = Hutchinson (self-similar, $K^* = 2.0$), E = Chung (1D fluid, floating BC), F = Chung (1D fluid, fixed BC), G = Stangeby (1D, fluid, $K^* = 1.0$).

velocity as

$$M_\perp \approx M_E + (1 + M_{\|\infty})M_{T_e} + M_{D_i} + [(1 - \sin\Theta)/(1 + \sin\Theta)](M_{D_i} - M_{D_e}), \quad (71)$$

where Θ is the angle between the probe surface and the magnetic field, while θ is the angle within the plane containing the field and external drift. Here M_E, M_{D_i}, M_{D_e} and M_{T_e} are the $E \times B$ drift, ion diamagnetic drift, electron diamagnetic drift and electron temperature gradient drift, respectively.

From Hutchinson's self-similar model, the parallel length of the presheath (L_s) in given as $a(M_\| + 1)/M_\perp \approx a/M_\perp$ for $0 \leqslant M_\| \leqslant 1$, which is much smaller than the parallel presheath length of the diffusive model ($L_\| = a^2 C_s/D_\perp$). For $M_\perp \to 1$, this reproduces the case of an unmagnetized plasma, where the size of perturbation is of the order of the probe size (a). However for $M_\perp \to 0$, L_s becomes infinite, which is not only unphysical but also indicating the breakdown of the self-similar problem, since self-similarity holds when far from the edge of the obstacle, i.e. there should be enough distance, from the edge toward the half-infinite plane, to generate an electric field to draw ions toward the vacuum (wake center) with a constant vertical velocity ($M_\perp$ = constant). Figure 22 shows the summary of ratios of current densities in magnetized plasmas. Except for Stangeby's inviscid model, all other 1D fluid, 2D fluid, 1D kinetic and self-similar models have similar values with about $\pm 10\%$ of deviations in K values.

Hutchinson's general model keenly explained the case of general shape and oblique angle incidence, with a simple form, however, there are a few points to discuss.

(i) Although Hutchinson's model covers the case of oblique flow to the arbitrary shape from the 3D continuity and momentum equations, atomic processes such as ionization, recombination and charge exchange could invalidate the self-similarity [119]. For example, if one considers charge exchange, the momentum equation cannot be self-similar unless the rate of momentum transfer by charge exchange is proportional to the self-similar variable, where z is the direction of the ambient steady-state flow. Quasi-neutrality for plasma expansion is only approximate, since the potential structure is determined by the Poisson equation for the plasma expansion into vacuum.

(ii) Hutchinson's approach to generate the ion collection to an object with arbitrary shape is unique and consistent to get analytic solutions of density. Although the method of the characteristics is good mathematically for deriving current densities in the upstream and downstream regions, the physics of ion collection in the downstream side (wake) and the upstream side (ram) may be different. In the wake, ion collection to a negatively-biased object may be the same as the free expansion of the neutral particles to the vacuum, as Hutchinson mentioned [10]. However, there might be a question of whether we could have a clear observation of self-similarity in the ram, as we have such behavior in the wake.

(iii) Patacchini and Hutchinson [161] expanded the kinetic model of Chung and Hutchinson [8] to analyze the transversely flowing magnetized plasma including both convection and diffusion to the cross-field transport. By adding a parallel contribution of the perpendicular convective transport ($v\partial f/\partial y$) to the ion kinetic transport equation of Chung and Hutchinson (equation (12)), they developed a generalized kinetic equation. With the introduction of a self-similar position variable ($\zeta = z/y$) and a shifted parallel velocity ($\hat{v} = v - v_\perp \zeta$), they built the following ion kinetic equation:

$$\hat{v}\frac{\partial f}{\partial \zeta} - V_s^2 \frac{\partial \phi}{\partial \zeta}\frac{\partial f}{\partial v} = -\frac{\hat{z}}{\zeta - \zeta_p}\left[\hat{v}_p \frac{\partial f}{\partial \hat{z}} - V_s^2 \frac{\partial \phi}{\partial \hat{z}}\frac{\partial f}{\partial v}\right] + \frac{\hat{z}}{\zeta - \zeta_p} v_\perp (f_\infty - f(y, z, v)),$$

which has a similar form to the previous one-dimensional kinetic equation (equation (12)), so that they could utilize a similar numerical scheme. Here $v, v_\perp, \zeta, \hat{z} = (z - y\zeta_p)W/v_\perp$ are the parallel velocity, perpendicular velocity, cotangent of the angle between the magnetic field and the position vector, and normalized distance to the probe along the parallel direction, respectively, and the subscript p indicates the variable at the probe surface. They calculated the calibration factor as $K^* \approx [0.4 - 0.1\kappa]^{-1}$, where $\kappa = 0.5\mathrm{erfc}(0.12 + 0.40 \ln \tau)$. Figure 23 shows the ratio (R) of ion saturation current densities against the shifted parallel Mach number ($M^*_\infty - M^*_\perp u_p$) for different ion temperature ratios ($\tau = T_i/T_e$). R increases with τ, and so does the calibration factor (K^*), which seems to be opposite to the result of Chung and Hutchinson (K decreases with τ(K = 1.9, 1.7, 1.3 for τ = 0.2, 1.0, 2.0, respectively), but considering $K^* = \sqrt{1 + \tau}K$, $R = \exp[K v_d/\sqrt{T_e/m_i}] = \exp[K^* v_d/\sqrt{(T_e + T_i)/m_i}$, both would produce similar results). They also provided a efficient method to measure both parallel and perpendicular drift flows simultaneously by locating the two Mach probes perpendicular to each other, and the middle of the two Mach probes is in the direction of the magnetic field.

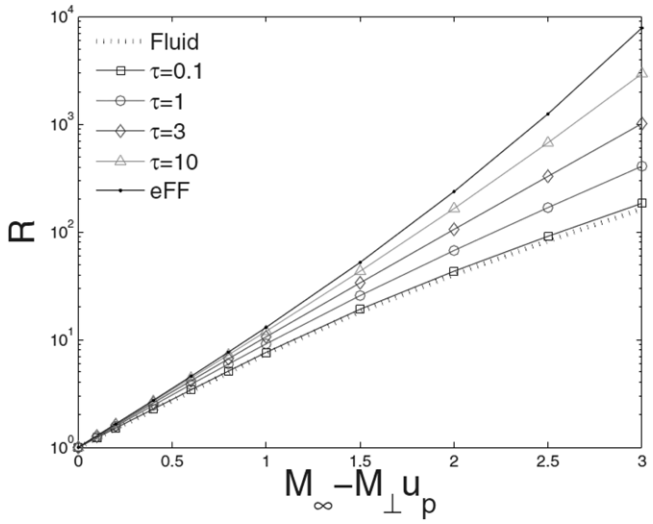

Figure 23. Ratio of current density of upstream to downstream against $M^*_\infty - M^*_\perp u_p$. Fluid is from the model of Hutchinson and eFF means by extended free flight limit [161].

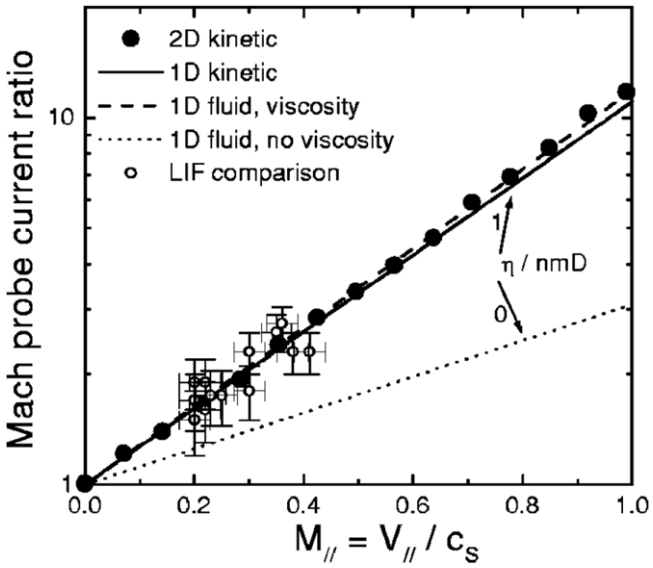

Figure 24. Calibration of MMP by the LIF method. Full circles are the 2D kinetic results of Gunn [87]. The solid line is the 1D kinetic model of Chung. The dashed line is the 1D fluid model of Hutchinson. The dotted line is the 1D fluid model of Stangeby. Open circles are the experimental LIF measurements of Poirier and Boucher [153].

2.4. *Measurement of shear viscosity*

Although shear viscosity should be included for the analysis of MPs in strongly magnetized plasmas, the normalized shear viscosity (α) is assumed to be unity in most tokamak experiments. However, a large difference in Mach numbers between those by simulation (or optical measurement) and MP measurement raised a question on MP interpretation [46, 61, 140]. Even if one cannot measure the exact value of the normalized viscosity (α), theoretical and experimental results support the strong shear viscosity ($\alpha = 1$).

Poirier tried to calibrate the MP using LIF in strongly magnetized plasmas for $0.2 \leqslant M_\infty \leqslant 0.4$ [153], and Gunn confirmed this with his 2D kinetic code, ensuring the result of 1D kinetic analysis, as shown in figure 24 [87].

Hutchinson re-analyzed the experimental data of Chung *et al*, claiming $\alpha = 0.5$ with kinetic theories for the free presheath, to show that $\alpha = 1$ by using a consistency test with the fluid theory of the connected presheath, since the presheath generated by the probe is connected to the dump, so that the model of connected presheath should be used instead of using that of the free presheath [95] (see figure 25).

Chung and Bengtson developed a probe which can measure both the viscosity (α) and flow velocity (M_∞) simultaneously (called a VMP), using similar fluid equations to those of Hutchinson. They measured the normalized shear viscosity as $0.7 \leqslant \alpha \leqslant 1.3$ at the SOL of the TEXT-U limiter tokamak. For this purpose, two MPs were used, one of which was located within the ion flux tube (presheath) generated by a larger MP, leading to generate three free presheaths and one bounded presheath. Figure 26 shows the schematic diagram of two small presheaths, one of which is bounded and the other is free, within the free presheath of a large object. The density profiles (curves 6 and 8 in figure 26) along the free presheaths in the upstream side (regions 4 and 5) have the same shapes. Assuming the absorbing surface, plasma density decreases monotonically toward the surface of the object. Along the bounded presheath (region 3), the maximum density cannot

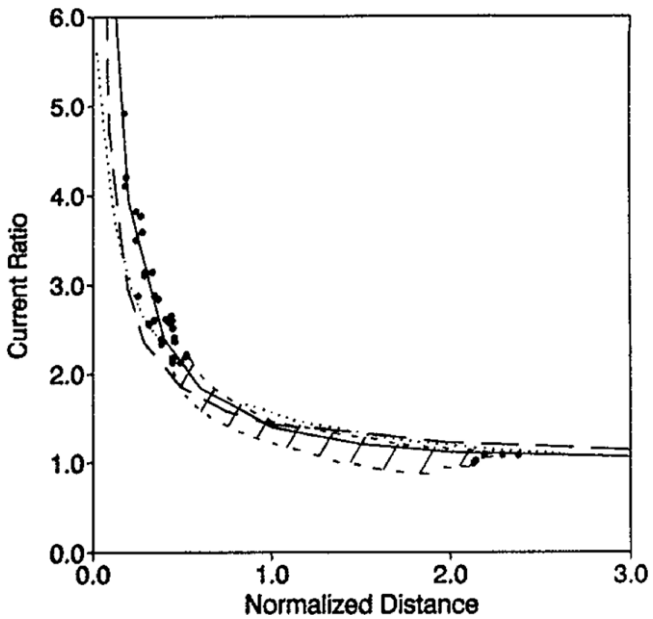

Figure 25. Determination of α by the model of the connected presheath. Points and the shaded area are the data of Chung *et al* [113, figure 11(*a*) 1]. The solid line is the theory with $\alpha = 1$, which fits the data well. The dashed line is the $\alpha = 0$ theory (over normalized distance), which cannot be made to fit. The dotted line is the free-presheath fit (for $\alpha = 0.5$) [113], which also shows substantial discrepancies [95].

exceed the reference density (n_o) and the plasma contacts two surfaces (objects 1 and 2).

The equations for both free and bounded presheaths have exactly the same form as the case of MP, but there are two solutions: one is numerical one by Hutchinson [95], and the other is analytical by Chung [12, 103]. Chung was able to

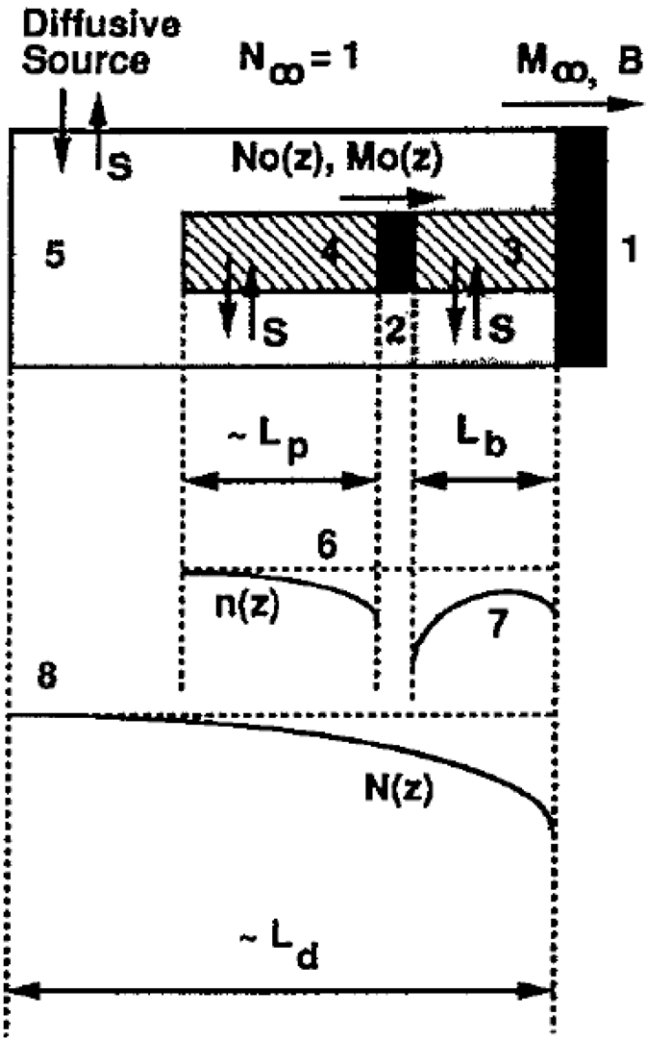

Figure 26. Schematic diagram of a bounded and a free presheath within a free presheath of a large object: 1 = large separator for generating a free presheath: 2 = small separator for generating a free and a bounded presheath; 3 = bounded presheath by a small separator (downstream); 4 = free presheath by a small separator (upstream); 5 = free presheath by a LS (upstream); and 6–8 indicate the density profiles along each presheath. a = half-size of the small separator, d = half-size of the LS. 'S' represents the diffusive plasma source indicating the particle and momentum exchange between outside and inside the presheath, flow Mach number, and the normalized shear viscosity [97].

obtain an analytical solution for $n(M^*)$ and the first-order differential equations for $\mathrm{d}y/\mathrm{d}M^*$ and $\mathrm{d}y/\mathrm{d}n$ to be solved for a given explicit integrand by partial integration. For the bounded presheath, n_∞ and M^*_∞ are replaced by the reference density and Mach numbers (n_o and M^*_0) at each L_b, where L_b is the position of the small object (i.e. size of the bounded presheath). Variations of density ($n(z)$), flow velocity ($M^*(z)$) along the bounded and free presheaths due to a small object (or MP) are obtained by a procedure similar to that in Hutchinson [95]. However, $n_0(L_\mathrm{b})$ and $M^*_0(L_\mathrm{b})$ are obtained analytically in Chung's [12], while they are assumed in Hutchinson's [95]; and $n(z)$ and $M^*(z)$ along the bounded presheath are calculated in Chung's model by direct integration for $0 < n_m < n_0(L_\mathrm{b})$, while they are obtained by numerical analysis with Patankar's numerical methods [157] in Hutchinson's case. The ion collection toward probes will be different depending on the size of the bounded presheath (L_b). If we apply the above theory to the free and bounded presheaths, we can analytically obtain the normalized density and the flow Mach number (M^*_∞) in terms of the normalized viscosity (α) and the distance between two separators, which form the bounded presheath. Applying the Dirichlet boundary condition, the density along the bounded presheath can be given with the maximum density (n_m) along the bounded presheath as follows:

$$n(M^*) = n_m \left[(1+\alpha)M^{*2} - (1+\alpha)M^*_\infty M^* + 1\right]^\delta \times \exp\left\{\frac{\alpha M^*_\infty}{\sqrt{\omega}}\left[\tan^{-1}\left(\frac{(1+\alpha)(2M^* - M^*_\infty)}{\sqrt{\omega}}\right) - \tan^{-1}\left(\frac{(1+\alpha)M^*_\infty}{\sqrt{\omega}}\right)\right]\right\}, \tag{72}$$

where $-1 \leqslant M^*_\infty \leqslant +1$ and $\omega = 4(1+\alpha) - (1+\alpha)^2 M^{*\,2}_\infty$. Putting equation (72) into equation (37) results in the position along the bounded presheath as

$$y(M^*) = \int_1^{M^*_\infty} \frac{n_m G(M)^{-\delta}\exp[H(M^*)]}{1 - n_m G(M^*)^{-\delta}\exp[H(M^*)]} \frac{1 - M^{*2}}{G(M^*)}\,\mathrm{d}M^*, \tag{73}$$

where $G(M) \equiv (1+\alpha)M^{*2} - (1+\alpha)M^*_\infty M^* + 1$, $H(M) \equiv (\alpha M^*_\infty/\sqrt{\omega})\{\tan^{-1}[(1+\alpha)(2M^* - M^*_\infty)/\sqrt{\omega}] - \tan^{-1}[(1+\alpha)M^*_\infty/\sqrt{\omega}]\}$.

Since the integrand of equation (73) is an explicit equation of M^*, $y(M^*)$ can be obtained explicitly in terms of M^*_∞ and n_m. From this one can obtain the flow velocity $M^*(y)$ in terms of the normalized position y, and the density is also obtained by inserting $M(y)$ into equation (72). Chung's analytical results give larger density $n_0(z)$ and smaller velocity $M^*_0(z)$ than those of Hutchinson [95] along the free presheath of the LMP. The ratios of the current densities of the SMP are smaller or larger depending on L. The difference in R rises as L gets larger, and the biggest difference between these result and those by a kinetic model is about 17%. Once one calculates the ratios of a LMP ($R_\mathrm{l}(M^*_\infty, \alpha)$) and a small one ($R_\mathrm{s}(\alpha, M^*_\infty)$), then α and M^*_∞ can be obtained by iteration, and this VMP could be called an iterative VMP (IVMP) (figure 6) [97], while there is another VMP, to be called a direct VMP, by which both α and M^*_∞ can be deduced by a current ratio of R_s of the MP within a free presheath by a large separator (LS) with a fixed ratio of probe separators [12].

Practical application of IVMP [96] was made in TEXT-U [97] using the actual probe as figure 6. TEXT-U was a limiter tokamak with a major radius $R_\mathrm{M} = 1.05\,\mathrm{m}$ and minor plasma radius $r_\mathrm{m} = 0.27\,\mathrm{m}$ defined by three-point limiters at a single toroidal location. For the data presented here, the toroidal magnetic field $B_\mathrm{t} = 2.0\,\mathrm{T}$, plasma current $I_\mathrm{p} = 170\,\mathrm{kA}$ with a line-averaged density $n_{\mathrm{e}0} = 4 \times 10^{19}\,\mathrm{m}^{-3}$. Measured edge parameters for these plasma conditions at the limiter are $T_\mathrm{e} = 30\,\mathrm{eV}$, $n_\mathrm{e} = 2 \times 10^{18}\,\mathrm{m}^{-3}$, and $T_\mathrm{e}/T_\mathrm{i} = 1$ is assumed. Radial profiles of the ion current density ratios ($R_\mathrm{s} = J_1/J_2$) measured by the SMP (probes 1 and 2) and those ($R_\mathrm{l} = J_4/J_3$) measured by the LMP (probes 3 and 4) are given as $1 < R_\mathrm{l} < 1.5$ and $50 < R_\mathrm{s} < 80$, respectively.

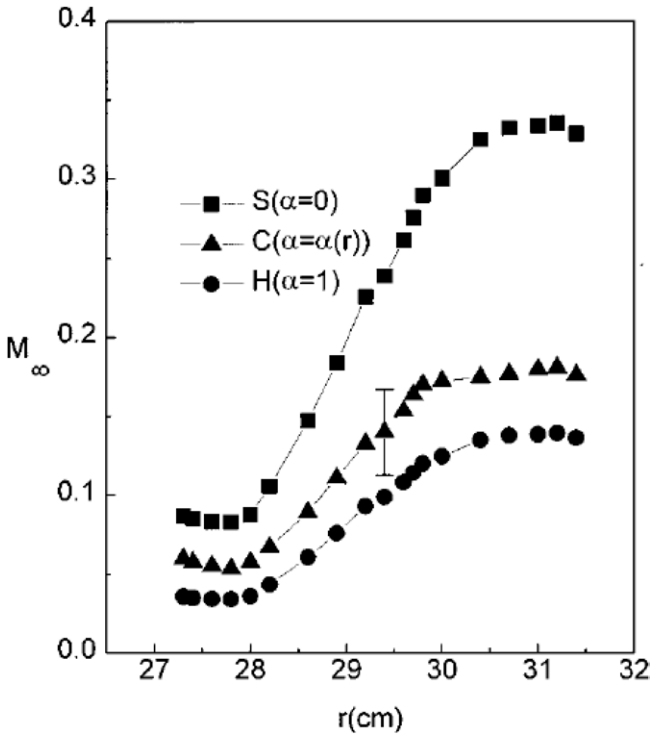

Figure 27. Radial profiles of the parallel Mach number $[M_\infty(r)]$ deduced by the analytic fluid theory (▲) from the measurement of R_s and R_l. Comparisons are made with those of Hutchinson [6] (solid circle: $\alpha = 1$) and Stangeby [5] (solid square: $\alpha = 0$) [97].

Using these theoretical values, for a set of measured values of R_s and R_l, they obtained a profile of M_∞ based on an analytic model [96], and the results are shown in figure 27. Normalized shear viscosity varies as $0.7 \leqslant \alpha \leqslant 1.3$ with an error of $\pm 40\%$ for $r_l = 27 < r < 31.5$ cm, where r_l is the limiter radius.

2.5. Overestimation of Mach number in SOL plasmas?

Porter *et al* simulated the flow in the SOL of the DIII-D, JET and JT-60U tokamaks using the 2D fluid code UEDGE [138], and found that the experimental values of the parallel velocities, deduced by Hutchinson's fluid model [6], are much larger (for JET a factor of 2–4, and for JT60-U more than a factor of 5) than those by the simulation. They include the effect of impurity radiation with multi-species plasmas, especially the intrinsic carbon impurities.

Erents *et al* [46] showed the overestimation of the parallel Mach numbers measured by the MP comparing the simulation results using the EDGE2D/Nimbus code [139] in the JET SOL plasma. They explained this by the following: (1) the difference of the measurement in magnetic fields between forward and reverse directions, producing $M \sim 0.2$ across the SOL, (2) ballooning like transport at the outer mid-plane, or (3) (atomic processes due to) impurity generated at the probe by plasma–surface interactions during the measurement. The Mach numbers predicted by the EDGE2D code are smaller by a factor of 5–10. However, an alternative and non-perturbing measurement is required to clarify the amplification of Mach numbers by the probes.

Gangadhara and LaBombard [140] also showed the overestimation of the parallel Mach numbers, measured by the MP, toward the divertor in the far SOL of Alactor C-Mod, comparing those by the spectroscopic (CCD) method. They intentionally made carbon plumes by puffing deuterated ethylene gas (C_2D_2) through the tip of the reciprocating probe. Near the separatrix, this dispersed impurity plume provides information on the bulk plasma flows and cross-field drifts. The ratio of the Mach numbers measured by the MP to those by the plume measurement is about 2.6 (=0.46/0.18) for the forward (normal) field discharge and 2.8 (=0.59/0.21) for the reverse field discharge.

Hidalgo *et al* [65] showed that there is a dynamical relationship between turbulent transport and parallel flows of tokamak edge plasmas via Reynolds stresses: 'Turbulent transport can partially derive parallel flows in the plasma boundary of fusion plasmas. Parallel flows could be directly coupled to transport via Reynolds stresses, which provide a nonlocal energy transfer between high and low wave numbers.' Based on their data, parallel flows seem to grow with the size of the transport event. They showed experimental data taken from JET edge plasmas with a time resolution of about 2–80 μs.

Assume the following SOL conditions of JET: $T_e \approx 50$ eV, $T_i(D^+) \approx 100$ eV, $n_e = 4 \times 10^{12}$ m^{-3}, $B_T \approx 3$ T, $L_c = \pi R_0 q^* = 40$ m, where L_c and q^* are the connection length and the safety factor. From these we get the following values: $s \approx 10 \times \lambda_D \approx 2 \times 10^{-2}$ cm, $\rho_i \approx 5 \times 10^{-2}$ cm, $D_B \approx 1$ m^2 s^{-1}, $C_s \approx 10^5$ m s^{-1}.

Then for a 1 inch-diameter probe (holder ~20 mm, $a \sim 10$ mm), the time for ions to fill the wake region across the magnetic field is about 1 μs, while the time to arrive at the probe surface from the end of the presheath traveling with ion acoustic speed parallel to the field, e.g. the time to move along the length (≈8.5 m) of the free presheath generated by the probe holder, is ~85 μs. So if they take the data averaging over 50–100 μs order, then the ratio of averaged current densities can be used to deduce the Mach number, while they cannot if the averaging time is less than 50–100 μs. In data shown by Hidalgo, they used data averaging 2–80 μs. So if the above JET condition would be right, their data might not represent the steady-state current density. By averaging more than 50–100 μs, the MP may produce similar values to those by the steady-state MP, while for less than 50–100 μs, care should be taken, since fewer ions are collected on the wake side, so the MP (turbulent) may be overestimated than the MP (average). There is always particles in the wake, since particles arrive at the wake region close to the probe surface across the magnetic field very quickly. If $M_{avg} \approx M(t)$, then his argument may be true: 'Turbulent transport partially contributes to the parallel flow,' where avg indicates the averaged value of a certain amount of time, say 1 ms, with $M(t) = \ln[I^u(t)/I^d(t)]/K$.

If the size of the turbulence is larger than the probe, fewer particles could be collected on the probe, especially on the wake side, since the potential fluctuation in the wake would be bigger than those in the ram region. This could lead to a large current ratio, leading to a larger parallel flow.

However, in his self-similar analysis, as Hutchinson mentioned, even in the case of larger eddies than the probe

size, the relation between the ratio of currents and the Mach number would be the same. So a more plausible reason should be given.

3. MP analyses in unmagnetized plasmas

As mentioned in the introduction, there have been experiments [2, 15, 38–42] involved with plasma flow in unmagnetized plasmas, especially in space plasmas with satellites, processing plasmas with a torch, or in fusion plasmas with $\boldsymbol{E} \times \boldsymbol{B}$ rotation or shear flows. Recently, Hutchinson raised a question [73] on the validity of applying a fluid model of Hudis and Lidsky [3] in various experiments [40, 114, 115] in unmagnetized plasmas, which indicates the necessity of a valid theory for MPs in unmagnetized plasmas.

3.1. PIC and kinetic models of MPs in unmagnetized plasmas

Consider the flow of ions to a probe whose characteristic size is smaller than the ion gyro-radius in drifting plasmas($\rho_i > a$), where ρ_i is the ion gyro-radius and a is the probe radius. Mott-Smith and Langmuir [72] derived an analytical formula of ion collection for the cylindrical probe with a thick sheath by assuming a shifted Maxwellian ion distribution at the sheath. Chung [78] developed a 1D kinetic model, by which numerical solutions of the self-consistent plasma-sheath equations are obtained for arbitrary external temperature and parallel plasma flow velocity. Hutchinson [77] developed a PIC code using the specialized-coordinate electrostatic particle and thermals in the cell (SCEPTIC) system for a spherical probe in unmagnetized plasmas, where ions are governed by Newton's law in the electrostatic potential. The Boltzmann relation for electrons and the Poisson equation for the electrostatic field are used. In all three approaches, the ratio of the upstream to downstream current can be represented by the form $R = \exp[K M_\infty]$, where v_d is the drift velocity in units of V_s and K is a constant depending on the type of source in the sheath-transition region.

3.1.1. PIC model—spherical. Hutchinson [77] developed a PIC model (or material point method: MPM) using specialized-coordinate electrostatic particle and thermals in the cell (SCEPTIC) coordination system for a spherical probe in unmagnetized plasmas. He added a background plasma flow, extending the stationary problem of Al'pert *et al* [122] and Laframboise [68], which breaks the conservation of the angular momentum in the spherical symmetric geometry. His model is also compared with those by Parrot [69] and Al'pert, and shows that his model is in good agreement with Al'pert's model [122], especially for the potential profile, partially due to the difference in mesh spacing, which indirectly indicates that the average normalized ion flux is dependent on the mesh spacing, even with the SCEPTIC code. From subsonic to supersonic flows, the SCEPTIC code seems to work for $T_i/ZT_e \geqslant 1$, but it may become unstable for $T_i/ZT_e < 0.1$ due to the finite-grid instability, which is common to the electron PIC codes with the nearest grid point (NGP) version for $T_i/ZT_e \leqslant 0.2$.

For the PIC code, ions are governed by Newton's law in the electrostatic potential, and electrons are expressed by the Boltzmann relation as follows: Force equations for the ions at position $\vec{x}$

$$m_i \frac{d^2\vec{x}}{dt^2} = -Ze\nabla\phi, \tag{74}$$

$$n_e = Zn_i = n_\infty \exp[e\phi/T_e], \tag{75}$$

with shifted Maxwellian ions. Then the Poisson equation on the electrostatic field is used for self-consistency. Hutchinson adopted the spherical coordinate for the potential variation and the Cartesian coordinate for the 7.2 million ion particles for the position and velocity with a similar non-uniform meshing technique ($r \equiv \zeta^2/2+1$) as Emmert *et al* [60] and Chung [78] chose in their kinetic models ($y \equiv s^\delta$, $\delta > 1$) for numerical stability. However, he chose a different mesh spacing (uniform in r, non-uniform in ζ) from that of Emmert and Chung's (uniform in s, non-uniform in y).

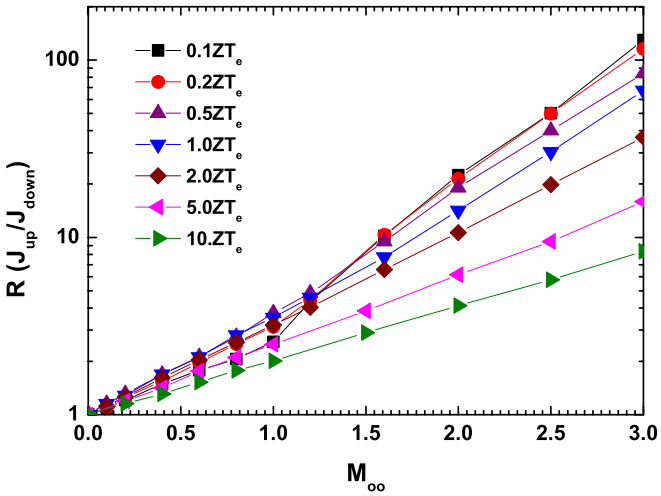

Figure 28. Ratio of upstream to downstream current densities by Hutchinson's PIC model [77].

The calibration factor of the exponential form ($R = \exp[K M_\infty]$), K, is averagely given as 1.34 for $\tau < 3$ and $0 \leqslant M_\infty \leqslant 3$ assuming zero Debye length from Hutchinson's model, although K is slightly dependent on the ion temperature (T_i) similar to the kinetic model [78]. Figure 28 shows the ratio of current density for $0 < T_{i\infty}/T_e < 10$ and $0 < M_\infty < 4$. Since the ratios fluctuate for subsonic Mach number and $0 < T_{i\infty}/T_e < 2$, we re-plot his data, as shown in figure 29. Here, there could be two expressions for R, i.e. $R = \exp[K M_\infty] = \exp[K^* M^*_\infty]$, where $M_\infty = v_d/V_s$, $M^*_\infty = v_d/C_s$ and $K^* = K\sqrt{1 + T_i/T_e}$. If one re-plots the same data of SCEPTIC and kinetic models for $0 \leqslant M^*_\infty \leqslant 1.2$, the ratio R increases for $0.1 \leqslant T_i \leqslant 1.0$ then decreases for $T_i = 2T_e$, while R of Chung's model increases with T_i, which is shown in figures 29. Moreover, K (K^*) of Hutchinson is around 0.67–1.10 (1.1–1.26) not 1.34, while that of Chung is around 0.9–1.24 (1.36–1.57), which is shown in table 1 and figure 30.

Hutchinson also extended his model with the non-zero Debye length calculation, which shows an unexpected reversal of the current ratio [123]. This has been observed in a recent experiment by Ko and Hershkowitz [124], where both a planar and a spherical probe are used for comparison. They found

the reversal of the current ratio or more ion collection on the downstream side than the upstream side for low-density plasmas with a short Debye length. However, there are discrepancies between the two probe data, say, there is a clear flow reversal in the data of the spherical probe, but not so clear in those by the planar MP for the same plasma conditions. This might indicate that for the low-density plasma with a large Debye length the planar MP would be preferable for the flow measurement, or the wake problem of planar geometry is quite different from that by a spherical object. There is another point on this experimental verification: the PIC model presumes drifting ions in a collisionless plasma and a thick sheath ($\lambda_D/a = 1$ for $T_i = T_e$ with $\phi_p = -15T_e$ and $\lambda_D/a = 3$ for $T_i = 0.1T_e$ with $\phi_p = -15T_e$ up to $v_d = 1.5C_s$), while Ko and Hershkowitz's experiment had the conditions that there are ion beam and background ions in a weakly collisional plasma and a thin sheath ($\lambda_D/a = 0.22$ for $T_i < 0.1T_e$ with $\phi_p = -20T_e$ up to $v_d = 2.5C_s$ with the planar MP and up to $v_d = 3.7C_s$ with the spherical MP). Recently, Kharapak *et al* measured the ion flow velocity around a sphere in a highly collisional plasma, but they did not observe the flow reversal. Although collisionality may play a role in these, all these may lead to the necessity of further detailed experiment and analysis [160].

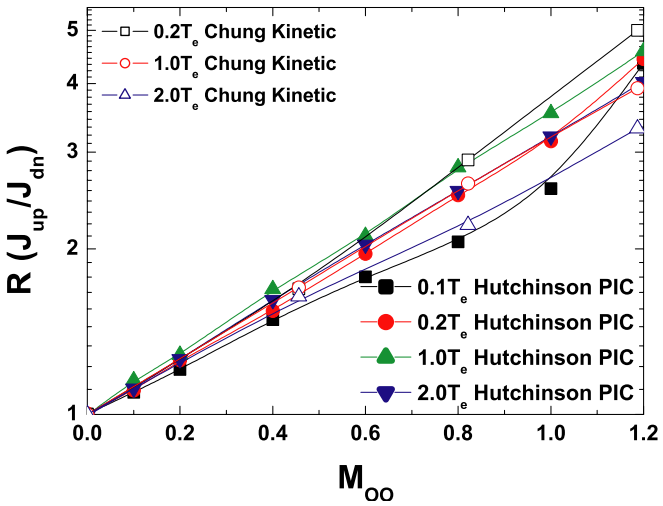

Figure 29. Ratio of upstream and downstream current in unmagnetized plasma ($0 \leqslant M_\infty \leqslant 1.2$). Solid squares: Hutchinson's PIC code ($T_i = 0.1T_e$), $K = 1.05$; solid circles: Hutchinson's PIC code ($T_i = 0.2T_e$), $K = 1.10$; solid up-triangles: Hutchinson's PIC code ($T_i = 1.0T_e$), $K = 0.89$; solid down-triangles: Hutchinson's PIC code ($T_i = 2.0T_e$), $K = 0.67$; open squares: Chung's kinetic code ($T_i = 0.2T_e$), $K = 1.24$; open circles: Chung's kinetic code ($T_i = 1.0T_e$), $K = 1.05$; open triangles: Chung's kinetic code ($T_i = 2.0T_e$), $K = 0.91$ [77, 78].

3.1.2. Kinetic model with self-consistency—planar. Experimental data of wake experiments using a planar disk showed that the scale lengths of potential or density variation along the presheath can be expressed in terms of the disk size for stationary weakly collisional plasmas ($v_d = 0$) and for subsonic to supersonic plasmas ($0.5 \leqslant v_d/\sqrt{2T_i/m_i} \leqslant 6$) [116]. In particular, for the experiment of wake with supersonic flows ($1 \leqslant M_\infty = v_d/\sqrt{T_e/m_i} \leqslant 20$), the size of the wake is expressed in terms of the object size regardless of the shape for the following supersonic Mach numbers: $M_\infty = 1$–2 [117], $M_\infty = 2$–4 [118], $M_\infty = 5$–14 [119], $M_\infty = 10$–23 [121]. In describing the ion distribution and density in the wake of ionospheric plasmas, Gurevich *et al* [75] expanded ion density in terms of the size of the planar disk or cylindrical radius. From the analysis of a 2D kinetic theory, Grabowski and Fisher [76] expressed the density variation in terms of the radius of the cylindrical probe (up to 6–8a). They even calculated the weakly magnetized case, which produces similar values to those without a magnetic field, while for the marginal case, $\rho_i \approx R_0$, density variation shows the oscillatory behavior along the magnetic field direction. Hutchinson [77] also described particle motion around a spherical probe in terms of radius (up to $\sim 5R_0$). From this, it could be justified that one can describe the presheath of a planar probe in terms of the size of the probe. And one can consider the source of the wake as the particle inflow from outside to fill the wake due to the density gradient and potential gradient to pull the particles. In modeling the MP in unmagnetized flowing plasmas, the critical physics lies in the wake. Although the analysis of the wake should be performed by the 2D or multidimensional model, as shown in figure 31, it would be difficult to solve the 2D kinetic model, but it might be useful to use a 1D model with inclusion of the 2D transport information.

Chung [78] developed a 1D model in order to deduce the flow velocity from the sheath current density, by treating the perpendicular component to the streaming direction as a source in the perturbed region, i.e. by taking into account the convective inflow toward the perturbed region (sheath-transition region) as a source. His model seems to simplify the models of Grabowski, Gunrevich and/or Merlino, as shown in figure 31. The normalized sheath densities, hence the sheath current densities at the center of the probes in the wake of

Table 1. Calibration factor K and K^* of UMP (Hutchinson's PIC and Chung's kinetic results in the ranges $0 \leqslant M_\infty \equiv V_d/\sqrt{T_e/m_i} \leqslant 1.3$).

T_i/T_e	$K^*\left(C_s = \sqrt{\frac{T_e+T_i}{m_i}}\right)$	$K\left(V_s = \sqrt{\frac{T_e}{m_i}}\right)$	Range	Ref
0.1	1.10	1.05	$0 \leqslant M_\infty \leqslant 1.2$	Hutchinson's PIC [77]
0.2	1.21	1.10	$0 \leqslant M_\infty \leqslant 1.2$	Hutchinson's PIC [77]
1	1.26	0.89	$0 \leqslant M_\infty \leqslant 1.2$	Hutchinson's PIC [77]
2	1.17	0.67	$0 \leqslant M_\infty \leqslant 1.2$	Hutchinson's PIC [77]
0.2	1.36	1.24	$0 \leqslant M_\infty \leqslant 1.3$	Chung's kinetic [78]
1	1.49	1.05	$0 \leqslant M_\infty \leqslant 1.3$	Chung's kinetic [78]
2	1.57	0.91	$0 \leqslant M_\infty \leqslant 1.3$	Chung's kinetic [78]

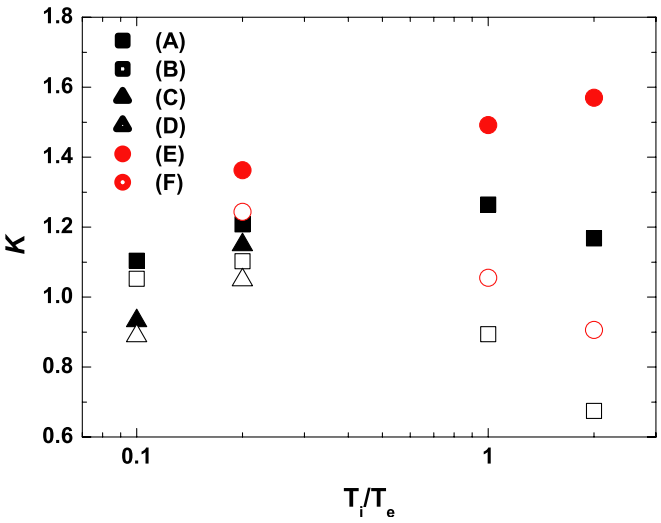

Figure 30. Relation between the calibration factor (K) and the temperature (T_i/T_e). (A): Hutchinson's PIC—K^* for $0 \leqslant M_\infty \leqslant 1.2$, (B): Hutchinson's PIC—$K$ for $0 \leqslant M_\infty \leqslant 1.2$, (C): Hutchinson's PIC—$K^*$ for $0 \leqslant M_\infty \leqslant 1$, (D): Hutchinson's PIC—$K$ for $0 \leqslant M_\infty \leqslant 1$, (E): Chung's kinetic—$K^*$ for $0 \leqslant M_\infty \leqslant 1.3$ and (F): Chung's kinetic—K for $0 \leqslant M_\infty \leqslant 1.3$ [77, 78].

flowing unmagnetized plasmas, are summarized as follows for M_∞ = (0, 0.5, 1.0): (0.46, 0.40, 0.22) by Grabowski (2D, cylindrical); (0.62, 0.46, 0.33) by Hutchinson (1D, spherical); and (0.76, 0.57, 0.44) by Chung (1D, planar).

For an unmagnetized plasma, ion transport into the presheath is assumed to be governed by the coherent external flow, so the inviscid model would be used, i.e. there is a certain amount of particle inflow as a source, and this inflow is presumably driven by the density difference between inside and outside of the perturbed region. Therefore, it is taken to be proportional to the density difference (perpendicular convection with a constant perpendicular velocity). The distribution of the inflowing particles is that of the external plasma. Hence we convert the 2D Vlasov equation into 1D Boltzmann equation without destroying the 2D physical mechanism.

The governing equations of electrons (Boltzmann equation), energy equation for ion motion, the Poisson equation for the electrostatic potential are the same as the kinetic model for magnetized plasmas, i.e. equations (13)–(15). Only different equation is the Boltzmann transport equation for ions, whose source term is composed of

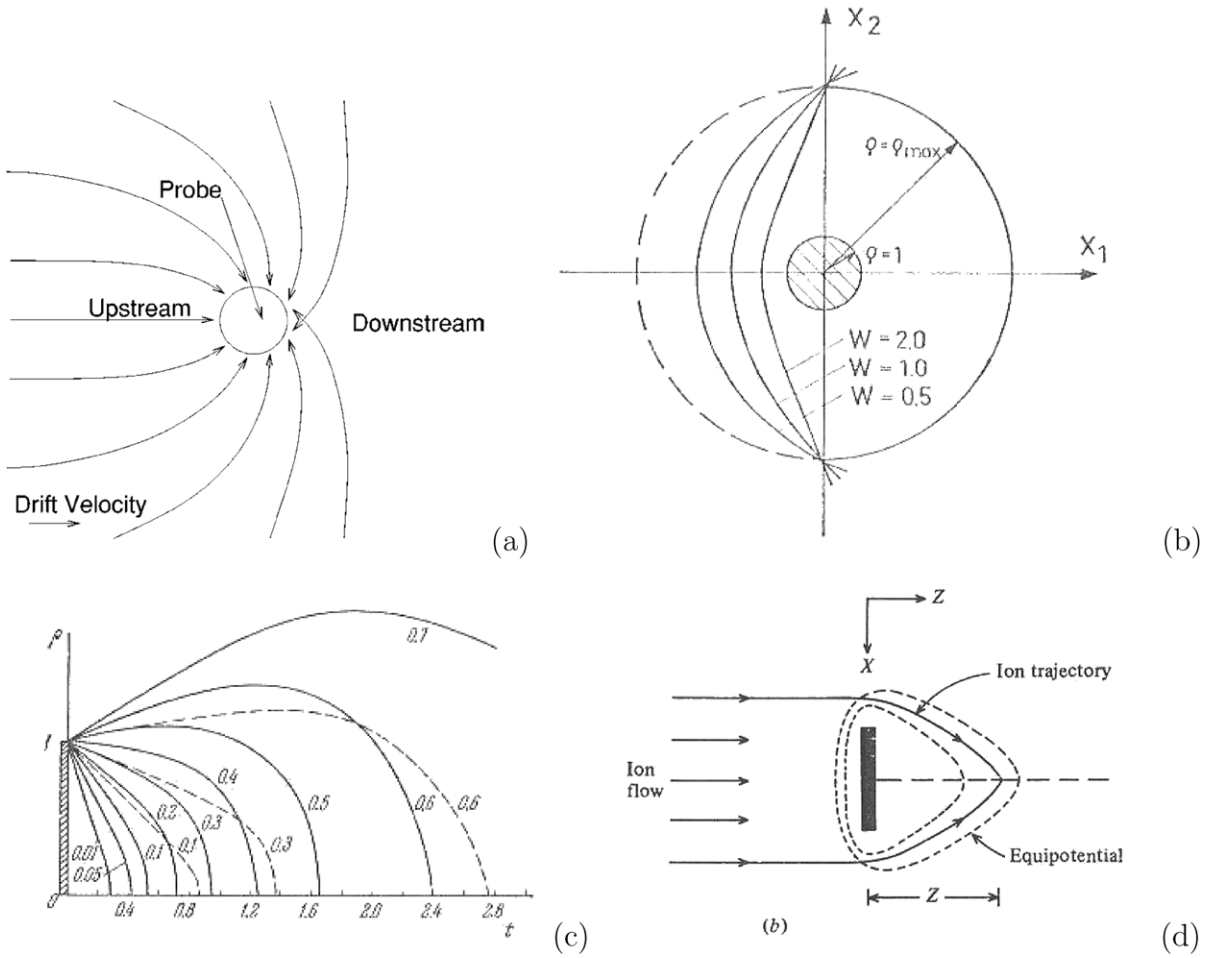

Figure 31. Schematic illustrations of ion orbits in UMP. (a) An illustration of possible ion orbits showing how collection to the downstream side of the spherical probe is essentially multidimensional [73], (b) perturbation (presheath) region around cylindrical probe [75], (c) constant concentration surfaces in the case of flow around a plate; the values of $n = N/N_0$ are indicated on the figure ($\beta = 1$) [75], (d) continuous deflection of ions in a body sheath extended to the wake axis [118].

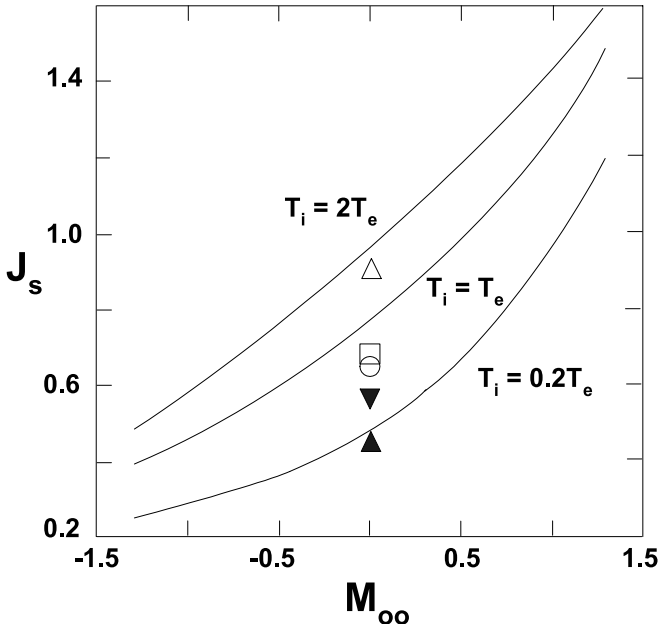

Figure 32. Sheath current densities. Comparisons are made with the kinetic model for $M_\infty = 0$ and $T_{i\infty} = T_e$. Emmert *et al* (△) [60], Laframboise (□) [68], Bissel and Johnson (○) [71], Parrot *et al* (▼) [69], and Grabowski (▲) [76]. Note that negative sign means the plasma drifts away from the probe (here, $M_\infty = v_d/V_s$, $V_s = \sqrt{T_e/m_i}$, $Z = 1$, $\lambda = 0$ (zero Debye length, quasi-neutral case), $\psi_w (\equiv e\phi_{wall}/ZT_e) = 3$).

convection transport and which is given by

$$\left[v\frac{\partial}{\partial z} - \frac{q}{m_i}\frac{d\phi}{dz}\frac{\partial}{\partial v}\right] f_i(z, v) = \frac{v_{th}}{a}\left(1 - \frac{n_i}{n_\infty}\right) f_{i\infty}, \quad (76)$$

where the variables are defined the same way as in the magnetized plasmas, except that v_{th} and a are the ion thermal speed ($= (T_{i\infty}/m_i)^{0.5}$) and the probe size, respectively. Then with non-dimensional parameters of $\lambda_a \equiv \lambda_D/a$ and $\xi \equiv z/a$, which is similar to the self-similar variable $\zeta = z/y$, the above equation can be non-dimensionalized as

$$\left[\xi\frac{\partial}{\partial \xi} + \frac{d\psi}{d\xi}\frac{\partial}{\partial u}\right] g(\xi, u) = \tau^{0.5}(1 - n) g_{i\infty}(u). \quad (77)$$

In figure 32, we show the ion current density flowing into the sheath as a function of the external drift velocity, for three values of ion temperature. The sheath current density (J_s) increases as the plasma drifts toward the probe (M_∞). Comparisons with other kinetic results are also shown in the same figure. Since there have been no kinetic analysis with drift, we just compare those without drift for $\tau = 1$. From Chung's kinetic model [78] for a planar probe, K is given as 1.2, 1.0 and 0.9 for $T_i/T_e = 0.2$, 1.0 and 2.0, respectively. For the kinetic model, the Boltzmann transport and energy conservation equations are used for ions, and the Boltzmann relation for electrons and the Poisson equation for the electrostatic field are used as a way of self-consistent analysis.

3.1.3. Kinetic model with neutral approximations—cylindrical. From Mott-Smith and Langmuir's kinetic model for a cylindrical probe with a thick sheath [72] in an unmagnetized plasma, one cannot get an analytic form for R, since it is composed of integration forms in terms of collection angle and potential difference between the sheath and probe wall, which should be solved numerically. They adopted energy and momentum equations such as

$$\tfrac{1}{2}m_i\left[v_\perp(a)^2 + v_{||}(a)^2\right] + q\phi = \tfrac{1}{2}m_i\left[v_\perp^2 + v_{||}^2\right],$$
$$a v_{||}(a) = b v_{||}, \quad (78)$$

where m_i, $v_\perp$, $v_{||}$ ($= v$), a, b, q and ϕ are the ion mass, radial velocity, tangential velocity, probe radius, sheath radius, ion charge and applied voltage with respect to the plasma, respectively. Here, '$b - a$' becomes the sheath thickness. Assuming a thick sheath ($b \to \infty$) and shifted ion Maxwellian distribution with a negative applied potential (i.e. ion collection), the normalized current densities of the upstream (J_{up}) and downstream (J_{dn}) sides can be calculated as

$$J_{up} = \frac{1}{\tau\pi^2}\int_0^{\pi/2} d\theta \int_0^\infty dM M\sqrt{M^2 + 2\psi}\exp\left[-\frac{f_{M\theta}}{2\tau}\right], \quad (79)$$

$$J_{dn} = \frac{1}{\tau\pi^2}\int_{\pi/2}^{\pi} d\theta \int_0^\infty dM M\sqrt{M^2 + 2\psi}\exp\left[-\frac{f_{M\theta}}{2\tau}\right], \quad (80)$$

where $f_{M\theta} \equiv M^2 - 2MM_\infty\cos\theta + M_\infty^2$, $M \equiv v/V_s$, $\psi \equiv -e\phi/T_e$, $\tau \equiv T_i/T_e$, $V_s \equiv \sqrt{T_e/m_i}$ and θ is the angle between the reference direction (usually, one sets it as the z direction) and the incident direction of the plasma flow. Here, if one assumes the charged particles as neutrals by neglecting the effect of electric field as done by Harbour and Proudfoot [1], these become the form consisting of exponential and error functions such as the following:

$$J_{up} = \frac{1}{2\sqrt{\tau\pi}}[\exp[-\tau M_\infty^2] + \sqrt{\tau\pi}M_\infty\{1 + \mathrm{erf}(\sqrt{\tau}M_\infty)\}], \quad (81)$$

$$J_{dn} = \frac{1}{2\sqrt{\tau\pi}}[\exp[-\tau M_\infty^2] - \sqrt{\tau\pi}M_\infty\{1 - \mathrm{erf}(\sqrt{\tau}M_\infty)\}]. \quad (82)$$

Interestingly, these equations are exactly the same as equation (82) of Hutchinson [77] on a spherical probe in the limit of $v_\perp \to \infty$ with $\cos\theta = -1$ for the upstream flow, and $\cos\theta = +1$ for the downstream. This implicitly indicates the independence of geometry on the particle collection, or behavior of a spherical probe is similar to that of a cylindrical probe.

Then the ratio of the current densities ($R \equiv J_{up}/J_{dn}$) can be reduced as

$$R = \frac{\exp[-\tau M_\infty^2] + \sqrt{\tau\pi}M_\infty\{1 + \mathrm{erf}(\sqrt{\tau}M_\infty)\}}{\exp[-\tau M_\infty^2] - \sqrt{\tau\pi}M_\infty\{1 - \mathrm{erf}(\sqrt{\tau}M_\infty)\}}$$
$$\approx \exp[K M_\infty], \quad (83)$$

where the calibration factor K can be approximated as an exponential form with $K = 2\sqrt{\pi\tau}/(1 + \tau M_\infty^2) \approx 2(\pi\tau)^{1/2}$, for $\tau < 1$ and $|M_\infty| < 1$.

3.2. Fluid theory of MP in unmagnetized plasmas

3.2.1. Planar probes.

A. The free-fall model

Hershkowitz and Oksuz [14, 74] introduced a new model in terms of electron densities, based on the free-fall motion of ions by the potential difference along the presheath. Using the quasi-neutrality and Boltzmann relation, the ratio of the upstream to downstream current densities is

$$R = \frac{n_\infty \exp[e\phi_{su}/T_e]}{n_\infty \exp[e\phi_{sd}/T_e]} = \exp\left[\frac{e}{T_e}(\phi_{su} - \phi_{sd})\right], \quad (84)$$

where ϕ_{su} and ϕ_{sd} are taken as the plasma-sheath potentials for the cases of upstream and downstream. The potential difference between the sheath and plasma potentials along the presheath causes a change (or gain) in kinetic energy, and the change in the upstream side ($e\nabla\phi_u$) is different from that in the downstream side ($\nabla\phi_d$) if there is plasma flow. The sum of these differences is approximately equal to difference of the sheath potentials:

$$e(\phi_{su} - \phi_{sd}) \approx |e\nabla\phi_u| + |e\nabla\phi_d|, \quad (85)$$

and considering the gain of the kinetic energy of both sides, sum of these differences is approximately equal to double of the kinetic energy of the drift plasmas:

$$|e\nabla\phi_u| + |e\nabla\phi_d| \approx m_i v_d^2. \quad (86)$$

Then a combination of these equations leads to

$$\frac{n_{eu}}{n_{ed}} \approx \exp[M_\infty^2], \quad (87)$$

where the potential differences were measured when the probes were biased to the plasma potentials, and they fitted their data with $\tau = T_l/T_e = 0.1$ in a drifting, unmagnetized and non-uniform plasma. Although they showed good agreement to those of Hudis and Lidsky, it would be incidental since the model of Hudis and Lidsky is only applicable for very low T_i/T_e, and it cannot be applied for $T_i = 0$. This method is better than the measurement of ion currents due to a high signal-to-noise ratio of electron currents.

The final form of Oksuz and Hershkowitz would be recovered by using the following parallel component of the momentum equation near the sheath with the Boltzmann electrons, the constant temperatures of ions and electrons, and quasi-neutrality:

$$m_i n_i V_z \frac{dV_z}{dz} = -\frac{dP_i}{dz} + en_i E = -(T_i + T_e)\frac{dn_i}{dz} \equiv -T\frac{dn_i}{dz},$$

where m_i, e, P_i, E, T_i and T_e are the ion mass, electron charge, ion pressure, electric field intensity, ion and electron temperatures, respectively, and $T = T_i + T_e$. By multiplying both terms by dz this equation becomes

$$\frac{1}{n_i}\frac{dn_i}{dz} = -\frac{m_i}{T}V_z\frac{dV_z}{dz} \to \frac{d}{dz}\ln(n) = -\frac{d}{dz}\left(\frac{M^2}{2}\right),$$

where $n = n_i/n_\infty$, $M = V_z/C_s$ and $C_s \equiv \sqrt{(T_e + T_i)/m_i}$, which has the same form as in [13] except for the sign. This leads to the following by direct integration:

$$\int_1^n d[\ln(n)] = -\int_{M_\infty}^{M} d\left[\frac{M^2}{2}\right] \to n(M) = \exp\left[\frac{M_\infty^2}{2} - \frac{M^2}{2}\right],$$

which recovers the Bohm value (0.61) at the sheath ($M = -1$) without drift ($M_\infty = 0$). Then the normalized sheath density with drift flow can be expressed as

$$n(M = -1, M_\infty) \equiv n_s(M_\infty) = 0.61\exp\left[\frac{M_\infty^2}{2}\right].$$

Although $n_s(M_\infty)$ is an even function of M_∞, $n_s(+|M_\infty|)$ (upstream) should be different from $n_s(-|M_\infty|)$ (downstream), physically, which can be clearly seen in figure 7 due to a flow reversal for the wake side, when $M_\infty < 0$. The sheath density at the upstream side should be increased by the drift, i.e. $n_s(M_\infty > 0) = n_{su} = 0.61\exp[M_\infty^2/2]$, while that at the downstream side should be decreased, i.e. $n_s(M_\infty < 0) = n_{sd} = 0.61\exp[-M_\infty^2/2]$. Then the ratio of the upstream to downstream sheath densities can be given as

$$R = \frac{J_{su}}{J_{sd}} = \frac{n_{su}}{n_{sd}} = \exp[M_\infty^2],$$

which is exactly the same form as that of Oksuz and Hershkowitz.

B. The self-consistent model

Taking the moment of Chung's kinetic model [78], equation (76), as follows:

$$n_i\frac{dV}{dz} + V\frac{dn_i}{dz} = \frac{v_{th}}{a}(n_\infty - n_i), \quad (88)$$

$$m_i n_i V\frac{dV}{dz} = en_i E - T_i\frac{dn_i}{dz} + m_i\frac{v_{th}}{a}(n_\infty - n_i)(v_d - V), \quad (89)$$

where the electron is assumed to follow a Boltzmann relation, $n_e = n_\infty\exp(e\phi/T_e)$. Then the non-dimensional forms of the parameters are given as follows: $n = n_i/n_\infty$, $y = z/a$, $M^* = v/C_s$, $C_s = \sqrt{(T_e + T_i)/m_i}$ and $\tau = T_i/T_e$. In terms of these parameters the equations can be written as

$$\frac{dn}{dy} = \frac{(1-n)}{\sqrt{1+\tau}}\frac{M_\infty - 2M}{1 - M^2}, \quad (90)$$

$$\frac{dM}{dy} = \frac{(1-n)}{n\sqrt{1+\tau}}\frac{M^2 - M_\infty M + 1}{1 - M^2}, \quad (91)$$

which leads to the following:

$$\frac{dn}{dM} = n\frac{M_\infty - 2M}{M^2 - M_\infty M + 1}. \quad (92)$$

Then the solution of this equation becomes

$$n(M) = \frac{n_\infty}{M^2 - M_\infty M + 1}, \quad (93)$$

and this leads to the ratio of the upstream to the downstream current densities as

$$R(M_\infty) = \frac{n(M=+1)}{n(M=-1)}) = \frac{2+M_\infty}{2-M_\infty} \approx \exp[M_\infty], \quad (94)$$

where the approximation is for $0 < M_\infty < 0.5$. Although the final equations of $\mathrm{d}n/\mathrm{d}M$, $n(M)$ and $R(M_\infty)$ are the same as Stangeby's [5] for magnetized flowing plasmas, the equations of $\mathrm{d}n/\mathrm{d}y$ and $\mathrm{d}M/\mathrm{d}y$ are different indicating the different transport rate in the perpendicular direction. In addition, the perturbation length (a) is much less than that of Stangeby ($L_\parallel$), and the (temporal) rate of flux flowing into the perturbed region are totally different (v_{th}/a-[high] versus $D_\perp/a^2$-[low]).

Comparing equations (88) and (89) with the self-similar equations with proper approximation, they have very similar forms:

$$n_\mathrm{i}\frac{\partial V}{\partial z} + V\frac{\partial n_\mathrm{i}}{\partial z} = -v_\perp\frac{\partial n}{\partial y} \approx \frac{v_\perp}{a}(n_\infty - n) \quad (95)$$

$$n_\mathrm{i}\frac{\partial V}{\partial z} + C_\mathrm{s}^2\frac{\partial n}{\partial z} = -nv_\perp\frac{\partial v_\perp}{\partial y} \approx nv_\perp(n_\infty - n) \quad (96)$$

by replacing v_{th} by $v_\perp$ (which loosely indicates the validity of the 1D kinetic model and its moment equation).

Since it is not easy to get the calibration factor for very low ion temperatures ($0.1 < T_\mathrm{i}/T_\mathrm{e} < 0.1$) from both PIC and kinetic models, it is worthwhile to fit the calibration factor. Figure 33 shows the fitted values of the calibration factors (K, K^*) for the unmagnetized plasmas (unmagnetized Mach probe (UMP)), which are defined as $R = \exp[K v_\mathrm{d}/\sqrt{T_\mathrm{e}/m_\mathrm{i}}] = \exp[K^* v_\mathrm{d}/\sqrt{(T_\mathrm{e}+T_\mathrm{i})/m_\mathrm{i}}]$, where $T_\mathrm{i} = T_{\mathrm{i}\infty}$. For UMP, K (K^*) values of Hutchinson($K(H)$) and Chung($K(C)$) show the same trend with $\tau \equiv T_\mathrm{i}/T_\mathrm{e}$, and the difference of K is almost constant, i.e. $K(C) - K(H) \approx 0.2$, for $0 \leqslant \tau \leqslant 2.0$. The fitting function of $K(C)$ or $K^*(C)$ would be useful, since it is not easy to get the calibration factor either by the PIC code or the kinetic model for very low ion temperatures ($T_\mathrm{i}/T_\mathrm{e} \ll 1$). Then the calibration factor over a wide range of ion temperatures, say $0 < T_\mathrm{i}/T_\mathrm{e} < 2$, is given as

$$K(C,\tau) = 1.31 - 0.31\tau + 0.056\tau^2,$$

where $K(\tau \to 0) \approx 1.31$ for Chung's case, and $K(\tau \to 0) \approx 1.1$ for Hutchinson's case. By fitting K and K^*, one can easily find the calibration factor for $T_\mathrm{i}/T_\mathrm{e} = 0$.

However, the calibration factors of Hudis and Lidsky, Mott-Smith and Langmuir, and Solomon and Shats show larger difference from those of Hutchinson and Chung. Accidently, they coincide with those of Hutchinson and Chung at specific values of $T_\mathrm{i}/T_\mathrm{e}$: K(Hudis) $\approx K(H)$ at $\tau \approx 0.075$; K(Hudis) $\approx K(C)$ at $\tau \approx 0.1$; and K(Solomon) $\approx K(H)$ at $\tau \approx 0.6$; K(Solomon) $\approx K(C)$ at $\tau \approx 0.75$, which indicates that Hudis and Lidsky's model accidently happened to be applied for the plasma with cold ion temperature, say, $\tau \sim 0.1$, and produced similar values to those by Chung and Hutchinson (with a modified calibration factor). As for those of Solomon and Shats, their model does not seem to be compatible with those of Hutchinson and Chung for the high ion temperature model, i.e. $\tau > 1$.

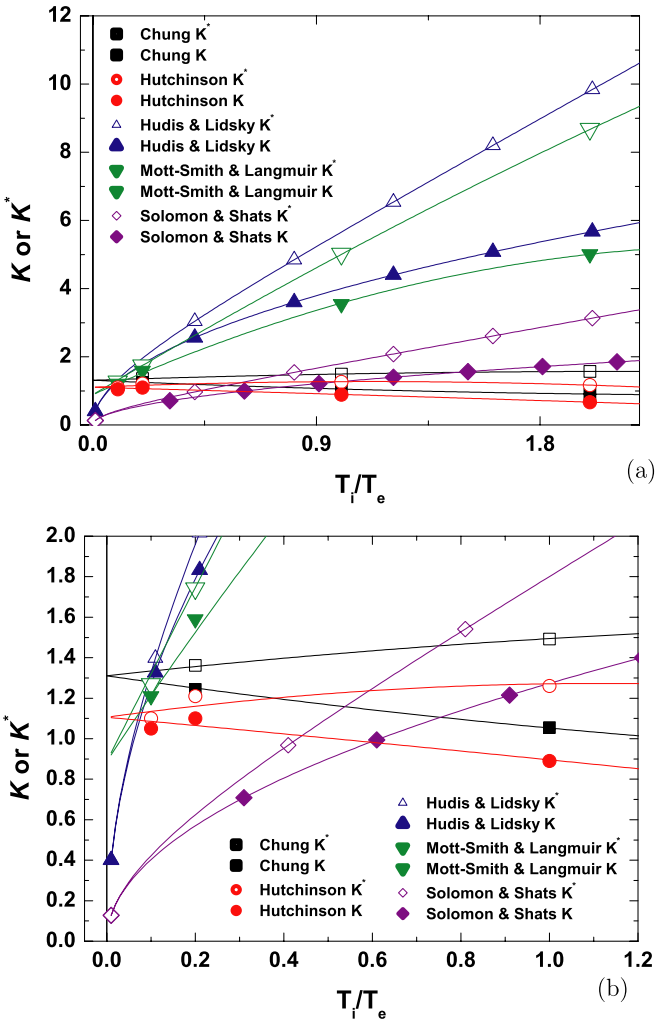

Figure 33. Fitted calibration factor: the second polynomial fitting ($K(T_\mathrm{i}/T_\mathrm{e}) = a + b(T_\mathrm{i}/T_\mathrm{e}) + c(T_\mathrm{i}/T_\mathrm{e})^2$). K and K^* are in the following form: $R = \exp[K v_\mathrm{d}/\sqrt{T_\mathrm{e}/m_\mathrm{i}}] = \exp[K^* v_\mathrm{d}/\sqrt{(T_\mathrm{e}+T_\mathrm{i})/m_\mathrm{i}}]$.

3.2.2. *Cylindrical probes.*

A. Low ion temperature ($T_\mathrm{i}/T_\mathrm{e} \ll 1$)

Hudis and Lidsky [3] set up a fluid model for a 1D cylindrical probe neglecting the influence of the electric field on the ion motions and obtained the ion saturation current difference in terms of the drift velocity, which is limited to collisionless high-density plasmas with $v_\mathrm{d} \ll v_\mathrm{th}$ and $T_{\mathrm{i}\infty} \ll T_\mathrm{e}$, adopting a similar idea of Mott-Smith and Langmuir [72]. As for the unmagnetized plasmas ($\rho_\mathrm{i} > a$), where ρ_i is the ion gyro-radius and a is the probe radius, the ion sheath current is given by Bohm's formula, $J_\mathrm{s} = 0.61 q n_\infty C_\mathrm{s}$.

Assuming that the difference in the potential drops at the downstream and upstream sides is caused by the drift velocity and can be given by the ion energy conservation, the ion fluid velocity is obtained from the free-fall motion and almost cold plasma approximation around the sheath boundary:

$$V(z) = \left[-\frac{2e\phi}{m_\mathrm{i}} + (v_\mathrm{th} \pm v_\mathrm{d})^2\right]^{0.5},$$

where v_{th} is the ion thermal velocity given as $\sqrt{T_i/m_i}$, and v_d is the drift velocity. The ion density within the sheath is calculated as $n_i = J_s/qV(z)$, and the electron density is given by the Boltzmann relation like equation (14). To these equations, applying the boundary conditions at the sheath as $n_i(z_s) = n_e(z_s)$, and $dn_i/d\phi\big|_{z_s} = dn_e/d\phi\big|_{z_s}$, then flux ratio is calculated as

$$R = \frac{J_{up}}{J_{dn}} = \exp[K M_\infty], \tag{97}$$

where $K = 4\sqrt{\tau}$, where $\tau \equiv T_i/T_e$ and the velocity is normalized by $V_s(\equiv \sqrt{T_e/m_i})$.

Hutchinson [73] showed that this model is neither physical nor consistent, but data of Hershkowitz and Oksuz [14, 74] suggested that this model can be used to fit the data of only very low ion temperatures with 1D ion motion through measurement of potential in the wake region. However, $K(\tau = 0)$ leads to a very large Mach number or $R = 0$ regardless of M_∞, which is unphysical.

B. High ion temperature ($T_i/T_e > 1$)

Shats *et al* [125] used a MP ($a \approx 3$ mm $\rho_i = 20$–50 mm) to measure the poloidal and toroidal velocities of the H-1 heliac ($B < 0.2$ T, $n_e \sim 10^{12}$ cm^{-3}, $T_e = 8$–30 eV, $T_i = 30$–120 eV). They adopted the formula of Hudis and Lidsky even for the case of $T_i/T_e > 1$, and normalized the flow velocity by $C_s(= \sqrt{(T_e + T_i)/m_i})$ instead of $V_s(= \sqrt{T_e/m_i})$, so their calibration factor is larger than that of Hudis and Lidsky by a factor of $\sqrt{(T_e + T_i)/T_i}$.

Solomon and Shats [126] derived a formula of a cylindrical MP for a small drift flow ($v_d/v_{th} \leqslant 0.4$) in the H-1 heliac. They considered that ions far from the probe have initial velocity as the vector sum of the thermal velocity and drift velocity, and they calculated the average velocity of ions traveling toward the probe as

$$\langle (V(z)^{\pm})^2 \rangle \approx v_{th}^2 \pm \frac{4 v_{th} v_d}{\pi}, \tag{98}$$

where the positive sign is for the upstream (u) flow and negative is for the downstream (d). Then the sheath potential comes from the energy conservation

$$\phi_s^{\pm} = \frac{m_i}{2e}[\langle (V(z)^{\pm})^2 \rangle - C_s^2], \tag{99}$$

which leads to the sheath current ratio as

$$R = \exp\left[\frac{e}{T_e}(\phi_s^+ - \phi_s^-)\right] \approx \exp\left[v_d \frac{4 m_i v_{th}}{\pi T_e}\right] = \exp[K M_\infty], \tag{100}$$

where $K \equiv 4\sqrt{\tau}/\pi$.

Figure 34 shows the summary of the current ratios with flow velocity according to various models for unmagnetized plasmas. As $T_i/T_e \to 0.1$, the curves of Hutchinson, Chung, Hudis, and Mott-Smith get closer for lower M_∞, while the curves of Hutchinson, Chung, Solomon and Oksuz get closer as $T_i/T_e \to 1.0$, indicating why a certain model has its own, but narrow region of applicability (also refer to table 2). Although one needs independent calibration for the wide range of ion temperatures, the models of Hutchinson (spherical probe) and Chung (planar probe) would produce consistent results with proper physical models.

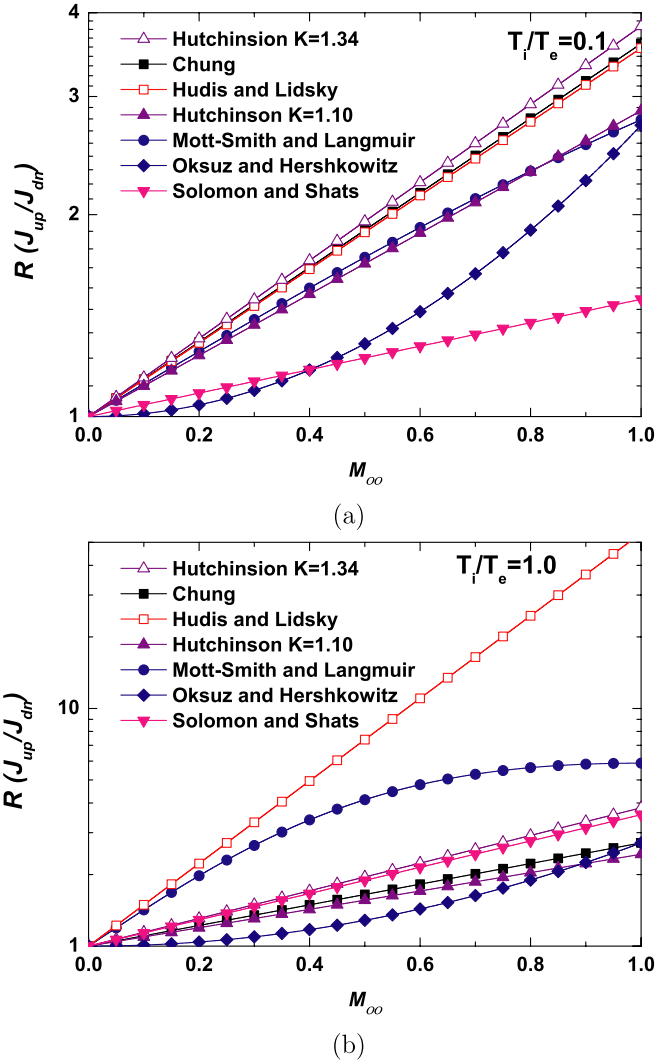

Figure 34. Ratio of up- and down-stream currents of the UMPs. (*a*) $T_i = 0.1T_e$, and (*b*) $T_i = T_e$. For low ion temperatures ($T_i/T_e = 0.1$), models of Hutchinson, Chung and Hudis produced similar results, while those of Hutchinson, Chung and Oksuz and Solomon produced similar values for higher ion temperatures ($T_i/T_e = 1.0$). This indicates that models of Hutchinson (PIC, spherical) and Chung (kinetic, planar) show (better) consistent result for a wide range of ion temperatures.

3.3. PMP in unmagnetized plasmas

For a high pressure plasma (0.32–3.68 Torr), Johnson and Murphree measured the Mach number $(v_d/(2T_i/m_i)^{\frac{1}{2}})$ as 1.12 and 1.18 from the ratios of 1.54 and 1.59 using a PMP with assumption of ion temperature equal to the gas temperature. They adopted the theory of Kanal [91], and the ratio of ion currents for PMP is given as

$$R_\perp \equiv \frac{I_\perp^*}{I_\parallel^*} = \frac{2}{\pi}\exp\left[-\frac{M_\infty^2}{2\tau}\right]\sum_{n=0}^{\infty}\left[\left(\frac{M_\infty}{\sqrt{2\tau}}\right)^n/n!\right]^2 \Gamma\left(n + \frac{3}{2}\right), \tag{101}$$

where $\tau \equiv T_i/T_e$, $M_\infty \equiv v_d/\sqrt{T_e/m_i}$. Here $I_\perp^*(I_\parallel^*)$ is the ion current collected by a cylindrical probe perpendicular(parallel)

Table 2. Calibration factor K for Hutchinson, Chung, Hudis and Lidsky, Solomon and Shats, and Oksuz and Hershkowitz ($0 \leqslant M_\infty \leqslant 1.2$).

T_i/T_e	Hutchinson	Chung	Hudis and Lidsky	Solomon and Shats	Oksuz and Hershkowitz
0.1	1.05	1.28	1.26	0.40	M_∞
0.2	1.10	1.24	1.79	0.57	M_∞
1.0	0.89	1.05	4.0	1.27	M_∞
2.0	0.67	0.91	5.66	1.80	M_∞

to the plasma flow (i.e. the longitudinal axis of the probe is perpendicular(parallel) to the plasma velocity vector), which is different from those of others. This can be derived without the presheath effect using the ion current collected by the cylindrical probe for the attractive potential, i.e. strongly negative bias. Johnson and Murphree's method produces a large Mach number even from a very small ratio of $I^*_\perp/I^*_{||}$. If one considers a usual error of probe measurement of about 20%, their method draws a large uncertainty ($|I^*_\perp/I^*_{||}|_{\max} \simeq 1.2/0.8 \simeq 1.5$ for $I^*_\perp \simeq I^*_{||}$).

To determine the plasma velocity of an atmospheric torch (15 kW, $I = 500$ A, $V = 30$ V), Chung *et al* [38] used a probe set combining a regular MP and a perpendicular Mach probe (PMP), which consists of two cylindrical electric probes, which are mutually perpendicular. Without reliable theories, they adopted the existing collisionless theories for MPs, by Chung [78], Hudis and Lidsky [3] and Mott-Smith and Langmuir [72], and a mathematical formula by Johnson and Murphree [90] based on the theory of Kanal [91] for PMPs. They compared the absolute flow speed ($\simeq$1700 m s^{-1}) deduced by the PMP using the model of Johnson and Murphree with those deduced by (parallel) MP. For the analyses of (parallel) MP, they adopted the average value ($K = 1.6$) of three calibration factors estimated by three collisionless theories for MP, which gives the speed as $\simeq$910 m s^{-1}.

As a suggestion to measure ion flows in a positive column or in discharges with dust particles by using electric probes, Stangeby and Allen [94] set up a fluid model for a cylindrical probe in a flowing plasma assuming cold ions ($T_i = 0$), collisionless plasmas, and quasi-neutrality. They adopted the isothermal electrons, i.e. $n_i = n_e = n_\infty \exp[e\phi/T_e]$, and continuity equations

$$\frac{\partial n_i}{\partial t} + \nabla \cdot (n_i \vec{V}) = 0, \tag{102}$$

where $\vec{V}$ is the velocity of the fluid, which is defined as $\vec{V} = -\nabla\varphi$ (φ is the velocity potential). Then, they solved the equation for the normalized velocity potential ($\Phi = \varphi/\sqrt{T_e/m_i}$) in terms of Mach number ($M_\infty \equiv v_d/\sqrt{T_e/m_i}$), radial ($\rho = r/r_0$) and azimuthal angle ($\theta$) with the boundary condition at the surface as $\partial\Phi/\partial n = 1$, indicating the highly absorbing surface, where n is measured normal to the surface. They obtained the stagnation density as $n_{st} = n_\infty \exp[M^2_\infty/2]$, where the normalized sheath potential (ψ_s) is given as ($M^2/2$), and n_{st} is larger than the unperturbed density. The sheath density is

$$n_s = 0.61 n_\infty \exp[-M^2_\infty(4\sin^2\theta - 1)/2], \tag{103}$$

where θ is the angle between the incident direction of ions and z, so that the ratio of ion currents collected at $\theta = 0$ (normal incidence) and $\pi/2$ (grazing incidence) is

$$R_\perp = J(0)/J(\pi/2) = \exp[2M^2_\infty]. \tag{104}$$

Kuriki and Inutake [92] measured the super-Alfvénic and supersonic flow produced by a magneto-plasma-dynamic arc (MPDA) jet using a pair of plane Langmuir probes whose surfaces are parallel and perpendicular to the flow. They used Stangey's formula for the subsonic flow analysis, but with reduced K values as $\exp[{M_\infty}^2/2]$ not $\exp[2{M_\infty}^2]$ to match R at $M_\infty = 1$, and used the following formula for the supersonic flow:

$$R_\perp = \frac{J_\perp}{J_\parallel} = \frac{e n_\infty v_d}{0.61 e n_\infty (T_e/m_i)^{0.5}} = 1.65 M_\infty. \tag{105}$$

The parallel ion saturation current is just the Bohm current density and the perpendicular current density is just the unperturbed current density, which is lacks physics.

Ando *et al* adopted the idea of Kuriki and Inutake for the measurement of supersonic flow in a magneto-plasma-dynamic arc (MPDA) jet using an MP and PMP. However, they switched the parallel and perpendicular current densities by using a different shape and position of two probes, since their perpendicular probe only collects particles at grazing angle, and the parallel probe collects the particles at the normal angle to the upstream side. For supersonic flows, $1.4 < M_\infty < 2.3$, they introduced a semi-empirical formula including the effect of ion temperature ($T_i > T_e$): $R_\perp = J_\parallel/J_\perp = \exp[k(M_\infty/\sqrt{1 + T_i/T_e})^{1/k}]$, where $k = 1.1$ for $T_i = 2T_e$ by fitting their data to the result of the PIC simulation of Hutchinson [77]. To fit their data to the result of the PIC simulation, they used the calibration factor ($K = 1.34$) of the PIC simulation for the case of supersonic flow (for $M_\infty > 1.5$, $0.7 \leqslant K \leqslant 1.5$, and $K \approx 1.34$ at $T_i/T_e = 2$). For $M_\infty < 1.5$, the calibration factor becomes smaller (see table 1 and figure 30), and the specific heat ratio of ions (γ_i) was chosen as 5/3, which was found to be 1.0–1.2 later [107]. This may cause the error of $\sim$16% in deducing Mach number.

Figure 35 shows the overall trend of $R_\perp = J_\perp/J_\parallel$ with M_∞. Even for plasmas with high collisionality, and supersonic flow in unmagnetized plasmas, they often used PMP to measure the parallel flow velocity. Although the wide spread of the ratio of current densities for M_∞ indicates that there is no prevailing theory and requires an independent calibration, the idea of Kuriki and Inutake seems to be plausible for the deduction of the supersonic flow velocity: the formation of the Bohm velocity at the sheath of the normal surface of the probe in the upstream region would not occur for the supersonic flow; the formation of the sheath itself is questionable, unless the kinetic energy of the supersonic fluid is lost during the

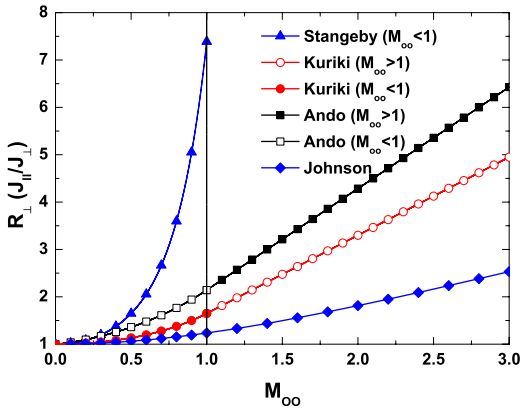

Figure 35. Ratio of parallel to perpendicular current densities in the unmagnetized plasmas.

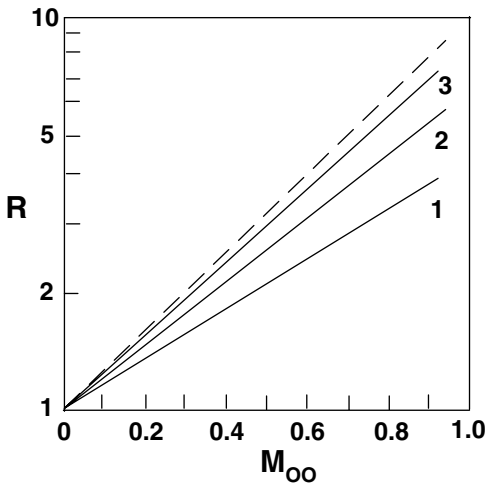

Figure 36. Effect of ionization. Sheath current density ratios shown for $\sigma_i = 0.1$ (line 3), 0.3 (line 2) and 0.5 (line 1) with $T_{i\infty} = T_e$. The broken line is from the case of $\sigma_t = 0.0$ (no ionization); $\sigma_t + \sigma_i = 1.0$ is applied to all the lines [7].

passage to the probe. It would be plausible to assume that all the particle are to be collected without being influenced by the presheath potential drop, if there is any. Hence the current density of the upstream supersonic flow would be enu_d.

4. MP analyses in special cases

4.1. Effect of collisions on MP analysis

Along the magnetized presheath formed by the probes, not only the diffusive ion source in the magnetized presheath with Boltzmann electrons [12], but also other sources such as charge exchange [79], ionization [80, 81] and recombination [82] are important in the SOL of diverted tokamaks.

4.1.1. Effect of electron–neutral collision: ionization. Since ions are born within the presheath due to electron–neutral collisions, with a velocity given by the local ion temperature, there is no way where the ion drift velocity outside the presheath can be introduced. The ion distributions (hence their moments) along the presheath are affected more strongly by the source shapes than the characteristics of the presheath (e.g. collisional or collisionless). If the ionization mean free path is shorter than the characteristic length of the ion flux tube, the total source term of the Boltzmann transport equation (equation (12)) becomes

$$S_f(z, v) = \sigma_t S_t + \sigma_i S_i = \sigma_t S_t + \langle \sigma v \rangle_{ion} n_e(z) f_n(z, v), \qquad (106)$$

where σ_t and σ_i are the ratios of each contribution ($\sigma_t + \sigma_i$), $\langle \sigma v \rangle_{ion}$ is the ionization rate, n_e is the electron density and f_n is the distribution of neutral particles. The choice of σ_i is related to the normalization factor, i.e. the source strength or the ion collection length. Assuming f_n to be Maxwellian with neutral temperature equal to ion temperature outside the presheath, if $n_e(z)\langle \sigma v \rangle_{ion} \propto |v|$, Chung [109] recover the same source term as Emmert *et al* [60], and if $\langle \sigma v \rangle_{ion} =$ constant, that of Bissel and Johnson is recovered. For transport source we choose $\alpha = 1.0$ (strong viscosity), and for the ionization term Chung and Hutchinson [7] choose Bissel and Johnson's model [71] since it is considered as more physical for the ionization source, although it produces a less physical ion distribution at the end of the ion flux tube. The combination of transport with Bissel and Johnson's model does not produce a Maxwellian at the end of the ion flux tube, while introduction of a modified Bissel type does. Figure 36 shows the relation of current density ratio with the drift velocity. K in $\exp(K M_\infty)$ is given by 1.07, 1.35 and 1.56 for $\sigma_i = 0.5, 0.3$ and 0.1, respectively. The overall trend is the same as the strong viscosity case, but the slope of the ratio (K) decreases with ionization. So a higher drift velocity is expected for the same current ratio measurement if we choose a model to which ionization is added (or less viscous).

In experiments, ionization occurs in the presheath and outside the presheath, but in the model, it is assumed that the plasma parameters are uniform outside the presheath (i.e. $\partial f_\infty / \partial z = 0$). This seems to be inconsistent with strong ionization. However, it is inconsistent not because Chung assumed uniform parameters outside the presheath, but because he included only the ionization source within the presheath. So, if one adds the additional ion flow into the presheath from (strong) ionization along with a cross-field transport source, then Chung's model might be a reasonable one, although it would be very difficult to find the actual ionization ratio due to lack of information on neutral density and the ratio of ion inflow by strong ionization to that by transport. Yet, for sufficient and consistent analyses more work is necessary.

4.1.2. Effect of electron–neutral collision: recombination and ionization. Recombination and charge exchange processes in fusion edge plasmas to achieve a detached plasma is important for the reduction of particle and heat fluxes onto the divertor targets. MAR processes induced by hydrogen or hydrocarbon puffing recently have shown the capability of contributing to the volume recombination [82, 83], along with electron–ion recombination processes characterized by radiative and three-body recombinations. In particular, hydrogen-MAR process can play a major role in cooling the plasma for low electron temperatures of 1–3 eV [84]. The conditions for each process to be effective strongly depend on the electron temperature and the electron density.

As for the recombination, there are two cases:

$$S_r = -\langle \sigma v \rangle_{rec} n_e f_i(v),$$

for electron–ion recombination (EIR), which is dominant for low temperatures ($T_e < 2$ eV) in hydrogen plasmas, and

$$S_r = -\langle \sigma v \rangle_{rec} n_e f_M(v),$$

for MAR, which exists over a wide range of electron temperatures in hydrogen plasmas. Here $f_M(v)$ is the distribution function of molecular ions. Dominant hydrogen-MAR processes are (a) dissociative attachment (DA: $H_2 + e \rightarrow (H_2^-)^* \rightarrow H^- + H$) followed by mutual neutralization (MN: $H^- + H^+ \rightarrow H + H^*$), (b) ion conversion (IC: $H_2 + A^+ \rightarrow (AH)^+$) followed by dissociative recombination (DR: $(AH)^+ + e \rightarrow A + H^*$, and (c) charge-exchange ionization (CX: $H_2 + A^+ \rightarrow H_2^+ + A$) followed by dissociative recombination (DR: $H_2^+ + e \rightarrow H + H^*$. With negligible negative hydrogen ions (neglecting channel (a)), DR prevails, yet channel (b) is more dominant than channel (c) [84]. Hence the reaction rate of hydrogen MAR can be approximated as

$$\begin{aligned}\langle \sigma v \rangle_{MAR} &\approx \langle \sigma v \rangle_{MN \leftarrow DA} + \langle \sigma v \rangle_{DR \leftarrow IC} + \langle \sigma v \rangle_{DR \leftarrow CX} \\ &\approx \langle \sigma v \rangle_{DR \leftarrow IC},\end{aligned}$$

where A is a neutral atom such as H, He or Ar, since some portion of $(AH)^+$ is dissociated into A and H^* after recombining with electron. Here the second term on the left-hand side is larger than the third, although for hydrogen plasmas they are not distinguishable [84]. Since molecular ion density ($n_M \equiv n_i((AH)^+)$) is increased by IC, while it is decreased by DR, the contribution of DR to MAR can further be approximated as

$$\begin{aligned}&\langle \sigma v \rangle_{DR \leftarrow IC} n_e f_M \\ &\quad \approx (1 - \delta) \langle \sigma v \rangle_{DR} ((AH)^+ + e \rightarrow A + H^*) n_e f_M,\end{aligned}$$

where δ ($\equiv \langle \sigma v \rangle_{non\text{-}IC} / \langle \sigma v \rangle_{IC}$) is the ratio of the non-IC process among IC, so that $1 - \delta$ is the probability that DR occurs after IC. For an example of hydrogen-MAR molecules, $\langle \sigma v \rangle_{MAR} \approx 3 \times 10^{-10}$ cm^3 s^{-1}, assuming $n(H_2)/n_e \approx 0.1$ and $T_e \approx T$ (heavy particles) ≈ 1 eV ($T_e < 4$–5 eV) and $n_N \approx n_i$, indicating that the main channel of plasma recombination is the dissociative recombination of molecular ions for $10^{14} < n_e < 10^{15}$ cm^{-3} [82, 127]. The Boltzmann equation with cross-field transport, recombination and ionization sources becomes [85]

$$\begin{aligned}v_z \frac{\partial f_i}{\partial z} + \frac{q}{m} E_z \frac{\partial f_i}{\partial v} &= S_t + S_a \qquad (107) \\ &\approx W \left[\alpha (f_{i\infty} - f_i) + (1 - \alpha) \left(1 - \frac{n}{n_\infty} \right) f_{i_\infty} \right] \\ &\quad + n_e \left[-K_M f_M - K_E f_i + K_I f_n \right],\end{aligned}$$

where f_M, f_i, f_n, K_M, K_E and K_I are the distributions and reaction rates of molecular ions, atomic ions, atomic neutrals, the reaction rates of MAR ($\equiv \langle \sigma v \rangle_{MAR}$), electron–ion recombination ($\equiv \langle \sigma v \rangle_{EIR}$), and ionization ($\equiv \langle \sigma v \rangle_{ion}$), respectively, and

$$S_a = n_e \left[-K_M f_M - K_E f_i + K_I f_n \right].$$

Assuming the same temperature of atomic neutrals as that of molecular ions, i.e. $T_N = T_M \equiv \tau T_i$, and $m_N = m_i$, the distribution functions of atomic neutrals ($f_N \equiv f_{N\infty}$) is given as

$$f_n(v) = \nu n_\infty \sqrt{m_i / 2\pi\tau T_i} \exp[-m_i v^2 / 2\tau T_i]$$

and $\nu_1 \equiv n_N / n_\infty$, while $f_{i\infty}$ is the shifted Maxwellian ion distribution.

By taking moments of equation (107) and using the dimensionless parameters such as $L \equiv C_s / W(z)$, $y \equiv \int [W(z)/C_s]\, dz$, or $y \equiv zW/C_s$, $M \equiv v/C_s$, $n \equiv n_i/n_\infty$, these become the following dimensionless equations:

$$M \frac{dn}{dy} + n \frac{dM}{dy} = 1 - n + k_i n - k_r n^2, \qquad (108)$$

$$\frac{dn}{dy} + nM \frac{dM}{dy} = (M_\infty - M)[1 - (1 - \alpha)n] - k_i n M, \qquad (109)$$

where k_i, k_m, k_e and k_r are the normalized ratios of ionization ($\equiv (K_I Z n_N a / C_s)(L/a)$), MAR ($\equiv (K_M Z n_M a / C_s)(L/a)$), electron–ion recombination ($\equiv (K_E Z n_\infty a / C_s)(L/a)$) and total recombination ($\equiv k_m + k_e$) with respect to the cross-field transport contribution, respectively, and n_M is the density of relevant molecular ions. After some arrangements, one can get the following equations for dn/dy and dM/dy:

$$\frac{dn}{dy} = \frac{M_\infty - 2M - (M_\infty - M)(1 - \alpha)n + (1 + k_r n) n M}{1 - M^2}, \qquad (110)$$

$$\begin{aligned}\frac{dM}{dy} &= [1 - n - M(M_\infty - M)[1 - (1 - \alpha)n] \\ &\quad + k_i n (1 - M^2) - k_r n^2][n(1 - M^2)]^{-1}, \qquad (111)\end{aligned}$$

Dividing equation (110) by equation (111) leads to

$$\begin{aligned}\frac{1}{n} \frac{dn}{dM} &= [M_\infty - 2M - (M_\infty - M)(1 - \alpha)n + (1 + k_r n) n M] \\ &\quad \times [1 - n - M(M_\infty - M)[1 - (1 - \alpha)n] \\ &\quad + k_i n (1 - M^2) - k_r n^2]^{-1}. \qquad (112)\end{aligned}$$

Figure 37 shows the normalized density (n) profiles in terms of normalized fluid velocity (M) for $\alpha = 1$ and $M_\infty = 0.4$ with different ionization contributions ($k_i = 0.001$, 0.1, 1.0) with respect to the cross-field transport contribution. Both results by solving equations (110) and (111), and equation (112) are exactly matched for this case. However, there are cases with $n(M) > 1$, which seems to be unphysical for the larger ionization ($k_i \geqslant 0.1$), indicating that even the model combining ionization source with the Hutchinson collisionless model can produce unphysical solutions, while the kinetic model does not [7]. Since this may be too early to maintain this argument, we need to further explore the singularity problem in 1D fluid approximation for flowing magnetized plasmas.

Figure 38 shows the ratio of ion saturation currents ($R \equiv J_{up}/J_{dn}$) in terms of ionization and recombination as an application of Chung's model. For the small contribution, say less than 1% for ionization and much less than 0.1% for recombination, there is no visible change in R. Larger ionization contribution ($k_i \geqslant 0.01$) makes R decreased with

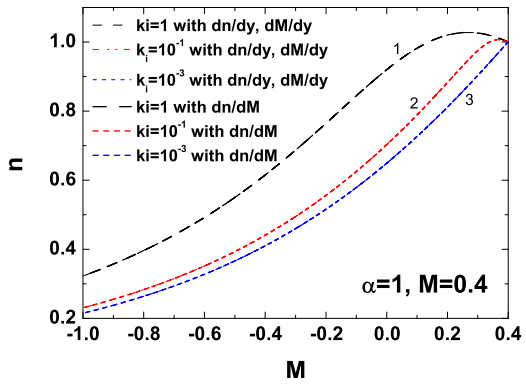

Figure 37. Normalized density (n) profiles in terms of normalized fluid velocity (M) for $\alpha = 1$ and $M_\infty = 0.4$ with different normalized ionization contributions ($k_i = 0.001$(line 3), 0.1 (line 2), 1.0 (line 1)) with respect to the cross-field transport contribution [85]. $n(M)$ is obtained by different calculations: (i) by solving dn/dy, dM/dy to obtain $n(y)$ and $M(y)$. Then plot $n(y)$ versus $M(y)$. (ii) By solving dn/dM as a conventional method. Both methods produce the same results (normalized ionization ratio $k_i = \langle\sigma v\rangle_{ion} Z n_N L/C_s$, normalized recombination ratio $k_r = (\langle\sigma v\rangle_{molecule} + \langle\sigma v\rangle_{e-i}) Z n_\infty L/C_s$).

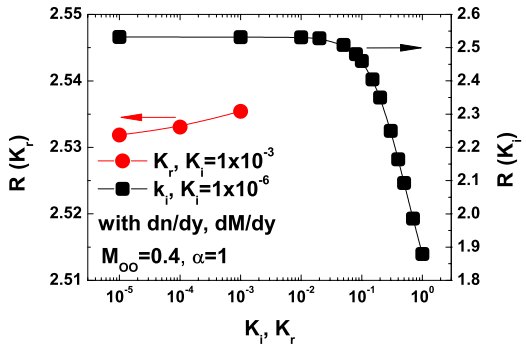

Figure 38. Ratio of ion saturation currents ($R \equiv J_{up}/J_{dn}$) of the magnetized plasma with $\alpha = 1$ (strong viscosity) and $M_\infty = 0.4$ in terms of the normalized ionization rate (k_i) and recombination (k_r). The solid circle is for the case of recombination with a fixed ionization ratio, and the solid square is for the case of ionization with fixed recombination [85].

the same Mach number (M_∞) indicating the decrease in the calibration factor ($K = \ln[R]/M_\infty$), which leads to a possible underestimation of Mach number with the same measured ratio (R), while R increases with recombination, although we cannot handle the case of somewhat larger contribution of recombination, say, larger than $k_r \geqslant 10^{-3}$ due to singularity of our fluid model or due to unknown numerical instability in our numerical code written in the Visual C^{++} and LabView program. There might be a solution for this if one would replace the atomic/molecular volume source of equation (107) with

$$S_a = -K_M n_e f_{M\infty}(v) - K_E n_e f_{i\infty}(v) + K_I n_e f_{N\infty}(v),$$

where ∞ indicates the unperturbed values.

4.1.3. Effect of ion–ion collisions. Clements *et al* [128] tried to get ion current of flowing plasmas by matching the velocity of the probe and (plasma) flame. Assuming diffusion dominant processes and thick sheath approximation, their model was applied to a spherical probe for a potassium plasma flame with the following conditions: $T_n \approx T_i \approx 1500$–$2300$ K, $n_e = 10^9 \sim 10^{12}\,\mathrm{cm}^{-3}$ and measured T_e. To analyze the experimental data, they used a time-dependent continuity equation without a volume source in spherical geometry with the ambipolar diffusion coefficient D_a:

$$\frac{\partial n}{\partial t} = -\nabla\cdot(n\vec{V}) = -D_a\nabla^2 n.$$

By integrating the density over the probe's residence time in the flame, they obtained the probe current for the thick sheath case as

$$I_i(t) = 4\pi(b-a)n_\infty\mu_i(T_e+T_i)\left(1+\frac{(b-a)}{[\pi\mu_i(T_e+T_i)t/e]^{0.5}}\right),$$

where $(b-a)$ is the sheath thickness, t is the residence time and μ_i is the ion mobility. The residence time is the time required for the probe to travel from the point of entry into the flame to the zero probe-flame velocity. Their model may be relevant for small electric Reynolds numbers ($R_e \ll 1$) with very low temperatures and very slowly moving plasmas ($v_d \ll C_s$). To apply their model to atmospheric plasmas, one has to know the ion mobility, ratio of ion to electron temperatures, and guarantee the residence time to match the probe speed to the plasma velocity, and yet it should be done for sufficient time to accomplish diffusion equilibrium. They also used the steady-state fluid equations for a cylindrical probe with a thin sheath for $v_d \ll C_s$ for a convection dominant ($\gg$ diffusion) case [129]. They assumed a floating(Neumann) boundary condition at the sheath, i.e. $E \to 0$ as $V \to 0$, which indicates that there is no transition layer between the sheath and the main plasma. This does not seem to be realistic, since most collisionless models and experiment indicate the existence of a transition layer or presheath whose size is the order of the probe or of the collecting object.

They showed no clear distinction between the ram and the wake side in terms of collected currents, instead they presented the total ion current for very large probe bias voltages ($V_p/T_e \approx 10^2$–10^3), which is given as

$$I_i = 5.3(en_e v_d)^{3/4}\phi_b^{1/2}[\mu_i\epsilon_o a]^{1/4},$$

and showed no tendency toward saturation at higher potentials. To get the Mach number from this, the following can be given:

$$M_\infty \equiv \frac{v_d}{\sqrt{T_e/m_i}} = \frac{0.11}{e\sqrt{T_e/m_i}(\mu_i\epsilon_0 a)^{1/3}}\frac{I_i^{4/3}}{n_e\phi_b^{2/3}}.$$

MacLactchy *et al* [130] showed that the thin sheath model of spherical probe is valid for $96 < R_e < 720$ and for $(b-a)/a < 0.5$. They conjectured that the time needed for ions to diffuse back into the vacant region is much longer than the flow time in the downstream (wake) side; if the plasma is highly collisional, then the entrained plasma carried very little charge into the probe. As for the plasma flows through the sheath, the probe extracts and drives away nearly all the charge. The probe and its wake are surrounded by a layer of fluid, which contains almost no charge. So one can expect

the higher ratio than the collisionless case for the same drift velocity of the plasma, i.e. the deduced Mach number with the collisionless model for the collisional flowing plasmas is overestimated. The interesting point is that they used the sheath thickness proportional to $\phi_b^{1/2}$, which is similar to the ion matrix sheath, while the collisional sheath is proportional to $\phi_b^{2/3}$ for the constant collision frequency model [131].

Smy gave an intensive review on the analysis of probe theory in collisional plasmas [132]. He adopted the steady-state ion fluid equation as

$$J_i = D_i \mathrm{d}n_i/\mathrm{d}r + \mu_i n_i \mathrm{d}V/\mathrm{d}r,$$

for a spherical probe, and the Boltzmann electrons for a highly negative applied voltage. However, he assumed a linear form of density variation:

$$n_e = n_i = n_0(1 - a/r) \rightarrow \phi = (T_e/e)\ln(1 - a/r),$$

for the thin sheath approximation. He also assumed the ion temperature profile to get the mobility profile. Then he got the ion currents in terms of electric Reynolds number ($R_e = 2ev_d a/\mu_i T_0$) and Damkohler number ($D = en_0\lambda_D/\mu_i T_0$) for four different dominant conditions: diffusion, convection, recombination and electric field convection. Here T_o is the bulk temperature of electrons and ions.

Models of MacLactchy and Smy need more information to deduce the Mach number, since they do not provide the direct relation between the current and the flow.

As for the effect of collision on the probe theory, one has to be cautious for the types of collisions (ion–neutral, ion–ion, electron–ion, electron–electron) and regions (sheath or presheath) to be applied. Ion–neutral collision along the presheath (or transition region) is totally different from i–i collision e–i/e–e collisions within the sheath, where the mobility is to be introduced.

4.1.4. Effect of ion–neutral collisions. The collisional fluid model on a Mach probe is expanded from Chung's model by adding the collision term and taking the moment as follows [162, 163]:

$$n_i \frac{\mathrm{d}V}{\mathrm{d}z} + V_z \frac{\mathrm{d}n}{\mathrm{d}z} = \nu_{iz} n_i + \frac{v_{th}}{a}(n_\infty - n_i), \tag{113}$$

$$m_i n_i V_z \frac{\mathrm{d}V_z}{\mathrm{d}z} = enE - T_i \frac{\mathrm{d}n}{\mathrm{d}z} - m_i n_i(\nu_{iz} + \nu_m)(V_z - v_d) + m_i \frac{v_{th}}{a}(n_\infty - n_i)(v_d - V_z), \tag{114}$$

where ν_{iz} and ν_m are the ionization collision frequency and momentum collision frequency, respectively, and the electron is assumed to follow the Boltzmann relation. Then the non-dimensional forms of the parameters are given as follows: $n = n_i/n_\infty$, $x = z/a$, $M = V_z/C_s$, $V_t = v_{th}/C_s = \sqrt{T_i/(T_e + T_i)} = \sqrt{\tau/(1+\tau)}$, $\mu = \nu_m a/C_s$, and $\sigma = \nu_{iz} a/C_s$. In terms of these parameters the equations can be written as

$$\frac{\mathrm{d}n}{\mathrm{d}x} = \frac{M_\infty - 2M}{1 - M^2}(1 - n)V_t - \frac{nM}{1 - M^2}(2\sigma + \mu) + \frac{nM_\infty}{1 - M^2}(\sigma + \mu), \tag{115}$$

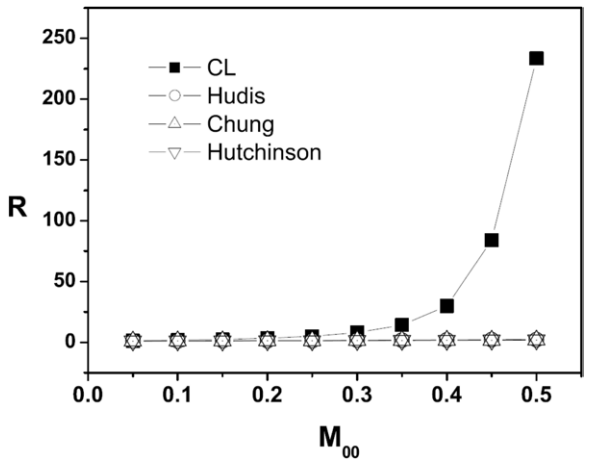

Figure 39. Theoretical ratios of ion saturation current for various models with Mach numbers ($M_\infty = v_d/\sqrt{(T_e + T_i)/m_i}$. Solid squares = collisional fluid model $K = 6.57(1 - 1.5M_\infty + 5.6M_\infty^2)$, open squares = fluid model of Hudis and Lidsky ($K = 1.79$), down triangles = kinetic model of Chung ($K = 1.24$) and upper triangles = PIC model of Hutchinson ($K = 1.34$). Due to a large difference between collisional and collisionless models the results of the last three models appear to coincide with each other although there is a large difference [162].

$$\frac{\mathrm{d}M}{\mathrm{d}x} = \frac{M^2 - M_\infty M + 1}{1 - M^2}\frac{(1 - n)}{n}V_t + \frac{(1 + M^2)\sigma + \mu M^2 - (\sigma + \mu)M_\infty M}{1 - M^2}, \tag{116}$$

which leads to the following as Stangeby tried:

$$\frac{\mathrm{d}n}{\mathrm{d}M} = [(M_\infty - 2M)n(1 - n)V_t - Mn^2(2\sigma + \mu) + M_\infty n^2(\sigma + \mu)][(M^2 - M_\infty M + 1)(1 - n)V_t + (1 + M^2)\sigma n + \mu n M^2 - (\sigma + \mu)M_\infty n M]^{-1}. \tag{117}$$

There would be some singularities in equation (78) in the range of interest ($-1 < M < 1$) and equation (78) cannot be used for the calculation of ratio for the MP. In order to avoid these singularities, we solved the full equation set ($\mathrm{d}n/\mathrm{d}x$ and $\mathrm{d}M/\mathrm{d}x$), and compared with that by a reduced equation ($\mathrm{d}n/\mathrm{d}M$) showing the singularity. They evaluated the data with plasma parameters such as $T_e = 4\,\mathrm{eV}$ and $n_e = 1.6 \times 10^{13}\,\mathrm{cm}^{-3}$ at the plasma center, using a MP whose size is $a = \sim 2\,\mathrm{mm}$. The experimental conditions for MP and normalized frequency are the following: Ar gas, pressure of 50 Torr, power of 800 W, $n_e = 1.5 \times 10^{13}\,\mathrm{cm}^{-3}$, $T_e = 4\,\mathrm{eV}$, $T_i = 0.8\,\mathrm{eV}$, $\sigma = 25$ and $\mu = 350$. Based on these conditions, one can find that the sheath is collisionless, and the presheath is collisional: $\lambda_D = 0.5\,\mu\mathrm{m}$, $\lambda_{i-n} = 60$–$400\,\mu\mathrm{m}$, $\lambda_{i-i} \sim 1000\,\mu\mathrm{m}$. Figure 39 shows the ratio of current densities including ion–neutral collisions comparing those without collisions. A fluid model including ion–neutral collisions produced 5 times reduced values than by collisionless kinetic, fluid and PIC models, i.e. $1\,\mathrm{km\,s^{-1}}$ versus $5\,\mathrm{km\,s^{-1}}$. Recent experiments of helium plasma with different neutral pressure also showed similar result [163].

Hutchinson and Patacchini [164] generalized their PIC model by adding the effect of charge-exchange in a stationary

plasma, so they could not show the relation of the calibration factor with the collision rate, but their model has the ability to include the case of drifting plasmas. For ion–neutral collisions, one could expect a smaller Mach number to be deduced than in the collisionless case from the same ratio of the ion saturation current densities, since momentum loss of ions to the neutrals is quite large due to the fact that (i) ion temperature is usually higher than that of neutral, (ii) neutral density is much higher than that of ion, and (iii) masses of ions and neutrals are similar. Hence the energetic ions are losing their energies severely, which leads to the decrease of average ion energy compared with the collisionless case.

4.2. Effect of multiple ions on MP analysis

LIF measurements along the presheath of two ion species in unmagnetized plasmas are shown by the Hershkowitz group that heavier ions reach the sheath edge faster than their Bohm velocity and lighter ones move slowly [40, 133–136], satisfying Riemann's generalized Bohm condition [137] due to mobility limitation [136]: $1 \geqslant \sum_j (n_{j0}/n_{e0})(c_j^2/v_j^2)$, where n_{j0}/n_{e0} is the fractional density of ion species, c_j Bohm velocity of individual species, v_j is the drift velocity of individual species at the sheath boundary, while each species arrive at the sheath with the sound speed of the system calculated in the bulk of the multiple ion species plasma [133]. Moreover, ions reach the Bohm velocity at the sheath edge [133] in single species ion plasmas, which is the same as the phase velocity of the bulk region.

Since the Bohm condition of each species is different, the flow along the presheath will be different, and the remaining question would be how to interpret the MP data. Although there has been no clear answer to this, but one can refer to the method of Samir *et al* [2], who used the effective mass and effective electron temperature to fit the data of hydrogen and helium ions collected by satellites of ionosphere and magnetosphere:

$$R = \frac{I_{up}(H^+ + H_e^+)}{I_{dn}(H^+ + H_e^+)} \approx a_1 \exp\left[b_1 \frac{V_s}{\sqrt{2T_{+av}/M_{+av}}}\right],$$

where a_1 and b_1 are fitting parameters depending on the satellite and collection angles, V_s is the satellite speed, $T_{+av} = T(H^+)n(H^+)/(n(H^+)+n(H_e^+)) + T(H_e^+)n(H_e^+)/(n(H^+)+n(H_e^+))$ and $M_{+av} = M(H^+)n(H^+)/(n(H^+) + n(H_e^+)) + M(H_e^+)n(H_e^+)/(n(H^+) + n(H_e^+))$.

As for an extreme case of multiply charged ions in plasmas, You *et al* [17] measured the current–voltage (I–V) curves with several multiple ion species in the electron resonance cyclotron ion source (ECRIS) for atomic spectroscopy and heavy ion cyclotron accelerators. The I–V curves show the extreme non-saturation of ion saturation currents. Therefore, the choice of ion saturation current may affect the ratio of the current densities, hence the deduction of the flow velocity.

The effect of multiple ion species or impurity on the Mach number deduction in strongly magnetized plasmas is given in the experiments of SOL of tokamaks: (1) Porter *et al* simulated the flow in the SOL of the DIII-D, JET and JT-60U tokamaks using the 2D fluid code UEDGE [138], and found that the experimental values of the parallel velocities are very larger than those by the simulation including the carbon impurity radiation; (2) Erents *et al* [46] showed the overestimation of the parallel Mach numbers measured by the MP comparing the simulation results using the EDGE2D/Nimbus code [139] in the JET SOL plasma, indicating possible (atomic processes due to) impurities generated at the probe by plasma–surface interactions during the measurement; (3) Gangadhara and LaBombard [140] also showed the overestimation of the parallel Mach numbers, measured by the MP, comparing those by the CCD method for carbon plumes by puffing deuterated ethylene gas (C_2D_2) around the tip of the fast-scanning probe. A similar type of impurity puffing experiment was conducted by Jalblonski *et al* [141] as a diagnostic tool for SOL of Alcator C-Mod. Although they expected ionization along the presheath they adopted the collisionless fluid model of Hutchinson to get the Mach numbers.

4.3. Effect of temperatures on MP analysis

For the plasma-sheath equations ($\lambda > 0$), there is no singular point in kinetic analysis [8] as the fluid analysis, and the sheath edge should be defined by using the ion acoustic velocity (C_s) toward the probe surface, which is defined by $C_s = \sqrt{(T_e + T_{is})/m_i}$, where T_{is} is the ion temperature at the sheath or at the point where $V(y) = \sqrt{T_e/m_i}$. Since T_{is} is not the same as T_∞ (usually $T_{is} < T_\infty$ for subsonic flow), there would be error/difference in deducing the absolute drift velocity using the fluid model, using $C_s = \sqrt{(T_e + T_\infty)/m_i}$.

Referring to figure 40, one can see that there is a balance between the acceleration due to the electric field, which draws the ions to the probe, and the influx of ions with the external velocity distribution. If the external flow is toward the probe, the distribution tends to be narrow. If it is away from the probe, so that the external and internal flow velocities are opposite, the distribution tends to get wider.

For subsonic ion drift flows ($|M_\infty| < 1$), the ion temperature at the sheath has smaller values than that outside the presheath. This is an interesting result because most previous fluid treatments assume that there is no temperature gradient along the presheath. Our results show that this is a bad approximation. The temperature appears to satisfy approximately an adiabatic law: $pn^{-\gamma_i} = \text{constant}$, with $\gamma_i = 2$–2.5. The sheath temperature due to drift is slightly lower than that of Laux *et al* [45]. This increased cooling of ions may be due to the fact that our model allows only one degree of ion freedom (i.e. ratio of specific heat of ions $\gamma_i = 3$; 2–2.5 is observed to participate in the energy equation, while their model involves three degrees of ion freedom ($\gamma_i = 5/3$).

However, in order to meet the condition such as $\gamma_i T_{is} \approx T_{i\infty}$ the physics is probably much closer to the case of γ_i of order 2–2.5 and the effective ion temperature being 0.4–0.5 times $T_{i\infty}$. Yet the theoretical work of Burm *et al* [108] and the experimental results of Inutake and Woo [107] suggest that $\gamma_e \approx 1.0$, $\gamma_i \approx 1.17$, which leads to a reduction in the absolute drift speed by $[(1+1.17\tau_s)/(1+\tau_\infty)]^{0.5}$, where $\tau \equiv T_i/T_e$. For $M_\infty = 0.5$, $\tau_s = 0.08$, 0.3 and 0.5 for $\tau_\infty = 0.2$, 1.0 and 2.0,

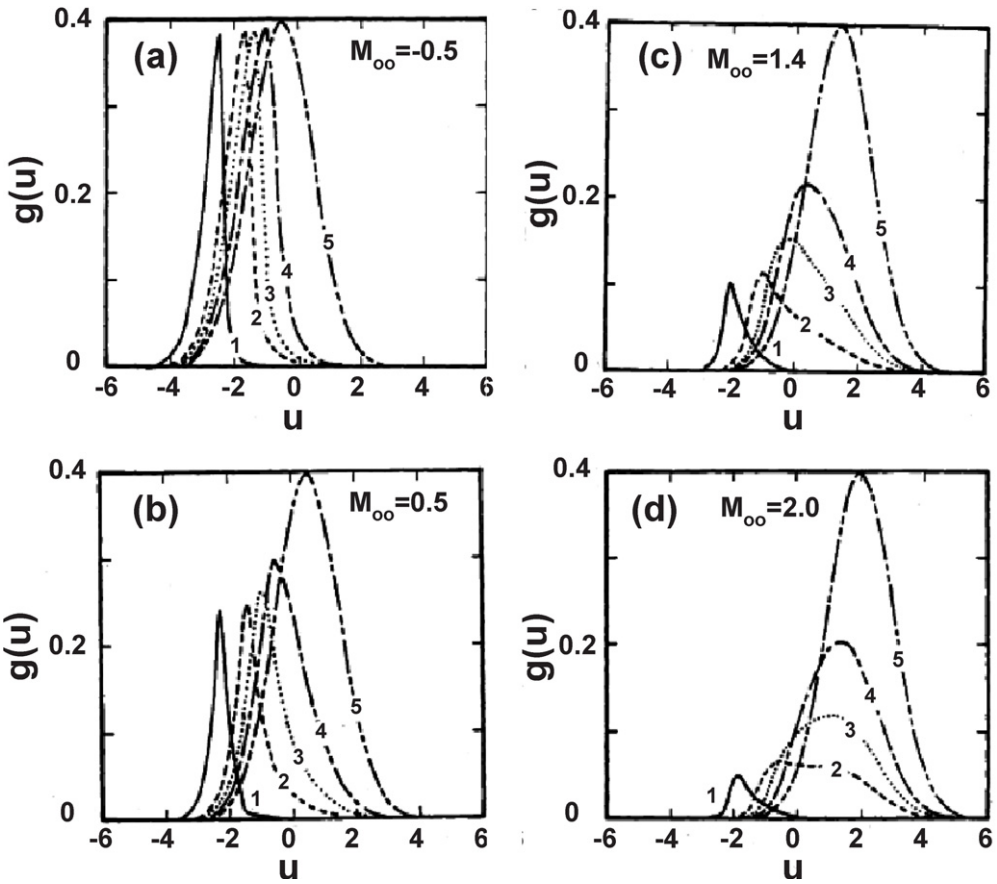

Figure 40. Ion velocity distribution functions for different ion drift velocities $u_d(=v_d/\sqrt{T_e/m_i}) = (a)\ -0.5$, $(b)\ 0.5$, $(c)\ 1.4$, $(d)\ 2.0$ when $\lambda = 0.001$, $T_{i\infty} = T_e$, $\psi_w = 3$. $\psi = \psi_w(1)$, $\frac{1}{2}\psi_w(2)$ $\frac{1}{3}\psi_w(3)$, $\frac{1}{4}\psi_w(4)$, $\infty(5)$, where $\lambda = \lambda_D/L_\parallel$, $\psi_w = -e\phi_{wall}/T_e$ and $\psi = -e\phi_{bias}/T_e$ [8, 109].

respectively, from the kinetic model. Then, the reduction ratio of each case would be 0.95, 0.82 and 0.73, respectively. So, in tokamak edge plasmas, for $\tau_\infty = 2$, 27% of absolute speed is reduced.

For transonic ion drift away from the probe (figures 40(*c*) and (*d*)), the sheath ion temperature increases again, as we have previously discussed. This effect for large drift is stronger when $T_{i\infty}$ is small. When the ion temperature outside the flux tube is $0.2T_e$, the sheath temperature is larger than that of $1.0T_e$ and $2.0T_e$ for the largest drift velocities. For low ion temperature and large ion drift (e.g. $T_{i\infty} = 0.2T_e$ and $M_\infty = 2.5$), there appears a double-humped ion distribution near the sheath. This is due to the fact that some particles are collected on the probe, and most of others are moving away from it. Clearly, the significance of attaching a temperature to such pathological distributions has been doubtful [8], but recent PIC model [77] shows a similar ion distribution in the azimuthal direction although it is with a different geometry (spherical) and is an unmagnetized plasma.

Gulick *et al* [142] measured the ion distribution function along the presheath of the magnetized plasma using the LIF method, and showed that the shape of the distribution is not Maxwellian and the broadening of the distribution toward the target surface gets wider, although they did not give the actual ion temperatures. Severn *et al* [133], Lee *et al* [135] and Claire *et al* [143] also measured the ion distribution function along the presheath of an unmagnetized multiple (Ar + Xe) plasma using the LIF method, compared with those by the ion acoustic wave measurements. Although they did not show the variation of the ion temperatures along the presheath, distributions seem to be narrowed for the Ar plasma, while those are broadened for the multiply charged plasmas (Ar + He and Ar + Xe) along the presheath.

These are contradictory to (1) the results of kinetic analysis of Chung and Hutchinson [8]; (2) those by PIC for the retarding field analyzer by Valsaque *et al* [144], although they obtained the fitting parameter $0.3 \leqslant K_T \equiv \ln[T_{up}/T_{dn}]/M_\infty \leqslant 1.4$ for a wide range of ion temperatures ($0.1 \leqslant T_{i\infty}/T_e \leqslant 5$), despite $T_{i\infty} \approx (T_{up} + T_{dn})/2$; and (3) those measured by the retarding field analyzer in tokamak experiments of Matthrews and Wan [31]. These may be due to the following. (1) For Lee's experiment, the unperturbed ion temperature is very cold, say 0.032 eV (≈102 °C), and weakly collisional plasmas ($n_e \approx$ (5–8) $\times\ 10^9\,cm^{-3}$, $T_e \approx$ 0.6–0.8, pressure ≈0.7 mtorr ≈2 $\times\ 10^{13}\,cm^{-3}$ with $T_n \approx 100\,°C$). (2) For Gulick's experiment, there is a chance of ion–neutral collisions near the target surface, since a large fraction of incident ions are to be recycled as thermal atoms. Hence both experiments indicated the possible inclusion of ion–neutral collisions, and the effect of multiple ions for Gulick's.

Gunn and Fuchs [16] analyzed the effect of two-temperature electron distribution on the deduction of Mach

number using a quasi-neutral particle-in-cell (QPIC) method with an isotropic and two-temperature electron distribution. The effect of hotter electron on the ion flow in the wake is found to be relatively small, i.e. the deduced Mach number is reduced slightly with increasing portion of hotter electrons, and this may be related to the finding by Song *et al* [145] that the hotter electrons affect the Bohm condition very little at the sheath. However, the presence of hotter electrons does strongly affect the deduction of electron temperature, which leads to the overestimation of the absolute ion sound speed.

To avoid the error of MP interpretation by different collection areas due to sheath expansion and the asymmetry of electron temperatures, Dejarnac *et al* introduced an MP composed of two tunnel probes in the CASTOR tokamak [146], which is less sensitive to the non-thermal electrons.

4.4. Effect of supersonic flow on MP analysis

Tsalas *et al* [101] measured sonic and supersonic plasma flows at the high field side SOL of the ASDEX Upgrade tokamak. Usually flows in the ionosphere or magnetosphere are supersonic. When the drift velocity exceeds the sound speed, fluid treatments generally show singularities, which are interpreted as an indication of shock formation, as shown in the fluid equations of Hutchinson [6] and Chung [12] for magnetized plasmas. So in their models, they cannot treat the case of supersonic flow, but Stangeby extends his fluid theory up to supersonic cases such as not for the deduction of Mach number (i.e. R), but for the deduction of power flux to the plate [5, 59].

For unmagnetized plasmas, Hutchinson's PIC model [77] can cover the case of supersonic flow, using the same formula for the subsonic flow ($K = 1.34$) up to $M_\infty \approx 3$. For the magnetized plasma, Chung and Hutchinson's kinetic analysis provides a formula for the supersonic flow up to $M_\infty = 5$ [8]. In their kinetic analysis, there is no evidence of a shock for the transonic case and this remains true, as further code runs have shown, even up to $M_\infty = 5$. Substitution of our solutions indicates that the theoretical necessary conditions for rarefaction shock are not satisfied. Thus, the absence of shocks seems to be consistent, although we know of no *a priori* argument why there should be none. It seems likely that it is due to a broadening of the velocity distribution function, a sort of relaxation in the velocity space, inherent in a proper kinetic treatment, which is absent from the fluid models, that prevents shock formation. If so, the results for transonic and supersonic velocities require a kinetic treatment such as ours. However, since our treatment is 1D, we may need 2D treatment for detailed explanation.

For the measurement of supersonic flow (say, for $M_\infty > 5.0$), PMP would practically be useful with proper calibration since both probes could measure reasonable amounts of ions even for higher Mach number, while the downstream side probe of the (parallel) MP barely collects them. There is one question on the analysis of Mach probe for supersonic flows: when we apply a fluid model to deduce the Mach number of supersonic flows from the ratio of the sheath current densities, how can we justify or clarify the sheath formation in the upstream side, since fluid velocity should be decreased at the sheath if we define the sheath by the Bohm criterion?

4.5. Effect of ion beams on MP analysis

Choi *et al* [147] measured the plasma flow velocity by MP and LIF methods in unmagnetized argon plasmas (<200 G) with supersonic ion beams. In order to determine flow velocities, the MP is calibrated via LIF in the absence of an ion beam, where the existing probe theories may be valid although they use different geometries (sphere and plane) and analyzing tools such as PIC and kinetic models. For the comparison of average plasma flow velocities by MP and LIF, the supersonic ion beam velocity was measured by LIF and then incorporated into a simple formula for average plasma speed with provisions for background plasma density and beam-corrected electron temperature (T_e) measured by a triple probe.

In order to calculate the average flow velocity of the plasma with an ion beam present, one must know densities and flow velocities of the beam and the plasma. Since the electric probe basically measures the particle flux, one can assume that the flow velocity determined by the MP shows the averaged velocity of the ion beam with the background plasma, and it would be presented as

$$\langle v \rangle = (n_p V_p + n_b V_b)/(n_p + n_b), \tag{118}$$

where n_p and V_p are the density and velocity of the background plasma without the ion beam, and n_b and V_b are the beam density and velocity. Actually the MP is for the measurement of the drift velocity expressed as in a shifted Maxwellian distribution, but not for the thermal velocity as in a Maxwellian distribution, yet it can be used as a diagnostic tool even for the measurement of bulk flow velocity.

4.6. Effect of negative ions on MP analysis

Kado *et al* [41] presented a method to measure the thermal and flow velocities for negative ions by means of a laser photo-detachment technique, laser photo-detachment velocimetry (LPDV). The difference in the temporal evolution of the photo-detached excess electron current between the upstream and the downstream regions corresponds to the flow velocity, while the average of the recovery times corresponds to the thermal velocity, namely the negative ion temperature. The initial results in a divertor/edge plasma simulator MAP (material and plasma)-II showed that the negative ion temperature is similar to that of helium ion obtained for helium discharges. The velocity of the negative ion front traveling from the laser edge to the sheath edge is different between the upstream and downstream sides due to the flow field. The recovery time of the negative ions toward the plane probe from the upstream and downstream sides can be described as L/v_{up}, and L/v_{dn}, respectively, where L is the distance between the edge of the laser irradiating region and the sheath edge, while v_{up} and v_{dn} represent the drift velocity of the negative ions of upstream and downstream sides of the probe, respectively. The thickness of the sheath is constant during the experiment if the probe bias is kept constant. By letting the thermal and directional flow (from

upstream to downstream) components of the drift velocity to be v_{th} and v_d, respectively, then we have:

$$v_{th} = \frac{1}{2}(v_{up} + v_{dn}) = \sqrt{\frac{8T_-}{M_-}}, \qquad v_d = \frac{1}{2}(v_{up} - v_{dn}), \tag{119}$$

where T_- and M_- denote the temperature and mass of the negative ions, respectively. By plotting the measured recovery time for the upstream and downstream sides as a function of the thickness of the laser beam from the surface of the plane probe, the flow velocity and the negative ion temperature can be determined at the same time, because the reciprocal of the slope corresponds to the drift velocity.

Kharapak *et al* [160] derived a relation between the ratio of upstream to downstream ion current in terms of the normalized grain radius $(a_0) \equiv a/\xi^*$, where $\xi* \equiv \sqrt{|Z|e/mu}$, m is the ion mass, ν is the frequency of ion momentum loss, u is the drift velocity for the highly collisional, without ionization/recombination drifting plasmas. In the low-velocity limit, they measured $R \approx 1$, and in the high-velocity limit, the ratio is given as

$$R = \exp(0.55a_0^2) \equiv \exp[K M_\infty]$$

where $M_\infty = v_d/\sqrt{T_e/m_i}$, $K = 0.55a^2\sqrt{T_e T_i}/|z|el_i = 0.55a^2\sqrt{T_e m_i}/|z|e$, l_i is the ion mean free path $(\equiv v_{T_i}/\nu)$, $|Z|$ is the magnitude of (negative) ion charge of a grain. They assumed the trajectory of ions near the negatively charged dust (grain) with a controlled Coulomb-like potential. They did not observe any asymmetry reversal as predicted by Hutchinson, [123], and as experimentally shown by Ko and Hershkowitz [124].

5. Calibration and error analysis

5.1. Calibration

5.1.1. MP in unmagnetized plasmas.

A. The LIF method

Lee *et al* [135] measured the ion velocity distribution functions (IVDFs) of argon and xenon plasmas in a multi-dipole filament chamber, and the argon ion speed was slower than its own Bohm velocity near the sheath and presheath boundary. Their ion velocity distribution function at sheath is well fitted to that of the kinetic result of Chung [78], as shown in figure 41. Claire *et al* [143] obtained IVDFs in electrostatic presheaths and sheaths in argon plasmas with LIF in a multi-dipole filament discharge. The shape of the measured IVDF is in qualitative agreement, for the presheath, with Emmert's model [60] and exhibits: (1) a Maxwellian profile at the center of the device where the potential is zero; (2) a distribution function's shape made of three distinct parts at the entrance of the presheath. Their result can approximately fit to the kinetic result of Chung [78], as shown in figure 41, which is a better fit than Emmert's in unmagnetized plasmas.

As mentioned in the section for the PIC simulation (section 3.1.1), Ko and Hershkowitz [124] found the reversal

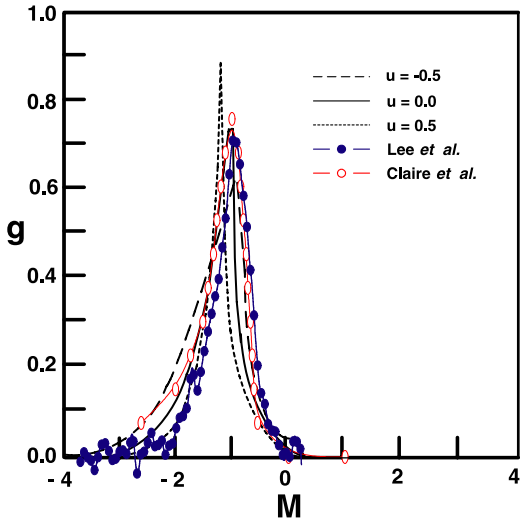

Figure 41. Ion velocity distribution functions at the sheath edge with different drift velocities ($u = v_d/\sqrt{T_e/m_i}$) of a kinetic model [78], LIF measurements without drift ($u = 0$) [135, 143].

of the current ratio or more ion collection using both a planar and a spherical probe as predicted by Hutchinson [123] on the downstream side than the upstream side for low-density plasmas with a short Debye length. However, there are discrepancies between the two probe data, say, clear flow reversal in the data of the spherical probe, but not so clear in those by the planar MP under the same plasma condition.

The characteristics of presheaths near an electrically floating plate in weakly collisional argon multi-dipole plasmas were investigated with a combination of data from LIF using a diode laser, MPs, emissive probes and Langmuir probes by Oksuz *et al* [40]. They fit their data to Hudis and Lidsky's model [3] up to $M_\infty = 0.7$. The maximum peak in velocity is approximately at $0.7C_s$ while the average flow velocity at the closest distance was somewhat less. Assuming collisionless ion motion, treating the ions as a single fluid, and assuming constant ion temperature are clearly questionable assumptions. The ion temperature changes by more than a factor of 3 in the measurement distance.

B. The electrostatic method

Oksuz and Hershkowitz [14] compared MP data with double-sided Langmuir probe data. The calculated plasma potential from the Langmuir probe is found to be approximately equal to the average of the plasma potentials calculated from data on each side of the MP. A new method is presented to determine the ion drift velocity using the electron saturation currents for $M_\infty < 1$ where M_∞ is the Mach number. They showed that their data are well fitted to the Hudis and Lidsky model [3] up to $M_\infty = 0.7$ assuming $T_i/T_e = 0.1$. The measured variation of plasma potential by an emissive probe supports their analysis, since they can deduce $M = 1$ at the sheath boundary. The ion drift velocities are calculated for $T_i = 0.1T_e$ or approximately 0.19 eV. This choice of ion temperature gave the best fit to the experimental Mach numbers.

Hala and Hershkowitz [151] suggested an independent and simple way of measuring plasma velocity by measuring the ion

acoustic wave velocity generated by a disk grid. As for the two ion species, the dispersion relation is approximately given as follows:

$$1 + \frac{1}{k^2\lambda_D^2} = \frac{\omega_{p1}^2}{\omega^2} + \frac{\omega_{p2}^2}{\omega^2}.$$

Then in the limit of small Debye length, the phase velocity becomes

$$v_{ph} = \omega/k \approx \sqrt{C_{s1}^2 + C_{s1}^2},$$

where $C_{s1} = \sqrt{n_j T_e/n_e M_j}$ is the concentration-weighted ion acoustic velocity for the j*th* ion species. This phase velocity becomes equal to the group velocity v_g for low-frequency and low-amplitude ion acoustic waves. This group velocity is measured by the time-of-flight method as Misra and Schott did by measuring a diverging spherical ion acoustic wave [152]: wave is generated so that density perturbation $\delta n_i/n_i$ of the launched pulse is very small, e.g. less than 0.5%, and is detected by a small probe, biased negatively to collect positive ion species, at different times of arrival.

5.1.2. MP in magnetized plasmas. Poirier and Boucher [153] measured the flow velocity of argon plasmas using LIF in the range $0.2 \leqslant M_\infty \leqslant 0.4$, and showed that Hutchinson's strong viscous model ($\alpha = 1$) fits to the data. Gunn *et al* [87] used these results to analyze the sensitivity of the alignment of MP in tokamak edge plasmas, using a GP and 2D kinetic code, called 'GUNDY', indicating the necessity of strong viscosity.

Gulick *et al* [142] measured the presheath ion flow velocity using the Doppler shift of LIF in singly ionized argon ions. The velocity shows a monotonic increase, from $0.15C_s$ far from the target to 0.5 at a distance of 5 mm from the surface. The experimental results are compared with those from a 1D isothermal single ion fluid model of the presheath and a kinetic electron fluid ion model. Both models agree well with the density profile, but underestimate the potential change and overestimate the velocity. The bulk flow velocity has been independently determined from 'MP' measurements, using various candidate theories to relate the Mach number to the ratio of the upstream to downstream saturation currents. A comparison with optical measurements indicate that the probe models which include viscosity provide reasonable agreement with MP data. Their data of $M_\infty = 0.15$ lies between the Hutchinson [6] and Harbour's and Proudfoot [1] model.

Using a VMP, Chung and Bengtson [97] measured the Mach number in the SOL of the TEXT-U tokamak as $0 < M_\infty < 0.2$ and $0.7 \leqslant \alpha \leqslant 1.3$ with an error of 40%. It would be necessary to expand their calibration up to the sonic point ($M_\infty \approx 1$) to give the exact number of α, since most models produce similar values of ratios for lower Mach number, e.g. $R(M_\infty = 0.3, \alpha = 1) = 1.93$, $R(M_\infty = 0.3, \alpha = 0.5) = 1.74$ and $R(M_\infty = 0.4, \alpha = 0.0) = 1.35$ by Hutchinson's analytic form.

5.2. Error analysis

5.2.1. Error in M due to error in R or J_s. If there is an error in measuring the ion sheath current density (J_s), σ_u, for upstream (J_{up}) and σ_d for downstream (J_{dn}), the error (σ_R) in the ratio ($R = J_{up}/J_{dn}$) is given by

$$\frac{\sigma_R}{R} = \left(\frac{\sigma_u^2}{J_{up}^2} + \frac{\sigma_d^2}{J_{dn}^2}\right)^{0.5}, \tag{120}$$

when J_{up} and J_{dn} are uncorrelated [154]. Since the flow Mach number is approximately given by

$$M_\infty = M_c \ln(R)$$

the error (σ_M) in the Mach number (M) can be calculated as

$$\sigma_M = M_c \frac{\sigma_R}{R} = M_c \left(\frac{\sigma_u^2}{J_{up}^2} + \frac{\sigma_d^2}{J_{dn}^2}\right)^{0.5}. \tag{121}$$

Here M_c is the inverse calibration factor ($M_c = 1/K$), which is calculated in terms of α and the ion temperature [7]. For example, if $\sigma_u/J_{up} = 10\% = \sigma_d/J_{dn}$, $R = 6$ and $\alpha = 1.0$, then $\sigma_M = (0.43)(0.1^2 + 0.1^2)^{0.5} = 0.061$ and the flow Mach number $M = 0.771 \pm 0.061$. Here $M_c = 0.43$ is used for $\alpha = 1$. Hence, the error in measuring M is about 8%, which is less than the error in the current density $J_s(\delta = 10\%)$. We apply the same 1D approximation to the SMP and LMP, which have different cross-field (vertical) positions, although the calibration factor (M_c) has different values with vertical position. Owing to this 2D effect, there might be an additional error in measuring M_∞ up to 10% [9].

5.2.2. Error in M_∞ due to K or α. According to Hutchinson's fluid model [6], the inverse calibration factor, M_c ($\equiv 1/K$), has the range 0.4–0.45 for $\alpha = 1$. According to Chung's argument [103] depending on the 1D fluid approximation, $\Delta R/R \simeq$ 20–26% with respect to Chung's kinetic model due to different values of K (or M_c).

If there is an error in the calibration factor by σ_M, then the error in measuring the flow Mach number is given by

$$\frac{\sigma_{M_\infty}}{M_\infty} = \left(\frac{\sigma_{M_c}^2}{M_c^2} + \frac{\sigma_R^2}{R^2}\frac{1}{(\ln R)^2}\right)^{0.5} \tag{122}$$

Hence, if we apply $\sigma_{M_c}/M_c = 10\%$, $\sigma_u/J_{up} = 10\% = \sigma_d/J_{dn}$, the largest error would be about 16% for $R = 3$ and 12% for $R = 9$.

According to Chung and Bengston's experiment in TEXT-U [97], they measured the normalized shear viscosity (α) and Mach number simultaneously, and they obtained α as 0.7–1.3. Hence, the tokamak data of Gunn *et al* [87] give $\alpha = 1$, if one uses the approximate formula of K as $K = 1 + \sqrt{\alpha^2/(1+\alpha)}\tan^{-1}\sqrt{1+\alpha}$, then $\Delta K = K(\alpha = 1.3) - K(\alpha = 1.0) = 0.17$.

5.2.3. Error in absolute velocity due to the specific heat ratio (γ_i). The effective acoustic velocity in the fluid treatments is $C_s \equiv \sqrt{(ZT_e + \gamma_i T_i)/m_i}$ and it is not obvious what to take for either γ_i or T_i. If the case of γ_i of order 2–2.5 and the effective ion temperature being 0.4–0.5 times $T_{i\infty}$ is used, then

the condition of $\gamma_i T_{is} \approx T_{i\infty}$ is met, as explained by Chung and Hutchinson [8] based on the well-matched results between their kinetic analysis with those of the isothermal fluid model by Hutchinson [6]. Experimentally, Ando *et al* determined γ_i as 1.2 by measuring the flow velocities coming out of the magnetic nozzle with an assumed calibration factor of the MP model [93], and Inutake and Woo [107] measured it as 1.17 using the LIF method, which was theoretically predicted by Burm *et al* [108]. If the ion acoustic speed should be used as $C_s = \sqrt{T_e + \gamma_i T_{is}}$, this leads to a reduction in the absolute drift speed by $r_\gamma \equiv [(1 + 1.17\tau_s)/(1 + \tau_\infty)]^{0.5}$, where $\tau_{s,\infty} \equiv T_{is,i\infty}/T_e$. Hence a smaller sheath ion temperature than the unperturbed ion temperature and smaller value of the specific heat ratio of ions make the absolute speed at the sheath smaller, so does the deduced drift speed. For example, from kinetic results of Chung and Hutchinson with $T_{i\infty} = 0.2, 1.0, 2.0T_e$, $T_{is} = 0.08, 0.3, 0.5T_e$ for $M_\infty = 0.5$, then $r_\gamma = 0.95, 0.82, 0.73$, which are 5%, 18%, 27% of reduction in the absolute speed measurement.

5.2.4. Geometrical error. Using the model of Van Goubergen *et al* [52], Gunn *et al* [87] used the following:

$$\frac{1}{K^*} \ln R = M_{||}^* - M_\perp^* \cot\theta, \tag{123}$$

where R is the current ratio, θ is the true angle, and K^* is a constant given by

$$K^* = 2[1 + 0.14\exp(M_{||}^*/0.862)]. \tag{124}$$

If there is a systematic error $\Delta\theta$ of the angular reference, then the apparent characteristic becomes, for $\Delta\theta < \theta = \pi/2$,

$$\frac{1}{K^*} \ln R = M_{||}^{*\prime} - M_\perp^{*\prime} \cot\theta' \approx M_{||}^{*\prime} + M_\perp^{*\prime}\Delta\theta' - M_\perp^{*\prime}\theta', \tag{125}$$

where the primes denote the falsely deduced values and $\theta' = \theta + \Delta\theta$.

$$\frac{1}{K^*} \ln R \approx M_{||}^{*\prime} + M_\perp^{*\prime}\Delta\theta - M_\perp^{*\prime}\theta'. \tag{126}$$

By equivalence with the correct expression, they found

$$M_\perp^* \approx M_\perp^{*\prime} \text{ and } M_{||}^{*\prime} \approx M_{||}^* - M_\perp^*\Delta\theta. \tag{127}$$

Although the perpendicular speed is not sensitive to misalignment, the parallel speed can be affected if the perpendicular speed is high enough, since an angular shift displaces the cot curve along the horizontal axis. To quantify the error in $M_{||}$ using Gunn *et al*'s argument [87], one should know not only the angle of misalignment, but also the perpendicular speed, which may be difficult in most experiments.

Shikama *et al* [155] raised a similar question and they calculated the effect of collection angle to the deduction of Mach number using the results of Hutchinson's PIC model [77], assuming that flow and magnetic field are independent of the angular distribution of current.

If we consider an error due to uncertainty of the sheath areas of ion collection, whether it comes from the misalignment (collection angle) or sheath expansion due to electron anisotropy, then the measured ratio can be expressed as

$$R_m = \frac{I_{um}}{I_{dm}} = \frac{I_{ut}(1+\epsilon)}{I_{dt}(1+\delta)} = R_t \frac{1+\epsilon}{1+\delta},$$

where subscripts m and t indicate measured and true. If $0 < \delta$, $\epsilon \ll 1$, then $1 + \delta \approx \exp[\delta]$, $1 + \epsilon \approx \exp[\epsilon]$, so

$$R_m = \exp[K M_{t\infty}] \exp[\epsilon - \delta].$$

Hence,

$$M_{t\infty} \approx M_{m\infty} - \frac{\epsilon - \delta}{K}.$$

If $\epsilon = \delta$, i.e. the same rate change of collection areas of up- and downstream sides, $M_{t\infty} = M_{m\infty}$. If $\epsilon \neq \delta$, then $M_{t\infty}$ is different from $M_{m\infty}$ by $(\epsilon - \delta)/K$. So if one gets exemplary numbers for this: for $M_{t\infty} = 0.5$ to be deduced as 0.4, then with $K = 1/0.4 = 2.5$, $(\epsilon - \delta) \approx 0.25$.

6. Conclusion

A Mach probe (MP) is an electric probe system to deduce the plasma flow velocity from the ratio of ion saturation currents. Generally, a typical MP is composed of two directional electric probes located at opposite sides of an insulator, but there are other MPs such as perpendicular MP (PMP), rotating (Mach) probe (RP), Gundestrup probe (GP), and visco-MP (VMP), depending on the shape of the probe holder, location of different probes or the method of collecting ions. Theories on the relation of the ratio of current densities with the Mach number are given for each Mach probe in terms of kinetic, PIC and self-consistent fluid or self-similar fluid models.

An exponential form for the ratio of current density ($R = \exp[K M_\infty]$) has been used as an empirical formula in order to deduce the plasma flow velocity at the SOL of tokamaks, ionospheric plasmas and other unmagnetized plasmas. This can be derived from continuity and momentum equations, using either self-similar or self-consistent methods. This exponential form seems to indicate the decay of flux (or current density) within the wake (or downstream) region of a collecting (or absorbing) object. The effects due to viscosity, ionization and charge-exchange (or recombination), and cross-field transport can play a role in reducing (or increasing) the flow speed as an additional drag (or pulling) force [7, 12, 80, 112].

As for theories of MP in magnetized plasmas, Stangeby [59] utilized the kinetic model of Emmert *et al* [60] to derive a simple analytic solution for MP [5] along with the experimental fitting of MP from DITE experiment [1]. Hutchinson [6] introduced a strong viscosity to build a physically and mathematically consistent fluid model. Later, Chung and

Hutchinson [8] introduced a kinetic model, which adopts the source term with ion drift consistently treating the diffusive source in a probe presheath along the strong magnetic field. This model and calculation seem to fit well to Hutchinson's fluid model with a strong shear viscosity [6]. Kinetic analysis (i) confirms the importance of viscosity in determining the ion drift velocity, (ii) has the ability to deal with ion drift kinetically without assuming the ion temperature along the presheath, and (iii) extends the ion drift velocity to the transonic regime. Chung and Hutchinson used the assumption that electron is isothermal (i.e. T_e is constant) even when ions drift transonically. Since there is no clear justification of this, we need better physical understanding about this even though there is a hint that viscosity plays a role. They also have generalized the source term in the Boltzmann equation by adding an ionization term. They obtained the relationship between the ion current density (and its ratio) and the drift velocity for the subsonic case. Introduction of ionization along the presheath decreases the value of K, while the cross-field contribution of the parallel viscosity contributes to increase K. Ion distributions near the probe surface get broader with viscosity, while they become narrower with ionization. For the deduction of parallel flow in strongly magnetized plasmas, it would be better either to use the kinetic model of Chung and Hutchinson, or Hutchinson's simple formula for an arbitrary normalized shear viscosity:

$$R(M^*_\infty, \alpha) = \exp[(1 + 1.2\sqrt{\alpha})M^*_\infty] = \exp[K M_\infty] = R(M_\infty, \alpha),$$

which produces the same value of the two-dimensional fluid model with $\alpha = 1$ and $M^*_\infty = v_d/\sqrt{(T_e + T_{i\infty})/m_i}(M_\infty = v_d/\sqrt{T_e/m_i})$: $K^*(K) = 2.2(1.6)$ (2D), 2.4(1.7) (1D), 2.3(1.66) (kinetic, $\tau_\infty = T_\infty/T_e$). This form can also be derived by the self-similar model ($(K^* = 2(K = 2.8))$ comparing with those of the inviscid model of Stangeby ($K^* = 1(K = 0.71)$): $R(M^*_\infty = \exp[2M^*_\infty]$. Figure 22 shows the ratios of sheath current densities with the parallel flow velocity (M_∞) in terms of viscosity, self-consistency and self-similarity.

To measure the rotation ($E \times B$) Mach number with the arbitrary angle ($30^o < \theta < 150^o$) of the probe tips, a Gundestrup or a rotating probe was proposed by using the model of Van Goubergen (and Hutchinson), by which the current ratio with parallel ($M_\parallel$), perpendicular ($M_\perp$) Mach numbers and incident angle (θ) is expressed as

$$R(M^*_\parallel, M^*_\perp, \theta) = \exp[K^*(M^*_\parallel - M^*_\perp \cot\theta)],$$

where $K^* = 2[1 + 0.14\exp(M_\parallel/0.862)] = 2.3$–$2.5$ (Van Goubergen), 2.2 (Hutchinson fluid) or 2 (Hutchinson, self-similar). However, the last value of Hutchinson should be expressed as 2.8 (without an ion pressure gradient). It would be better to use the Van Goubergen (or Hutchinson) model for the oblique angle incidence (or Gurdestrup/Rotating probe), because MacLachy's method is too complicated and requires several assumed values. For the oblique angle incidence to the arbitrarily shaped object, Hutchinson has keenly derived a formula of the current ratio with Mach number using self-similarity; $R(M_\parallel, M_\perp, \theta) = \exp[2(M_\perp - M_\parallel \cot\theta)]$, where a general cross-field transport, not necessarily cross-field diffusive, is assumed. It also needs further investigation on the application of the self-similar model to the Mach probe theory, especially with an ion pressure gradient and the atomic processes such as ionization and recombination. If one would use a vector probe, composed of two Mach probes with clear directionality, one of which is directed toward 0° or 180°, and the other toward 90° or 270° with respect to the magnetic field, one should apply the parallel magnetized Mach probe (MMP) model for the probe with 0° or 180°, but for the probe with 90° or 270° (grazing angle) it is not so clear which model should be applied. Depending on the sizes of ion Larmor radius and probe size toward the flow direction, either MMP or UMP model could be selected. However, Patacchini and Hutchinson derived a simple formula for the deduction of the parallel and perpendicular flows by locating two mutually perpendicular Mach probes [161]. And with mathematical consistency and comprehensiveness, Hutchinson showed that the collection of ions to an arbitrary shape with convex surface in the strongly magnetized plasmas seems to be similar to the case of his one-dimensional fluid model [10].

Although the insensitivity of this type of cross-field transport has been shown by Hutchinson and Patacchini, determination of the normalized shear viscosity (α) would be important to deduce Mach number: (i) By developing a fluid model for the connected-presheath Hutchinson incisively drew the number of α as unity by re-analyzing the experimental data of Chung *et al* for the free-presheath analysis, where they suggested $\alpha = 0.5$ without considering the case of connected (bounded) presheath. (ii) Later Chung analytically treated the bounded (connected) presheaths analytically using a one-dimensional fluid approximation comparing with those by a numerical one. From results using the bounded and free presheaths with mixed boundary conditions, a visco-Mach probe, which has one small Mach probe and one large Mach probe within one probe holder, was proposed to measure α and M_∞ simultaneously, and measured them in the TEXT-U tokamak, which produced $\alpha = 0.7$–1.3 in the SOL. (iii) Gunn elaborated on this problem by developing a two-dimensional kinetic model and comparing his numerical data with experimental data based on the LIF method by Poirier.

For the analysis of an MP in unmagnetized plasmas, kinetic models based on neutral approximation (cylindrical probe), and self-consistency (planar probe), are introduced along with PIC model (spherical probe). The fluid model obtained by taking moments of the kinetic model is compared with that by cold plasma approximation. Results of the existing PIC model are re-evaluated for subsonic to sonic flows, indicating that a possible overestimation would occur while using this model. Hutchinson's original PIC model suggested the calibration factor K as 1.34 for a large range of ion temperature ratios ($0 \leqslant T_i/T_e \leqslant 10$) and Mach numbers

($0 \leqslant M_\infty \leqslant 3$), although there are fluctuations of K with M_∞ depending on T_i/T_e. If one fits his numerical results for a narrow range of ion temperatures and subsonic Mach numbers, K becomes much smaller, 0.67–1.1, while those of the kinetic model is 0.91–1.24 (see table 1). Since it is not easy to get the calibration factor for very low ion temperatures ($0 < T_i/T_e < 0.1$) from both PIC and kinetic models, it is worthwhile to fit the calibration factor. The fitting function of $K(C)$ or $K^*(C)$ kinetic model for a wide range of ion temperatures ($0 < T_i/T_e < 2$) is given as

$$K(C, \tau) = 1.31 - 0.31\tau + 0.056\tau^2,$$

and K of the PIC model is $K(H) \approx K(C) - 0.2$, where C indicates the Chung and Hutchinson kinetic model, and H the Hutchinson PIC model. By fitting K and K^*, one can easily find the calibration factor for $T_i/T_e = 0$: $K(\tau \to 0) \approx 1.31$ for Chung's case, and $K(\tau \to 0) \approx 1.1$ for Hutchinson's case. However, the calibration factors of Hudis and Lidsky, Mott-Smith and Langmuir, and Solomon and Shats show larger difference from those of Hutchinson and Chung. Accidently, they coincide with those of Hutchinson and Chung at specific values of T_i/T_e: K(Hudis) $\approx K(H)$ at $\tau \approx 0.075$; K(Hudis) $\approx K(C)$ at $\tau \approx 0.1$; and K(Solomon) $\approx K(H)$ at $\tau \approx 0.6$; K(Solomon) $\approx K(C)$ at $\tau \approx 0.75$, which indicates that Hudis and Lidsky's model accidently happened to be applied for the plasma with cold ion temperature, say $\tau \sim 0.1$, and produced similar values to those by Chung and Hutchinson (with a modified calibration factor). As for those of Solomon and Shats, their model does not seem to be compatible with those of Hutchinson and Chung for the high ion temperature model, i.e. $\tau > 1$.

All the models of Hudis, Solomon and Hershkowitz treat the ion motions near the sheath and can be expressed in terms of the normalized potential difference between the ram and wake regions ($2e|\nabla\phi|/T_e$): (Hudis) $-m_i[{V_z}^2 - (v_{th} + v_d)^2] - [{V_z}^2 - (v_{th} - v_d)^2] = 4m_i v_{th} v_d/T_e = 4\sqrt{\tau}M_\infty$; (Solomon) $m_i[({v_{th}}^2 + 4v_{th}v_d/\pi) - ({v_{th}}^2 - 4v_{th}v_d/\pi)] = (4/\pi)m_i v_{th} v_d/\pi = (4/\pi)\sqrt{\tau}M_\infty$; (Oksuz) $m_i {v_d}^2/T_e = {M_\infty}^2$.

Hutchinson and Patacchini comprehensively summarized the ion collection to an absorbing spherical object using their PIC simulation, which covers the following general cases: magnetized and unmagnetized plasmas, collisionless to collisional plasma (charge-exchange), and oblique angle collection, etc [163].

For the supersonic flow or flows in highly collisional plasmas, perpendicular Mach probes have been used, although there is no prevailing and consistent model. Although kinetic theory or a self-similar model can extend their application range from subsonic to the supersonic flows, independent calibration is required for the validity of a certain model.

In addition to the existing collisionless models, atomic processes such as ionization and recombination are included to kinetic and fluid models resulting in a decrease in K for ionization and increase in K for recombination. But the effect of ion–neutral collision seems to be dominant, by which the deduced Mach number could be severely reduced. Hence it could be a clue for explaining the overestimation of Mach probe measurement in the tokamak edge. Although turbulent transport has been suggested as a candidate for the strong flow in the SOL of diverted tokamaks, one should be careful in taking the current densities for the steady-state MP analysis.

Not only does the ion temperature variation along the flux tube show that we should not neglect the temperature gradient along the presheath ($T_s \neq T_\infty$), but also the heat specific ratio γ_i is deduced as 1.2 by probe experiments, as 1.17 by LIF experiments and theory. If the ion acoustic speed should be used as $C_s = \sqrt{T_e + \gamma_i T_{is}}$, this leads to a reduction in the absolute drift speed by $r_\gamma \equiv [(1 + 1.17\tau_s)/(1 + \tau_\infty)]^{0.5}$, where $\tau_{s,\infty} \equiv T_{is,i\infty}/T_e$. Hence a smaller sheath ion temperature than the unperturbed ion temperature and a smaller value of the specific heat ratio of ions make the absolute speed at the sheath smaller, so does the deduced drift speed. For example, from kinetic results of Chung and Hutchinson with $T_{i\infty} = 0.2$, 1.0, $2.0T_e$, $T_{is} = 0.08$, 0.3, $0.5T_e$ for $M_\infty = 0.5$, then $r_\gamma = 0.95$, 0.82, 0.73, which are 5%, 18%, 27% of reduction in absolute speed measurements.

The effects of supersonic, negative ion, supersonic ion beams are also mentioned. As for the supersonic flow, results of kinetic and PIC models can be applied since there is no singular point near the probe surface even with a velocity bigger than the Bohm velocity in these models. Even the fluid model for magnetized plasmas with an arbitrary viscosity [12] can be used for the supersonic flow up to Mach number 2, while there would be a negative shear viscosity for larger flow than Mach number 2, theoretically.

Since there is a limitation for $\theta = 0^\circ$, to measure the velocity flowing perpendicular to the magnetic field such as $E \times B$ flow in cylindrical linear machines or propulsion systems, even in tokamaks, one may need a separate Mach probe with clear directionality and narrow collection angle, which does not collect any particle flowing in the parallel direction as Nagaoka *et al* [156] and Chung and Bengtson [97] tried, i.e. 'The tops of the cylindrical probes were recessed 1.0 mm $\sim$ ($>2.5 \times \rho_i$) from the boron nitride shielding to ensure that most of the ion saturation current is collected from the exposed sides of the cylindrical probes'.

So far the calibration of MMP has been made for $0.2 \leqslant M_\infty \leqslant 0.4$ by the LIF method and for $0 \leqslant M_\infty \leqslant 0.2$ by the VMP method, although self-consistent probe check is carried out using the connected-presheath model. Self-similar, 1D and 2D fluid models indicate 20% difference of K, besides the wide variation of $\alpha(\pm 40\%)$ by VMP experiments. If atomic processes are involved, the uncertainty would grow. All of these require a comprehensive calibration for a wide range of Mach numbers and ion temperatures ($0 \leqslant M_\infty \leqslant 1 \to 2$ and $0 \leqslant T_i/T_e \leqslant 2$).

As for the calibration of UMP, the spectroscopic method was used for $1.4 \leqslant M_\infty \leqslant 2.4$ to confirm the PIC model of Hutchinson using the ion specific heat ratio (γ_i) as a fitting parameter with high ion temperature ($T_i/T_e = 2$).

Formulae of the calibration factors are summarized in table 3.

Table 3. Mach probe formulae expressed by current density ratios, $K^* = K\sqrt{1+\tau}$, $\tau = T_{i\infty}/T_e$. α is the normalized shear viscosity, $M_\infty = v_d/\sqrt{T_e/m_i}$, $M^*_\infty = M_\infty/\sqrt{1+\tau}$, $M_o = M_\infty/\sqrt{2\tau}$, $M^*_{||} = M^*_\infty$. First authors are shown.

Models [Ref]	$R_{\|\|}R_\perp$ formula	$K[\tau=1,\alpha=1]$	Condition
Chung [8]	$\exp[K M_\infty]$	1.66	Kinetic, magnetized ($0 \leqslant \alpha \leqslant 1$)
Hutchinson [9]	$\exp[(1+1.2\sqrt{\alpha})M^*_\infty]$	1.56(2D), 1.7(1D)	Fluid, magnetized ($0 \leqslant \alpha \leqslant 1$)
Hutchinson [11]	$\exp[2M^*_\infty]$	1.41	Self-similar, magnetized
Stangeby [5]	$(2+M^*_\infty)/(2-M^*_\infty) \approx \exp[M^*_\infty]$	0.75	Fluid, magnetized ($\alpha = 0$)
Chung [12]	$\exp[(1+\sqrt{\alpha^2/(1+\alpha)}\tan^{-1}(\sqrt{1+\alpha}))M^*_\infty)]$	1.2	Fluid, magnetized ($0 < M_\infty \leqslant 0.5$)
Mott-Smith [72]	$\exp[(2\sqrt{\pi\tau}/(1+\tau M^2_\infty))M_\infty]$	2.7	Kinetic, unmagnetized
Chung [78]	$\exp[K M_\infty]$	1.0	Kinetic, unmagnetized
Hudis [3]	$\exp[(4\sqrt{\tau})M_\infty]$	4.0	Fluid, unmagnetized
Hutchinson [77]	$\exp[K M_\infty]$	$1.34(0 \leqslant \tau \leqslant 10)$	
		$1.1(0 \leqslant \tau \leqslant 1)$	PIC, unmagnetized
Solomon [126]	$\exp\left[\frac{4}{\pi}\sqrt{\tau}M_\infty\right]$	1.27	Fluid, unmagnetized
Hershkowitz [40]	$\exp[M^2_\infty]$	M_∞	Free fall
Van Goubergen [52]	$R_{\perp,\|\|} = \exp[K^*(M^*_{||} - M^*_\perp/\tan\theta)]$	1.7	Fluid, magnetized $\perp$ +$\|\|$
	$K^* = \exp[2(1+0.14\exp(M^*_{||}/0.862))]$	—	
Johnson [90]	$R_\perp = \frac{2}{\pi}\exp[-M^2_o]\sum_{n=0}^{\infty}[(M^2_o)^n/n!]^2\Gamma\left(n+\frac{3}{2}\right)$		PMP, unmagnetized
Kuriki [92]	$R_\perp = \exp[M^2_\infty/2]$ $(M_\infty < 1)$,		
	$= 1.65M_\infty$ $(M_\infty > 1)$		PMP, unmagnetized
Ando [93]	$R_\perp \approx \exp[1.1{M^*_\infty}^{0.9}]$ $(M^*_\infty < 1)$,		
	$\approx 1.65\sqrt{1+\tau}M^*_\infty$ $(M^*_\infty > 1)$		PMP, unmagnetized
Stangeby [94]	$R_\perp = \exp[2{M^*_\infty}^2]$		PMP, unmagnetized

Acknowledgments

The technical support of Hyun-Jong Woo in preparing the manuscript is greatly appreciated. This paper is much improved by the comments, references and suggested phrases of the referees during the review process, which is deeply appreciated. This work is supported by the National R&D Program through the National Research Foundation of Korea (NRF) funded by the Ministry of Education, Science and Technology (Grant number 2009-0082669 and 2012-0005926). This work is partially supported by the Basic Research Program of the National Fusion Research Institute (NFRI) of Korea. It is also partially supported by the Brain Korea 21 (BK21) program under the Ministry of Education, Science and Technology (MEST).

References

[1] Harbour P J and Proudfoot G 1984 *J. Nucl. Mater.* **121** 222
[2] Samir U, Comfort R H, Chappell C R and Stone N H 1986 *J. Geophys. Res.* **91** 5725
[3] Hudis M and Lidsky L M 1970 *J. Appl. Phys.* **41** 5011
[4] Hutchinson I H 1988 *Phys. Fluids* **31** 2728
[5] Stangeby P C 1984 *Phys. Fluids* **27** 2699
[6] Hutchinson I H 1987 *Phys. Fluids* **30** 3777
[7] Chung K-S and Hutchinson I H 1991 *Phys. Fluids* B **3** 3053
[8] Chung K-S and Hutchinson I H 1988 *Phys. Rev.* A **38** 4721
[9] Hutchinson I H 1988 *Phys. Rev.* A **37** 4358
[10] Hutchinson I H 2008 *Phys. Rev. Lett.* **101** 035004
[11] Hutchinson I H 2008 *Phys. Plasmas* **15** 123503
[12] Chung K-S 1994 *Phys. Plasmas* **1** 2864
[13] Chung K-S 2006 *Japan. J. Appl. Phys.* A **10** 7914
[14] Oksuz L and Hershkowitz N 2004 *Plasma Sources Sci. Technol.* **13** 263
[15] Boenig H V 1988 *Fundamentals of Plasma Chemistry and Technology* (Lancaster: Technomic Publishing Co.)
[16] Gunn J P and Fuchs V 2007 *Phys. Plasmas* **14** 032501
[17] You H-J, Woo H-J, Chung K-S, Liu Y, Meyer F W, Lho T and Lee M-J 2008 *Rev. Sci. Instrum.* **79** 02A319
[18] Malik S M, Muller D E, Sridharan K, Fetherston R P and Conrad J R 1995 *J. Appl. Phys.* **77** 1
[19] Stangeby P C 2000 *The Plasma Boundary of Magnetic Fusion Devices* (Bristol: Institute of Physics Publishing)
[20] Chung K-S, Kado S, Woo H-J, Seo Y-J, Shikama T, Scotti F, Choi G-S and Lho T 2007 *J. Nucl. Mater.* **363–365** 1403
[21] Chang-Diaz F R 2000 *Sci. Am.* **28** 90
[22] Berisford D F, Bengston R D, Raja L L, Cassady L D and Chancery W J 2008 *Rev. Sci. Instrum.* **79** 10F515
[23] La Belle-Hamer A L, Otto A and Lee L C 1994 *Phys. Plasmas* **1** 706
[24] Unruh W G 1981 *Phys. Rev. Lett.* **46** 1351
[25] Sakagami M 2003 *Math. Sci.* **478** 1
[26] Loureiro J, Mendonça J T, Brinca A L, Fonseca R, Silva L O and Vieira I 2005 *J. Atmos. Sol.—Terr. Phys.* **67** 1315
[27] Pospieszczyk A 2005 *Phys. Scr.* **T119** 71
[28] Kado S and Shikama T 2003 *J. Plasma Fusion Res.* **79** 841
[29] Woo H-J, Chung K-S, Lho T and McWilliams R 2006 *J. Kor. Phys. Soc.* **48** 260
[30] Proudfoot G, Harbour P J, Allen J and Lewis A 1984 *J. Nucl. Mater.* **128–129** 180

[31] Wan A S, LaBombard B, Lipschultz B and Yang T F 1987 *J. Nucl. Mater.* **145–147** 191
[32] Krasheninnikov S I 1992 *Nucl. Fusion* **32** 1927
[33] Kahn S A and Rognlien T D 1981 *Phys. Fluids* **24** 1442
[34] Montierth L M, Neuman W A and Morse R L 1992 *Phys. Fluids* B **4** 784
[35] Petrie T W *et al* 1992 *J. Nucl. Mater.* **196–198** 848
[36] Hutchinson I H *et al* 1994 *Phys. Plasmas* **1** 1511
[37] Porter G D, Rognlien T D, Rensink M E, Loarte A, Asakura N, Takenaga H and Matthews G 2003 *J. Nucl. Math.* **313–6** 1085
[38] Chung K-S, Hong S-H and Chung K-H 1995 *Japan. J. Appl. Phys.* **34** 4217
[39] Chung K-S, Kwak G Y, Choi Y-S, Lee M-J, Bak J G and Kwon M 2004 *Rev. Sci. Instrum.* **75** 4299
[40] Oksuz L, Khedr M A and Hershkowitz N 2001 *Phys. Plasmas* **8** 1729
[41] Kado S *et al* 2004 *Contrib. Plasma Phys.* **44** 656
[42] Tanga A, Bandyopadhyay M and McNeely P 2004 *Appl. Phys. Lett.* **84** 182
[43] Ohtsuka H, Kimura H, Shimomura S, Maeda H, Yamamoto S, Nagami M, Ueda N, Kitsunezaki A and Nagashima T 1978 *Plasma Phys.* **20** 749
[44] Allen J and Harbour P J 1987 *J. Nucl. Mater.* **145–7** 264
[45] Laux M *et al* 1989 *J. Nucl. Mater.* **162–164** 200
[46] Erents S K, Pitts R A, Fundamenski W, Gunn J P and Matthew G F 2004 *Plasma Phys. Control. Fusion* **46** 1757
[47] Boedo J A *et al* 1999 *J. Nucl. Mater.* **266–269** 783
[48] Asakura N *et al* 2002 *Plasma Phys. Control. Fusion* **44** 2101
[49] LaBombard B, Gangadhara S, Lipschultz B and Pitcher C S 2003 *J. Nucl. Mater.* **313–316** 995
[50] Tsois N *et al* 1999 *J. Nucl. Mater.* **266–269** 1230
[51] Gunn J P *et al* 2007 *J. Nucl. Mater.* **363–365** 484
[52] Van Goubergen H *et al* 1999 *Plasma Phys. Control. Fusion* **41** L17
[53] Boucher C *et al* 2001 *J. Nucl. Mater.* **290–293** 561
[54] Peterson B J *et al* 1994 *Rev. Sci. Instrum.* **65** 2599
[55] Samir U 1986 *Space Technology Plasma Issue in 2001* ed H Garrett, J Feynman and S Gabriel (Jet Propulsion Lab., California Institute of Technology) p 69
[56] Bohm D 1949 *The Characteristics of Electrical Discharges in Magnetic Fields* ed A Guthrie and R K Wakerling (New York: McGraw Hill) chapter 2–3
[57] Sanmartin J R 1969 *Phys. Fluids* **13** 103
[58] Laframboise J G and Rubinstein J 1976 *Phys. Fluids* **19** 1900
[59] Stangeby P C 1982 *J. Phys. D: Appl. Phys.* **15** 1007
[60] Emmert G A, Wieland R M, Mense A T and Davidson J N 1980 *Phys. Fluids* **23** 803
[61] Asakura N, ITPA SOL and Divertor Topical Group 2007 *J. Nucl. Mater.* **363–5** 41
[62] Gravier E, Gunn J P, Lachambre J-L, Loarer T, Mank G, Boucher C, Finken K-H, Jachmich S, Lehnen M and Van Oost G 2002 *Nucl. Fusion* **42** 653
[63] LaBombard B *et al* 2004 *Nucl. Fusion* **44** 1047
[64] LaBombard B, Hughes J W, Mossessian D, Greenwald M, Lipschultz B, Terry J L and the Alcator C-Mod Team 2005 *Nucl. Fusion* **45** 1658
[65] Hidalgo C *et al* 2003 *Phys. Rev. Lett.* **91** 065001
[66] Tonks L and Langmuir I 1929 *Phys. Rev.* B **34** 876
[67] Bernstein I B and Rabinowitz I N 1959 *Phys. Fluids* **2** 112
[68] Laframboise J 1966 *Theory of Spherical and Cylindrical Langmuir Probes in a Collisionless, Maxwellian Plasma at Rest* Institute for Aerospace Studies, Report No 100 (Toronto: University of Toronto Press)
Laframboise J 1966 *Rarefied Gas Dynamics* vol 2, ed. J H deLeeuw (New York: Academic) p 22
[69] Parrot M J M, Storey L R O, Parker L W and Laframboise J G 1982 *Phys. Fluids* **25** 2388
[70] Harrison E R and Thompson W B 1959 *Proc. Phys. Soc. London* **74** 145
[71] Bissel R C and Johnson P C 1987 *Phys. Fluids* **30** 779
[72] Mott-Smith H M and Langmuir I 1926 *Phys. Rev.* **28** 727
[73] Hutchinson I H 2002 *Phys. Plasmas* **9** 1832
[74] Hershkowitz N and Oksuz L 2002 *Phys. Plasmas* **5** 1835
[75] Gurevich A V, Pitaevskii L P and Smirnova V V 1970 *Sov. Phys.—Usp.* **99** 595
[76] Grabowski R and Fischer T 1975 *Planet. Space Sci.* **23** 287
[77] Hutchinson I H 2002 *Plasma Phys. Control. Fusion* **44** 1953
[78] Chung K-S 1991 *J. Appl. Phys.* **69** 3451
[79] Biehler S, Ecker G and Riemann K-U 1988 *Phys. Fluids* **31** 1999
[80] Chung K-S, Choi Y-S, Lee M-J and Woo H-J 2005 *32nd EPS Conf. on Controlled Fusion and Plasma Physics (Tarragona, Spain, 2005)* P2.079
[81] Chung K-S 1992 *J. Appl. Phys.* **71** 1177
[82] Krasheninnikov S I, Pigarov Yu A and Sigmar D J 1996 *Phys. Lett.* A **214** 285
[83] Janev R K, Kato T and Wang J G 2000 *Phys. Plasmas* **7** 4364
[84] Kado S, Iida Y, Kajita S, Yamasaki D, Okamoto A, Xiao B, Shikama T, Oishi T and Tanaka S 2005 *J. Plasma Fusion Res.* **81** 810
[85] Chung K-S, Woo H-J, Choi Y-S and Lee M-J 2008 *Contrib. Plasma Phys.* **48** 430
[86] Uehara K, Kawakami T, Amemiya H, Hoether K, Cosler A and Bieger W 1998 *Nucl. Fusion* **38** 1665
[87] Gunn J P *et al* 2001 *Phys. Plasmas* **8** 1995
[88] Dyabilin K, Hron M, Stöckel J and Žáček F 2002 *Contrib. Plasma. Phys.* **42** 99
[89] Hoethker K, Bieger W, Van Goubergen H 1998 *Contrib. Plasma Phys.* **38S** 121
[90] Johnson B H and Murphree D L 1969 *AIAA J.* **7** 2028
[91] Kanal M 1964 *J. Appl. Phys.* **35** 1697
[92] Kuriki K and Inutake M 1974 *Phys. Fluids* **17** 92
[93] Ando A *et al* 2006 *Contrib. Plasma Phys.* **46** 335
Ando A *et al* 2006 *Thin Solid Films* **506–507** 692
[94] Stangeby P C and Allen J E 1971 *J. Plasma Phys.* **6** 19
[95] Hutchinson I H 1991 *Phys. Fluids* B **3** 847
[96] Chung K-S 1994 *Nucl. Fusion* **34** 1213
[97] Chung K-S and Bengtson R D 1997 *Phys. Plasma* **4** 2928
[98] Hutchinson I H 2002 *Principles of Plasma Diagnostics* 2nd edn (Cambridge: Cambridge University Press)
[99] Stangeby P C 1989 *The Interpretation of Plasma Probes for Fusion Experiments*, in *Plasma Diagnostic* vol 2, ed O Auciello and D L Flamm (London: Academic)
[100] Stangeby P C 1988 *Phys. Fluids* **31** 2726
[101] Tsalas M, Herrmann A, Kallenbach A, Müller H W, Neuhauser J, Rohde V, Tsois N, Wischmeier M and the ASDEX Upgrade Team 2007 *Plasma Phys. Control. Fusion* **49** 857
[102] Hutchinson I H 1995 *Phys. Plasmas* **2** 1794
[103] Chung K-S 1995 *Phys. Plasmas* **2** 1796
[104] Stangeby P C 1987 *Phys. Fluids* **30** 3262
[105] Matthews G F, Stangeby P C and Sewell P 1987 *J. Nucl. Mater.* **145–147** 220
[106] Cohen S A 1978 *J. Nucl. Mater.* **76-77** 68
[107] Inutake M *et al* 2007 *Plasma Phys. Control. Fusion* **49** A121
Woo H-J 2011 *PhD Thesis* Hanyang University, Seoul
[108] Burm K T A L, Goedheer W J and Schram D C 1999 *Phys. Plasmas* **6** 2622
[109] Chung K-S 1989 Ion collection by probing objects inflowing magnetized plasmas *PhD Thesis* M.I.T., Cambridge, MA; also *M.I.T. Plasma Fusion Center Report* PFC/RR-89-13
[110] Lang S 1968 *Calculus* 2nd edn (Reading: Addison-Wesley) chapter 12
[111] Gunn J P 2005 *J. Nucl. Mater.* **337–9** 310

[112] LaBombard B, Conn R W, Hirooka Y, Lehmer R, Leung W K, Nygren R E, Ra Y, Tynan G and Chung K-S 1989 *J. Nucl. Mater.* **162–164** 314
[113] Chung K-S, Hutchinson I H, LaBombard B and Conn R W 1989 *Phys. Fluids* B **1** 2229
[114] Shinohara S, Matsuoka N and Matsuyama S 2001 *Phys. Plasmas* **8** 1154
[115] Hsu S C, Carter T A, Fiksel G, Ji H, Kulsrud R M and Yamada M 2001 *Phys. Plasmas* **8** 1916
[116] Bogashchenko I A, Gurevich A V, Salimov R A and Eidelman Yu I 1971 *Sov. Phys. JETP* **32** 841
[117] Morgan M A, Chan C, Cooke D L and Tautz M F 1989 *IEEE Trans. Plasma Sci.* **17** 220
[118] Merlino R L and D'Angelo N 1987 *J. Plasma Phys.* **37** 185
[119] Diebold D, Hershkowitz N, Intrator T and Baily A 1987 *Phys. Fluids* **30** 579
[120] Bezzerides B, Forslund D W and Lindman E L 1978 *Phys. Fluids* **21** 2179
[121] Stone N H 1981 *J. Plasma Phys.* **25** 35
[122] Al'pert Ya L, Gurevich A V and Pitaevskii L P 1965 *Space Physics with Artificial Satellites* (New York: Consultants Bureau)
[123] Hutchinson I H 2003 *Plasma Phys. Control. Fusion* **45** 1477
[124] Ko E and Hershkowitz N 2006 *Plasma Phys. Control. Fusion* **48** 621
[125] Shats M G, Rudakov D L, Boswell R W and Borg G G 1997 *Phys. Plasmas* **4** 3629
[126] Solomon W M and Shats M G 2001 *Rev. Sci. Instrum.* **72** 449
[127] Krasheninnikov S I 1997 *J. Nucl. Mater.* **241–243** 283
[128] Clements R M, MacLatchy C S and Smy P R 1972 *J. Appl. Phys.* **43** 31
[129] Clements R M and Smy P R 1970 *J. Appl. Phys.* **41** 3745
[130] MacLactchy C S, Budgel P C and Miner J R 1974 *Can. J. Phys.* **52** 1057
[131] Liebermann M A and Lichtenberg A J 1994 *Principles of Plasma Discharges and Material Processing* (New York: Wiley) chapter 5
[132] Smy P R 1976 *Adv. Phys.* **25** 517
[133] Severn G D, Wang X, Ko E and Hershkowitz N 2003 *Phys. Rev. Lett.* **90** 145001
[134] Lee D, Hershkowitz N and Severn G 2005 *Appl. Phys. Lett.* **91** 041505
[135] Lee D, Severn G, Oksuz L and Hershkowitz N 2006 *J. Phys. D: Appl. Phys.* **39** 5230
[136] Hershkowitz N and Ko E 2005 *IEEE Trans. Plasma Sci.* **33** 631
[137] Riemann K-U 1995 *IEEE Trans. Plasma Sci.* **23** 709
[138] Rognlien T D, Porter G D and Ryutov D D 1999 *J. Nucl. Maters.* **266–269** 654
[139] Erents S K *et al* 2000 *Plasma Phys. Control. Fusion* **42** 905
[140] Gangadhara S and Labombard B 2004 *Plasma Phys. Control. Fusion* **46** 1617
[141] Jalblonski D, LaBombard B, McCracken G M, Lisgo S, Lipschultz B, Hutchinson I H, Terry J and Stangeby P C 1997 *J. Nucl. Mater.* **241–243** 782
[142] Gulick S L, Stansfield B L, Z. Abou-Assaleh, Boucher C, Matte J P, Johnston T W and Marchand R 1990 *J. Nucl. Mater.* **176–177** 1059
[143] Claire N, Bachet G, Stroch U and Doveil F 2006 *Phys. Plasmas* **13** 062103
[144] Valsaque F, Manfredi G, Gunn J P and Gauthier E 2002 *Phys. Plasmas* **9** 1806
[145] Song S B, Chang C S and Choi D I 1997 *Phys. Rev.* E **55** 1213
[146] Dejarnac R, Gunn J P, Stoeckel J, Adamek J, Brotankova J and Ionita C 2007 *Plasma Phys. Control. Fusion* **49** 1791
[147] Choi Y-S, Woo H-J, Chung K-S, Lee M-J, Zimmerman D and McWilliams R 2006 *Japan J. Appl. Phys.* **45** 5945
[148] Stangeby P C and Chankin A V 1995 *Phys. Plasmas* **2** 707
[149] Cosler A, Höthker K, Kemmereit E, Schürer M, Bieger W and Heuser W 1995 *SOFE '95. Seeking a New Energy Era, 16th IEEE/NPSS Symp.* (Urbana-Champaign, IL: University of Illinois) vol 2 p 1051
[150] Stansfield B L, Boucher C, Gunn J P, Guo H, Fall T, Mailloux J, Meo F and Terreault B 1995 *J. Nucl. Mater.* **220–222** 1121
[151] Hala A M and Hershkowitz N 2001 *Rev. Sci. Instrum.* **72** 2279
[152] Misra S G and Schott L 1973 *Plasma Phys.* **15** 883
[153] Poirier D and Boucher C 1998 Validation of plasma velocity measurements with Mach probes using laser-induced fluorescence *Int. Congress on Plasma Physics and 25th European Physical Society (Prague, Czech Republic, 29 June–3 July)*
[154] Bevington P R and Robinson D K 1992 *Data Reduction and Error Analysis for the Physical Science* 2nd edn (New York: McGraw-Hill)
[155] Shikama T *et al* 2005 *Phys. Plasmas* **12** 44504
[156] Nagaoka K, Okamoto A, Yoshimura S and Tanaka M Y 2001 *J. Phys. Soc. Japan* **70** 131
[157] Patankar S V 1980 *Numerical Heat Transfer and Fluid Flow* (New York: Hemisphere)
[158] Back R and Bengtson R D 1997 *Rev. Sci. Inst.* **68** 377
[159] MacLactchy C S, Boucher C, Poirier D A and Gunn J 1992 *Rev. Sci. Instrum.* **63** 3923
[160] Khrapak S A, Klumov B A and Morfill G E 2007 *Phys. Plasmas* **14** 034502
[161] Patacchini L and Hutchinson I H 2009 *Phys. Rev.* E **80** 036403
[162] Choi Y-S *et al* 2009 *J. Phys. D: Appl. Phys.* **42** 225205
[163] Park E-K *et al* 2012 *Current Appl. Phys.* **12** 1497
[164] Hutchinson I H and Patacchini L 2007 *Phys. Plasmas* **14** 013505
[165] Hutchinson I H and Patacchini L 2010 *Plasma Phys. Control. Fusion* **52** 124005